

Ionized Plasma and Neutral Gas Coupling in the Sun's Chromosphere and Earth's Ionosphere/Thermosphere

Leake, J.E. [1] · DeVore, C.R. [2,3] · Thayer, J.P. [4] · Burns, A.G. [5] · Crowley, G. [6] · Gilbert, H.R. [3] · Huba, J.D. [2] · Krall, J. [2] · Linton, M.G. [2] · Lukin, V.S. [2] · Wang, W. [5]

Received: date / Accepted: date

Abstract We review our understanding of ionized plasma and neutral gas coupling in the weakly ionized, stratified, electromagnetically-permeated regions of the Sun's chromosphere and Earth's ionosphere/thermosphere. Using representative models for each environment we derive fundamental descriptions of the coupling of the constituent parts to each other and to the electric and magnetic fields, and we examine the variation in magnetization of the ionized component. Using these descriptions we compare related phenomena in the two environments, and discuss electric currents, energy transfer and dissipation. We present a coupled theoretical and numerical study of plasma instabilities in the two environments that serves as an example of how the chromospheric and ionospheric communities can further collaborate. We also suggest future collaborative studies that will help improve our understanding of these two different atmospheres which share many similarities, but have large disparities in key quantities.

1 Introduction

In a universe where partially ionized gases abound, interactions between ionized plasma and neutral gas play a critical role in planetary and stellar atmospheres, including those of the Earth and the Sun. They also are important at the heliopause, where the solar wind meets the interstellar medium, and in other astrophysical contexts. Plasma-neutral interactions modulate momentum and energy exchange among the neutral gas, electrons, and ions, and between the ionized plasma and electromagnetic fields. The physics of plasma-neutral coupling adds another layer of complexity to problems that previously have been addressed by assuming a fully ionized plasma or some other single-fluid approximation. The importance of these transitional layers in the inner heliosphere – in particular, the solar chromosphere and terrestrial ionosphere/thermosphere – lies in their impact on space weather processes that can profoundly affect Earth and society. This motivates our attention to the underlying physics of plasma-neutral coupling.

[1] George Mason University *email: jleake@gmu.edu* · [2] Naval Research Laboratory · [3] NASA Goddard Space Flight Center · [4] University of Colorado · [5] National Center for Atmospheric Research (NCAR) · [6] Atmospheric and Space Technology Research Associates

The solar chromosphere is the highly dynamic, complex region above the relatively cool visible surface of the Sun and beneath the very hot corona. It is characterized by several transitions that occur with increasing altitude: from predominantly neutral to ionized hydrogen; from essentially unmagnetized to strongly magnetized charged particles; from collisional to collision-less behavior; and from gas-dominated to magnetic field-dominated dynamics. These transitions vary in space and time as the chromosphere is driven continually from below by convective motions and magnetic evolution. The chromosphere is the source of the solar wind and also modulates the flow of mass and energy into the corona. The chromosphere's complexity is increased further by its state of thermodynamic and ionization non-equilibrium, which makes understanding its observed emission and absorption spectra very challenging.

The ionosphere/thermosphere (hereafter I/T) is a similarly transitional region in the Earth's upper atmosphere, in which the gas is ionized to varying degrees by incident solar radiation. It encompasses the same physical transitions as those occurring in the chromosphere. In this paper we use the term I/T to denote that region of the Earth's upper atmosphere between about 80-600 km altitudes. The word "thermosphere" technically denotes a distinct region based on the temperature profile of the neutral component of the upper atmosphere. The word "ionosphere" refers to the ionized component of the gas in the upper atmosphere, usually in the same 80-600 km altitude region. Thus, I/T includes both the neutral and ionized constituent parts of the weakly ionized mixture. The I/T is bounded below by the mesosphere, and above by the magnetosphere, and as a result it is driven continually from above and below. Understanding how the many various forcing mechanisms interact to cause variability in the I/T system remains a major challenge.

Previous authors have discussed similarities and differences between the Sun's chromosphere and the Earth's ionosphere (Haerendel 2006; Fuller-Rowell and Schrijver 2009). These authors emphasized the strong collisional coupling of the minority plasma constituents to the majority neutral species in both atmospheres; a collisional coupling of the neutrals to the plasma that is very substantial in the solar chromosphere but relatively weak in the terrestrial I/T; and the impact of these interactions on the highly anisotropic electrical conductivities along and across ambient magnetic fields in the two environments. Haerendel (2006) further presented analogies between density fluctuations in solar spicules and sporadic E layers, atmospheric heating by Alfvén waves in chromospheric plages and auroral arcs, and plasma erosion driven by currents aligned with the magnetic fields in solar flares and auroral ion outflows. Fuller-Rowell and Schrijver (2009) provided a detailed summary of processes occurring in the ionosphere, followed by a survey of phenomena in the Sun's chromosphere and comparisons between the two. They discuss the similar variability of the charged particle magnetizations in the two atmospheres and the role of convective overshoot from the photosphere/thermosphere below the chromosphere/ionosphere, and highlight major contrasts in the dynamic/static character of the magnetic fields and the resultant dominance of magnetohydrodynamics/electrodynamics in describing macroscopically the evolution of those fields.

One of the goals of this review is to highlight the commonalities and differences between the chromosphere and I/T in order to develop cross-disciplinary collaboration between the two communities, which typically use different approaches to the same fundamental physics. In doing so, we hope to identify important questions concerning the transition from weakly ionized dense mixtures to fully ionized tenuous plasmas linked by electromagnetic fields, and present methods by which we can enhance our physical understanding of such systems using improved analytical and numerical modeling of plasma-neutral coupling in the chromosphere and I/T.

The paper is structured as follows. In §2, we examine representative static models of the chromosphere and I/T, and compare the two environments in terms of their fundamental neutral, plasma, and magnetic properties and some key dimensionless ratios. In §3, we present the governing equations for a weakly ionized reacting plasma-neutral mixture. In §4 we investigate in detail the physics and the equations that govern the coupling of the ionized plasma and neutral gas to each other and to the electromagnetic field. We compare the magnetization and mobility of the ionized component of the two environments and relate them to the evolution of electric currents. In §5 we discuss processes which are examples of such coupling, and consider the contrasting approaches that the I/T and chromosphere communities use to describe essentially the same phenomena. In §6, we address the transfer and dissipation of energy, first focusing on the state of the field's knowledge. Then we discuss the importance of the conversion of electromagnetic energy into thermal and kinetic energy, and look at the efficiency of plasma-neutral coupling in this energy transfer. In §7, we present an illustrative analytical and numerical case study of the Rayleigh-Taylor instability, which is common to the chromosphere and I/T yet also highlights the contrasting conceptual and mathematical approaches employed by the two communities. We conclude in §8 with some parting thoughts about current challenges to our understanding of plasma-neutral coupling on the Sun and at the Earth.

2 Basic Properties

In this section, basic properties of the Sun's chromosphere and Earth's I/T are presented and compared. As we will show quantitatively, there are both significant similarities and substantial differences between these environments. From fundamental principles, we deduce qualitative implications about how the majority neutral and minority plasma constituents couple hydrodynamically in both atmospheres. Then in §4 we will discuss how they couple principally magnetohydrodynamically in the chromosphere (where the fluctuating and ambient magnetic fields frequently are of the same magnitude) but electrodynamically in the I/T (where the fluctuating fields are far smaller than the ambient field, in general). Several of the following general introductory considerations are elaborated on in more detail in the later sections of the paper, which deal with the governing multi-fluid equations, generalized Ohm's law and its low-frequency limit, the mobility of plasma and electric currents, electromagnetic energy transfer, and the Rayleigh-Taylor instability.

2.1 Models for the Chromosphere and Ionosphere/Thermosphere

The chromosphere may be best represented by the semi-empirical quiet-Sun model "C7" developed and tabulated by Avrett and Loeser (2008), hereafter referred to as the ALC7 model (see also Vernazza et al. 1981; Fontenla et al. 1993, 2006). In this model, simulated line and spectral emissions are matched to the observed spectra to obtain estimates of the total density, ionization level and temperature in the chromosphere. The transition region above is modeled by assuming an energy balance between the downward total energy flow from the overlying hot corona and local radiative loss rates. Downward diffusion through the background neutral gas of the predominant hydrogen and helium ions, enhanced by the ambipolar electric field generated by the more freely diffusing electrons, contributes significantly to the energy transport in the lower chromosphere, while electron thermal conduction dominates in the upper chromosphere. Although this one-dimensional model certainly does

not capture all variations, either temporally or in three dimensions, it is useful for characterizing the generic structure of the chromosphere.

The I/T may be best represented by the NCAR Thermosphere-Ionosphere-Mesosphere-Electrodynamical General Circulation Model (NCAR TIMEGCM). TIMEGCM is a time-dependent, three-dimensional model that solves the fully coupled, nonlinear, hydrodynamic, thermodynamic, and continuity equations of the neutral gas along with the ion energy, momentum, and continuity equations from the upper stratosphere through the ionosphere and thermosphere (Roble et al. 1988; Richmond et al. 1992; Roble and Ridley 1994). TIMEGCM predicts global neutral winds, neutral temperatures, major and minor species composition, electron and ion densities and temperatures, and the ionospheric dynamo electric field. The input parameters are solar EUV and UV spectral fluxes, parameterized by the F10.7 cm index, plus auroral particle precipitation, an imposed magnetospheric electric field, and the amplitudes and phases of tides from the lower atmosphere specified by the Global Scale Wave Model (Hagan et al. 1999). Many features of the model, such as increased electron temperature in the E and F layers, have been validated against observations (e.g., Lei et al. 2007). For the atmospheric profiles used in this paper, TIMEGCM was run under equinox conditions with a F10.7 value of 150, a Kp index of 2, and tidal forcing. The vertical profile was taken from 47.5° N latitude at 12:00 local time. Thus like the model chromospheric profile described above, we represent the I/T structure by a single 1-D, time-independent profile extracted from the TIMEGCM.

In displays of quantities provided by, or derived from, these models for the chromosphere and I/T, we use as the primary (left) ordinate axis the normalized total gas pressure (P/P_0), where P_0 is defined to be the pressure at a selected reference height in the domain. The approximate corresponding altitude is shown as the secondary (right) ordinate axis. For the chromosphere, we chose the Sun's visible surface, the photosphere, as the reference height. The pressure there is 1.23×10^4 Pa in the ALC7 model. For the Earth's atmosphere, we selected a reference height of 30 km, even though it is in the stratosphere and outside the I/T region. This choice of lower boundary is to allow comparison of electrodynamics between the two atmospheres later in this review. We set the top of the chromosphere where the pressure has decreased from its base value by six orders of magnitude; this occurs at an altitude of 1989 km, above which the temperature rises steeply in the transition region. Ten orders of magnitude of pressure reduction were included in the I/T, which extends up to about 640 km in altitude.

2.2 Neutral Gas, Plasma, and Magnetic Field

Figure 1 depicts the temperature profiles in the ALC7 chromosphere and the TIMEGCM I/T. Overall, the chromosphere is about one order of magnitude hotter (4,400–6,700 K) than the I/T (200–2,800 K). All species temperatures are assumed to be equal in the model chromosphere (left), whereas the neutral, electron and ion temperatures are allowed to differ in the model I/T (right). We also note that the I/T values are plotted down to the reference pressure level near 30 km (stratosphere), for comparison with the chromospheric profile, even though the I/T altitudes are at 80–600 km. Both the solar and Earth profiles show a decline with altitude in the lower atmosphere to a minimum value, beyond which the temperature begins to rise in the upper atmosphere. In the chromosphere, the temperature increase is due to both local heating, the nature of which is not well understood, and downward heat conduction from the overlying, much hotter solar corona. The increasing ionization fraction of the chromosphere and transition region above with height is a direct consequence of this

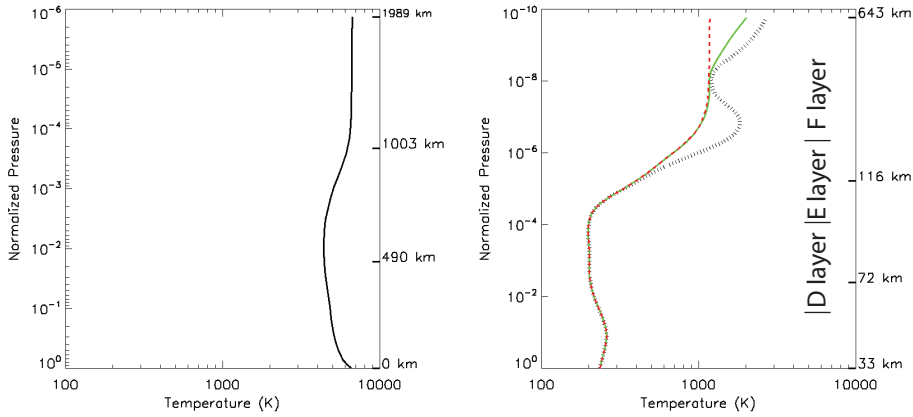


Fig. 1 Single-fluid temperature (K) in the ALC7 chromosphere (left) and neutral (red dashed line), ion (green solid line), and electron (black dotted line) temperatures in the TIMEGCM I/T (right).

temperature increase. In the I/T, on the other hand, the neutral gas is photo-ionized by incident UV radiation from the Sun. The excess kinetic energy of the liberated photoelectrons is thermalized by electron-electron collisions and is transferred to the ions and neutrals by collisional thermal equilibration, accompanied by additional electron liberation due to impact ionization. Additional heating processes contribute at high latitudes, including Joule heating and energetic particle precipitation in the polar caps. Because the equilibration rate is much higher between ions and neutrals than with electrons, the ion and neutral temperatures are essentially equal to each other and equal to (at low altitudes) or below (at mid altitudes) the temperature of the electrons. Above about 300 km altitude in the thermosphere, Coulomb coupling between electrons and ions becomes increasingly important, and the three temperatures increasingly separate, with electrons the hottest and neutrals the coolest. We speculate that a fully comprehensive model of the chromosphere would show similar qualitative trends in the coupling of the neutral and plasma temperatures, but the details of the temperature profiles of the species would depend sensitively on how the unknown heating mechanisms partition thermal energy among the particles.

The approximate altitude ranges of the ionospheric D, E, and F-layers are shown in the right-hand panel of Figure 1. The lowest, D, layer of the ionosphere extends from about 60 to 90 km in altitude. Its dominant neutral is molecular nitrogen (N_2), while its dominant ion is nitric oxide (NO^+) photo-ionized by penetrating Ly α radiation at λ 121.5 nm. Water cluster ions can also be significant in the D-layer. The middle, E, layer extends upward from 90 km to about 150 km altitude. N_2 remains the dominant neutral species, but at this height solar soft X-ray and far UV radiation, together with chemical reactions, add molecular oxygen ions (O_2^+) to the plasma. The highest, F, layer ranges from about 180 km to well over 500 km in altitude. At these heights, due to molecular dissociation at the elevated temperatures and ionization by extreme ultraviolet radiation, atomic oxygen is dominant in both its neutral (O) and ionized (O^+) states.

In contrast to the rich compositional structure of the Earth's I/T, the composition of the chromosphere is relatively uniform with altitude, consisting primarily of hydrogen (H, H^+), secondarily of helium (He, He^+) up to 10% that of Hydrogen, and thereafter a smattering of minority neutrals and ions up to iron at much smaller concentrations. However, the radi-

ation in the chromosphere is dominated by spectral lines in some of these minority species, such as calcium, magnesium and iron. Plasma-neutral coupling in the cool material of solar prominences (see §7) has been shown to lead to species separation and preferential draining of He relative to H (Gilbert et al. 2002, 2007). This occurs due to the very strong charge-exchange collisional coupling of H to H^+ , which retains the majority hydrogen atoms while the minority helium atoms leak out much more freely. In the solar chromosphere, the constantly churning convection driven from below maintains the roughly uniform composition through turbulent mixing. In contrast, in the Earth’s atmosphere, above about 100 km (the turbopause) turbulent mixing is too weak to homogenize the atmosphere and maintain a uniform composition, so the atmospheric composition becomes stratified under gravitational attraction according to the species molecular weights.

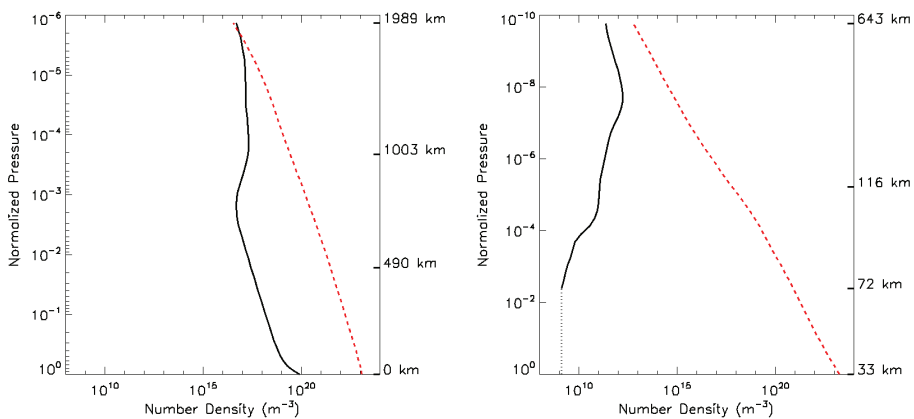


Fig. 2 Neutral (red dashed line) and plasma (black solid line) number densities (m^{-3}) vs. normalized pressure in the ALC7 chromosphere (left) and the TIMEGCM I/T (right).

The number densities of the neutral and plasma constituents of the atmospheres are shown in Figure 2. The neutral densities are nearly equal in the ALC7 chromosphere (left) and TIMEGCM I/T (right) over their common range of normalized pressures, falling from a value of about $10^{23} m^{-3}$ where the base pressure was chosen in each atmosphere. In contrast, the plasma densities differ by several orders of magnitude between the chromosphere and the I/T, due to the combination of their order-of-magnitude temperature difference and to the disparate ionization processes that dominate in the two atmospheres. Thus, the neutral and plasma densities become nearly equal at the top of the Sun’s chromosphere, whereas in the Earth’s I/T region, the plasma density is much smaller than the neutral density throughout the displayed altitude range. Equality of the plasma and neutral densities in the I/T occurs only at much higher altitudes than those shown in our graphs. The dotted line below 70 km in Figure 2 denotes a region below the ionosphere proper, where the plasma density is small and poorly characterized in TIMEGCM so we have elected to hold it fixed at its value at 70 km altitude.

These very similar neutral densities, but radically different plasma densities, in the chromosphere and I/T have important consequences for the roles of plasma-neutral coupling in the dynamics of the mixture. The collision frequencies of ions on neutrals (v_{in}) and of neu-

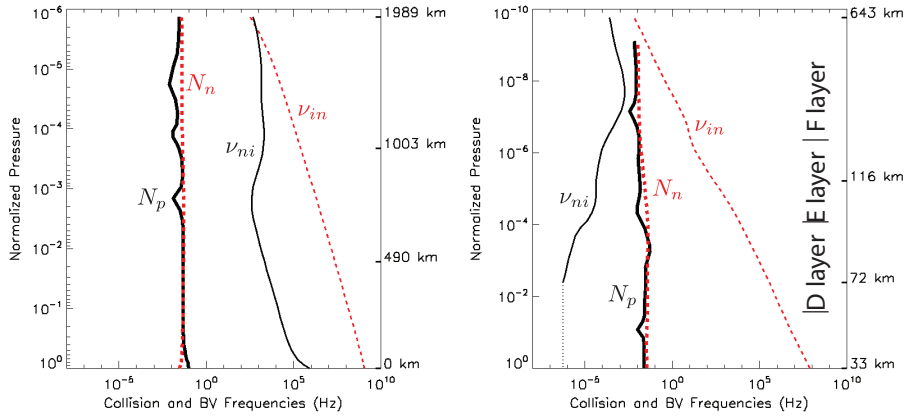


Fig. 3 Frequencies in the ALC7 chromosphere (left panel) and the TIMEGCM I/T (right panel). The thin lines show collision frequency for ions on neutrals (ν_{in} - red dashed line) and neutrals on ions (ν_{ni} - black solid line). The thick lines show the Brunt-Väisälä frequency for neutrals (N_n - red dashed lines) and plasma (N_p - black solid line). Note that $N_p/\nu_{in} < 1$ in both atmospheres, but that $N_n/\nu_{ni} < 1$ in the chromosphere while $N_n/\nu_{ni} > 1$ in the I/T.

trals on ions (ν_{ni}) are shown in Figure 3. Clearly, the profile shapes mostly reflect those of the neutral and plasma densities, respectively. A dependence on the thermal speed of the colliding particles introduces variations directly proportional to the square root of the temperature, and inversely proportional to the square root of the average particle mass; the ion-neutral collision frequency therefore is about an order of magnitude higher in the hydrogen-dominated chromosphere than in the nitrogen and oxygen-dominated I/T. The frequency ν_{in} reaches 1 GHz at the base of the ALC7 chromosphere (left) and about 1 MHz at the base of the TIMEGCM D layer at an altitude of about 70 km (right). Therefore the ions respond very strongly to the neutrals at the base of both the chromosphere and ionospheric D-layer and respond well above. In contrast, the neutral-ion collision frequency ν_{ni} is relatively high (~ 1 MHz) at the base of the chromosphere, but is miniscule ($\sim 1 \mu\text{Hz}$) at the base of the D layer; thus, the response of the neutrals to the ions is strong in the chromosphere but extremely weak in the I/T. As a result, it is generally a reasonable approximation to treat the neutral density and wind velocity as given in studies of the lower I/T, while feedback on the neutral gas from the ensuing plasma dynamics is ignored. However this is a poor approximation in Earth's polar regions during geomagnetic storms, where the ions can strongly influence the neutral gas, and it is not well justified in the chromosphere, particularly for disturbances occurring at long scale lengths and low frequencies.

An explicit example of how these considerations apply to important chromospheric and ionospheric phenomena can be found in incompressible motions of the atmospheres. As will be shown by a linear analysis of the multifluid equations in §7 below, the motions are characterized by the Brunt-Väisälä frequency N (Brunt 1927; Väisälä 1925),

$$N^2 \equiv \frac{g}{L}, \quad (1)$$

where g is the gravitational acceleration and L is the local scale height of the particle density, neutral or plasma. If the associated density is stably stratified (i.e., decreasing with height), then the motions are purely oscillatory. If, on the other hand, the density is unstably stratified

(increasing with height), then the motions consist of one exponentially damped and one exponentially growing mode, the Rayleigh-Taylor instability (Rayleigh 1882; Taylor 1950). A glance at Figure 2 indicates that the I/T must be susceptible to Rayleigh-Taylor instability, due to the high altitude peak in the plasma number density, in the F layer. The plasma number density also increases with altitude for a region of the model chromosphere.

Figure 3 shows the Brunt-Väisälä frequencies for the neutral gas and for the plasma, calculated from their density profiles in the ALC7 chromosphere (left) and the TIMEGCM I/T (right). The frequencies for the plasma are similar in magnitude to, but much more variable than, those of the neutral gas. The variability is due to changes in the slopes of the density profiles with height. The frequencies for the neutral gas turn out to be roughly equal in the chromosphere and I/T (between 0.01 and 0.05 Hz). This occurs because the Sun's much stronger gravity is compensated for by the much higher thermal speed of its neutrals: the neutral frequency N_n is essentially the ratio of those quantities, after using the pressure scale height to approximate the neutral-density scale height L_n . In both environments, the frequency N_p set by L_p is smaller than the ion-neutral collision frequency, $N_p/v_{in} < 1$, so that the Brunt-Väisälä oscillations (or Rayleigh-Taylor instabilities) of the plasma are affected by coupling to the neutrals. In the chromosphere, the oscillations and instabilities of the neutrals are similarly affected by coupling to the plasma, since there we have $N_n/v_{ni} < 1$. However, the opposite is true in the I/T, where $N_n/v_{ni} > 1$: the oscillations of the stably stratified neutral gas are unaffected by the plasma, and the neutral motion is essentially undisturbed by the evolution of the unstably stratified plasma. These contrasting consequences of the plasma-neutral coupling will be borne out by the analysis and numerical simulations shown below in §7.

Both the Sun's chromosphere and the Earth's I/T are permeated by magnetic fields. The Lorentz force on charged particles acts in the direction perpendicular to the field, so that when the field is sufficiently strong, the properties of the plasma become highly anisotropic although, as will be shown later, anisotropy also depends on magnetization, the ratio of gyrofrequency to collision frequency, and so also depends on plasma temperatures. Some consequences of this anisotropy will be discussed in subsequent sections of the paper. For the general considerations presented here, we will assume that the magnetic field of the I/T is locally uniform with a field strength of 5.15×10^{-5} T, which is a good approximation as the I/T magnetic field is basically a dipole. Combined with the 1D snapshot taken from the TIMEGCM model described above, this 1D, time-independent model for the I/T is simple but reasonable. The chromosphere's magnetic field, by contrast, has a temporally and spatially varying magnetic field. For example, the magnetic field is known to decay with height, but the field value at the surface is different above quiet Sun regions compared to active regions. To capture some of this variance we adopt the approach of Goodman (2000, 2004) and use a height-dependent 1D magnetic field model:

$$B(z) = B_0 \exp\left(-\frac{z}{2L_T}\right) \quad (2)$$

where $L_T = \frac{k_B T}{m_p g}$ is the local scale height. Furthermore we choose three different values for B_0 : 10, 100, 100 G.

A key parameter governing the coupling of the fluid to the magnetic field is the so-called β , the ratio of the thermal pressure (P) to the magnetic pressure ($B^2/2\mu_0$) appearing in the equations of motion,

$$\beta \equiv \frac{2\mu_0 P}{B^2}, \quad (3)$$

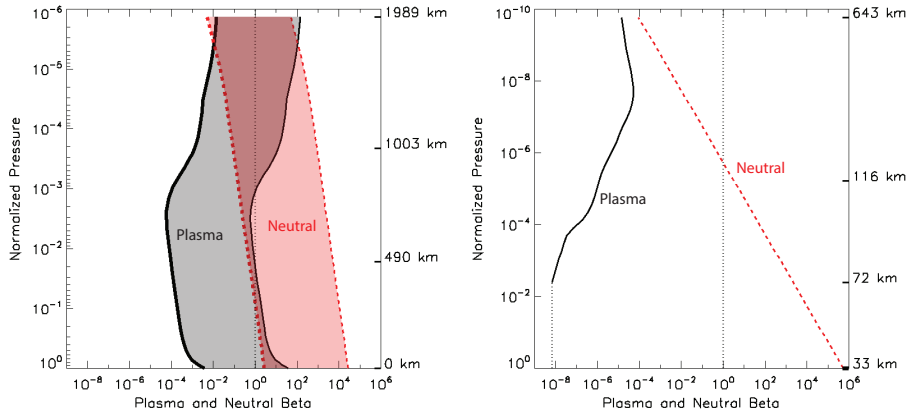


Fig. 4 Neutral (red dashed lines) and plasma (black solid lines) β in the ALC7 chromosphere (left) and the TIMEGCM I/T (right). The I/T magnetic field is assumed to be a single value of 5.15×10^{-5} T. For the chromosphere, a magnetic field height-dependence (Equation 2) is assumed, for a choice of three surface field values B_0 . The lines for the two extreme values of $B_0 = 10$ G (thin line) and $B_0 = 1000$ G (thick line) are shown, with a shaded area between them.

where μ_0 is the magnetic permeability. Values of β derived from both the plasma and neutral pressures are displayed in Figure 4 for the ALC7 chromosphere (left) and the TIMEGCM I/T (right). This dimensionless number measures the relative strength of the pressure and magnetic forces exerted on the fluid. It also measures the local amplification of the ambient magnetic field that can be accomplished by stagnation-point flows that compress the field in the perpendicular direction and evacuate the thermal pressure in the parallel direction. Total pressure balance between the pre- (B_0, P_0) and post-compression ($B = B_0 + \delta B, P = 0$) states implies a fractional amplification of the field strength given by

$$\frac{\delta B}{B_0} = (1 + \beta)^{1/2} - 1. \quad (4)$$

Direct dynamical compression of the field by plasma motions not coupled to the neutrals can occur only up to strengths set by the beta (β_p) associated with the plasma pressure (P_p). For the chromosphere, β_p has an approximate maximum of 100 (Figure 4) and the resulting maximum amplification is ~ 9 , while in the I/T β_p has a maximum of 10^{-4} and so the maximum amplification is $\sim 5 \times 10^{-5}$. In principle, plasma motions strongly coupled by collisions to flows of the neutral gas could compress the field up to strengths set by the beta (β_n) associated with the neutral pressure (P_n). Using maximum values of β_n from Figure 4 of 2×10^4 for the chromosphere and 2×10^5 for the I/T, would allow amplification factors as large as 140 and 450, respectively. However, this process requires the neutral gas to couple sufficiently strongly to the magnetic field to maintain total force balance through the intermediary of fast neutral-ion collisions. This coupling in the I/T is far too weak to maintain such a balance; therefore, such strong terrestrial magnetic-field fluctuations are never observed. The coupling in the chromosphere is much stronger, and likely is responsible for at least some of the much larger magnetic-field fluctuations observed in the lower solar atmosphere. As already noted, the strongest chromospheric magnetic fields originate above sunspots, which form in the higher-pressure photosphere and convection zone below the

chromosphere. Typical neutral (and plasma) flows can range from km/s in convective cells to as large as 1000 km/s in chromospheric jets. In the lower I/T typical neutral flows are 100 m/s, but at higher latitudes during storms these can increase to 500 m/s.

2.3 Summary

The basic atmospheric profiles, and quantities derived from them, that have been discussed in this section clearly show both quantitative similarities and differences between the solar chromosphere and the terrestrial I/T. The neutral number densities, neutral beta, ion-neutral collision frequencies and Brunt-Väisälä frequencies of both neutrals and plasma track reasonably closely over the common range of normalized pressures in the two atmospheres. On the other hand, the plasma number densities, plasma beta, and neutral-ion collision frequencies are very different, due to the much higher ionization fraction on the Sun vs. the Earth. The plasma is driven strongly by the neutral gas in both atmospheres, as a result, while the neutrals are driven by the ions fairly strongly in the chromosphere but relatively weakly in the I/T. Relative magnetic field fluctuations of order unity are ubiquitous on the Sun, but the fluctuations are far smaller in magnitude on the Earth. Both atmospheres exhibit regions of instability driven by a combination of gravity and convection where upward-increasing particle number densities occur, modulated by the frequency of collisions between the ions and neutrals. In the remainder of the paper, further implications of this rich combination of similarities and differences between the Sun's chromosphere and Earth's I/T will be elucidated.

3 Governing Equations

In the partially ionized, collisional mixture of the Sun's chromosphere and Earth's I/T, each species can be treated as a fluid, i.e. each species is collision dominated. There are phenomena where particle distribution functions that deviate from Maxwellian are important, such as during flares in the chromosphere and auroras in the ionosphere, but we consider only here the fluid description of the chromosphere and I/T.

Even though the species are collision dominated, for transient or high frequency (i.e., larger than the collision frequency between species) phenomena the coupling of the individual species to each other by collisions may not be sufficient to allow a description which disregards the difference in the inertial terms in the momentum equation for each species. We define such a description here as a single-fluid model. Here we present a multi-fluid model adopted for both the chromosphere and I/T. Multi-fluid here refers to a model which solves the continuity, momentum and energy equation for all three components, ions, electrons and neutrals. However, we subsequently combine the ion and electron equations to create a two-fluid model which solves the continuity, momentum and energy equation for the neutral fluid and the ionized fluid (electron-ion drift is captured by the Hall term in the generalized Ohm's law). This model is especially relevant when magnetic fields are present, as they directly affect the ionized component of the mixture but not the neutral component. The details of the model's application in the chromosphere can be found in Meier and Shumlak (2012), Leake et al. (2012), and Leake et al. (2013), where it is shown that the ionized and neutral fluids can decouple as current sheets form and thin in the chromosphere, and hence a multi-fluid model is vital. There are occurrences other than magnetic reconnection sites when multi-fluid models are required. Examples include when high frequency waves

from flares propagate down into the chromosphere (e.g., Voitenko and Goossens 2002; Kigure et al. 2010; Edmondson et al. 2011; Russell and Fletcher 2013), and when waves interact non-linearly to create flows and currents on smaller and smaller scales (see review by Narain and Ulmschneider 1990). Due to a low ionization level in the I/T compared to the chromosphere, neutral-ion collisions can be much less frequent than in the chromosphere, and phenomena that occur on timescales of minutes require a multi-fluid model (Roble et al. 1988; Richmond et al. 1992; Roble and Ridley 1994; Fuller-Rowell et al. 1996; Millward et al. 1996).

In the multi-fluid model, the three fluids, ions (i), electrons (e), and neutrals (n), can undergo recombination and ionization interactions. The ions are assumed to be singly ionized which is a good approximation for the dominant species in both atmospheres. The rate of loss of ions/electrons (or gain of neutrals) due to recombination is Γ^{rec} , and the rate of gain of ions/electrons (or loss of neutrals) due to ionization is Γ^{ion} .

3.1 Continuity

Assuming charge quasi-neutrality ($n_i = n_e = n$, where n_α is the number density of species α), the ion, electron, and neutral continuity equations are:

$$\frac{\partial n}{\partial t} + \nabla \cdot (n\mathbf{V}_i) = \Gamma^{ion} - \Gamma^{rec}, \quad (5)$$

$$\frac{\partial n}{\partial t} + \nabla \cdot (n\mathbf{V}_e) = \Gamma^{ion} - \Gamma^{rec}, \quad (6)$$

$$\frac{\partial n_n}{\partial t} + \nabla \cdot (n_n\mathbf{V}_n) = -\Gamma^{ion} + \Gamma^{rec}. \quad (7)$$

Subtracting Equation (6) from (5) then yields

$$\nabla \cdot (n[\mathbf{V}_i - \mathbf{V}_e]) = 0, \quad (8)$$

which is simply a statement of current conservation (see also Equation 22 below) in a quasi-neutral plasma.

3.2 Momentum

The ion, electron and neutral momentum equations are shown below:

$$\begin{aligned} \frac{\partial}{\partial t}(m_i n \mathbf{V}_i) + \nabla \cdot (m_i n \mathbf{V}_i \mathbf{V}_i + \mathbb{P}_i) &= en(\mathbf{E} + \mathbf{V}_i \times \mathbf{B}) + m_i n \mathbf{g} + \mathbf{R}_i^{ie} + \mathbf{R}_i^{in} \\ &+ \Gamma^{ion} m_i \mathbf{V}_n - \Gamma^{rec} m_i \mathbf{V}_i, \end{aligned} \quad (9)$$

$$\begin{aligned} \frac{\partial}{\partial t}(m_e n \mathbf{V}_e) + \nabla \cdot (m_e n \mathbf{V}_e \mathbf{V}_e + \mathbb{P}_e) &= -en(\mathbf{E} + \mathbf{V}_e \times \mathbf{B}) + m_e n \mathbf{g} + \mathbf{R}_e^{ei} + \mathbf{R}_e^{en} \\ &+ \Gamma^{ion} m_e \mathbf{V}_n - \Gamma^{rec} m_e \mathbf{V}_e, \end{aligned} \quad (10)$$

$$\begin{aligned} \frac{\partial}{\partial t}(m_n n_n \mathbf{V}_n) + \nabla \cdot (m_n n_n \mathbf{V}_n \mathbf{V}_n + \mathbb{P}_n) &= m_n n_n \mathbf{g} + \mathbf{R}_n^{ne} + \mathbf{R}_n^{ni} \\ &- \Gamma^{ion} m_i \mathbf{V}_n + \Gamma^{rec} (m_i \mathbf{V}_i + m_e \mathbf{V}_e). \end{aligned} \quad (11)$$

The velocity and mass of species α are denoted \mathbf{V}_α and m_α , respectively. The electric and magnetic field are denoted \mathbf{E} and \mathbf{B} , respectively. The pressure tensor is $\mathbb{P}_\alpha = P_\alpha \mathbb{I} + \boldsymbol{\pi}_\alpha$ where P_α is the scalar pressure and $\boldsymbol{\pi}_\alpha$ is the viscous stress tensor. For the neutral fluid this is isotropic, but for electrons and ions this has elements that are functions of the particle magnetization (the magnetization is the ratio of the gyrofrequency to the collision frequency), and is anisotropic. The reader can find derivations of these viscous stress tensors in Braginskii (1965). The Coriolis force has been omitted for simplicity in further derivations, although its effects can be important in the I/T (e.g., Fuller-Rowell et al. 1984). On the Sun, only long time-scale phenomena are affected by this force, for example, the rotation of sunspot groups and the large-scale solar dynamo. The transfer of momentum to species α due to a combination of identity-preserving collisions and charge-exchange collisions with species β is given by

$$\mathbf{R}_\alpha^{\alpha\beta} \equiv m_{\alpha\beta} n_\alpha \nu_{\alpha\beta} (\mathbf{V}_\beta - \mathbf{V}_\alpha), \quad (12)$$

where $m_{\alpha\beta} = m_\alpha m_\beta / (m_\alpha + m_\beta)$ and $\mathbf{R}_\alpha^{\alpha\beta} = -\mathbf{R}_\beta^{\beta\alpha}$. The relative importance of charge-exchange collisions and identity-preserving collisions varies in the solar atmosphere and the I/T, but for the purposes of a comparison of the two plasma environments we combine the two types of collisions into one general “interaction”. The collision frequency $\nu_{\alpha\beta}$ is then defined using a solid body approximation with a relevant choice of cross-section (e.g., Leake et al. 2013). The above equations are for a single “average” species of ions of mass m_i and neutrals of mass m_n .

3.3 Energy

The full derivation of the energy equations for all three components can be found in Meier and Shumlak (2012). The equation for the rate of change of the thermal plus kinetic energy $\varepsilon_\alpha = \rho_\alpha V_\alpha^2/2 + P_\alpha/(\gamma_\alpha - 1)$ of species α , neglecting ionization and recombination, is

$$\frac{\partial \varepsilon_\alpha}{\partial t} + \nabla \cdot (\varepsilon_\alpha \mathbf{V}_\alpha + \mathbf{V}_\alpha \cdot \mathbb{P}_\alpha + \mathbf{h}_\alpha) = \mathbf{V}_\alpha \cdot \left(q_\alpha n_\alpha \mathbf{E} + \sum_{\beta \neq \alpha} \mathbf{R}_\alpha^{\alpha\beta} + m_\alpha n_\alpha \mathbf{g} \right) + \sum_{\beta \neq \alpha} Q_\alpha^{\alpha\beta} + S_\alpha + U_\alpha \quad (13)$$

where $\rho_\alpha = m_\alpha n_\alpha$, γ_α is the ratio of specific heats, q_α is the charge,

$$Q_\alpha^{\alpha\beta} = \frac{1}{2} \mathbf{R}_\alpha^{\alpha\beta} \cdot (\mathbf{V}_\beta - \mathbf{V}_\alpha) + 3 \frac{m_{\alpha\beta}}{m_\alpha} n_\alpha \nu_{\alpha\beta} k_B (T_\beta - T_\alpha) \quad (14)$$

is the heating of species α due to collisions with species β , T_α is the temperature of the fluid, S_α and U_α are radiative and chemical process contributions, respectively, and \mathbf{h}_α is the heat flux. This heat flux involves a thermal conductivity tensor that depends on the magnetization of the species, see Braginskii (1965).

3.4 Maxwell’s Equations

The equations relating changes in the electric and magnetic field are

$$\nabla \times \mathbf{E} = -\frac{\partial \mathbf{B}}{\partial t}, \quad (15)$$

$$\nabla \times \mathbf{B} = \varepsilon_0 \mu_0 \frac{\partial \mathbf{E}}{\partial t} + \mu_0 \mathbf{J}, \quad (16)$$

$$\nabla \cdot \mathbf{B} = 0, \quad (17)$$

$$\nabla \cdot \mathbf{E} = \sigma / \epsilon_0. \quad (18)$$

Here σ is the charge density, ϵ_0 is the permittivity, and μ_0 is the permeability. The second of these Maxwell equations can be written as an equation for \mathbf{J} :

$$\mathbf{J} = \frac{\nabla \times \mathbf{B}}{\mu_0} - \epsilon_0 \frac{\partial \mathbf{E}}{\partial t}, \quad (19)$$

the second term being the displacement current. Taking the ratio of the magnitude of the two terms on the right-hand side gives

$$\frac{|\frac{\nabla \times \mathbf{B}}{\mu_0}|}{|\epsilon_0 \frac{\partial \mathbf{E}}{\partial t}|} \sim \frac{B_0 t_0}{L_0 \mu_0 \epsilon_0 E_0} \sim \frac{t_0^2 c^2}{L_0^2} \quad (20)$$

where $c = (\mu_0 \epsilon_0)^{-1/2}$ is the speed of light, subscripts “0” indicate representative values for each variable, and $B_0/t_0 \sim E_0/L_0$ is used from the first Maxwell equation (15). From Equation (20), the displacement current can be ignored in the equation for \mathbf{J} if the system time scale t_0 is longer than the time it takes light to travel across the system L_0/c . This is a reasonable assumption in the Sun and the Earth’s atmospheres, and leaves the equation for \mathbf{J} in the static form of Ampère’s law:

$$\mathbf{J} = \frac{\nabla \times \mathbf{B}}{\mu_0}. \quad (21)$$

For reasons discussed in detail later, in ionospheric literature, the current conservation equation

$$\nabla \cdot \mathbf{J} = 0 \quad (22)$$

is used, rather than Equation (21), with the \mathbf{B} field represented as a conservative field. We note that Equation (22) follows immediately from Equation (21) and the identity $\nabla \cdot (\nabla \times \mathbf{B}) = 0$, and is equivalent to Equation (8). In cases where the characteristic time scale of variation is long compared to the Alfvén wave travel time (Vasyliūnas 2012), one can assume that $\partial \mathbf{B} / \partial t \approx 0$, $\nabla \times \mathbf{E} = 0$, and the electric field can be written as the gradient of a scalar, $\mathbf{E} = -\nabla \Phi$.

3.5 Ohm’s Law

The generalized Ohm’s law can be interpreted as an equation for the temporal evolution of the current density $\partial \mathbf{J} / \partial t$. Thus, along with the momentum equations and Maxwell’s equations the system equations contain time derivatives for all four variables \mathbf{B} , \mathbf{V} , \mathbf{E} , and \mathbf{J} . As will be shown in this section, under certain assumptions (e.g. low-frequency or long timescale), we can ignore $\partial \mathbf{J} / \partial t$ and rewrite the Ohm’s law as a linear equation which relates the current density \mathbf{J} to the electric field \mathbf{E}^* in a specific rest frame using either the conductivity $\underline{\underline{\sigma}}$ or resistivity $\underline{\underline{\eta}}$ tensor. The time derivative $\partial \mathbf{E} / \partial t$ can also be dropped for timescales longer than the light crossing time of the system (see above). This leaves just the time derivatives for \mathbf{B} and \mathbf{V} (we will discuss this MHD approach in the following two sections). Ionospheric physicists prefer the use of the conductivity formulation $\mathbf{J} = \underline{\underline{\sigma}} \cdot \mathbf{E}^*$, since electric fields can persist due to the generally low conductivity of the plasma, while solar physicists generally use the resistivity formulation $\mathbf{E}^* = \underline{\underline{\eta}} \cdot \mathbf{J}$.

Below is a derivation of the generalized Ohm's law, valid for both the chromosphere and I/T. Firstly, we neglect the ionization and recombination terms in the three momentum equations (9-11). The generalized Ohm's law can be obtained by taking the momentum equation for each species α (9-11), multiplying by the charge to mass ratio q_α/m_α ($q_i = e = -q_e$ and $q_n = 0$), and summing over all species. Using the definition of $\mathbf{R}_\alpha^{\alpha\beta}$ in Equation (12), and the fact that for our singly ionized ion model $m_n = m_i + m_e$ so that $m_{in} \approx m_i/2$, $m_{ei} = m_{en} \approx m_e$, gives

$$\begin{aligned} \frac{\partial \mathbf{J}}{\partial t} = \frac{\partial(en\mathbf{V}_i - en\mathbf{V}_e)}{\partial t} = & \frac{ne^2}{m_e} \left(\mathbf{E} + \mathbf{V}_e \times \mathbf{B} + \frac{m_e}{m_i} \frac{\mathbf{j} \times \mathbf{B}}{en} \right) + e \left(\frac{\nabla \cdot \boldsymbol{\kappa}_e}{m_e} - \frac{\nabla \cdot \boldsymbol{\kappa}_i}{m_i} \right) \\ & - (\mathbf{v}_{ei} + \mathbf{v}_{en})\mathbf{J} + en \left(\mathbf{v}_{en} - \frac{\mathbf{v}_{in}}{2} \right) \mathbf{W}. \end{aligned} \quad (23)$$

where we have neglected terms of order $1/m_i$ relative to terms of order $1/m_e$. The tensor $\boldsymbol{\kappa}_\alpha \equiv \mathbb{P}_\alpha + \rho_\alpha \mathbf{V}_\alpha \mathbf{V}_\alpha$. We call Equation (23) the generalized Ohm's law, as it is derived from the momentum equations with minimal assumptions. In solar physics, the term "generalized Ohm's law" is often used to describe a linear relationship between the electric field and current density which includes more than just anisotropic resistivity. For example, fluid models which include Hall or Pedersen currents may all contain a "generalized Ohm's law". In this paper, the term applies only to Equation (23) and any algebraic manipulations of it. When certain assumptions and simplifications are made to Equation (23), we just refer to the result as "Ohm's law".

In ionospheric applications (e.g., Vasyliūnas 2012) Equation (23) can be recast so that the velocities on the right hand side are the plasma velocity \mathbf{V}_p , defined by

$$\mathbf{V}_p \equiv \frac{(m_i \mathbf{V}_i + m_e \mathbf{V}_e)}{(m_i + m_e)} \approx \mathbf{V}_i + \frac{m_e}{m_i} \mathbf{V}_e \approx \mathbf{V}_i - \frac{m_e}{m_i} \frac{\mathbf{J}}{en} \approx \mathbf{V}_e + \frac{\mathbf{J}}{en}. \quad (24)$$

where the approximations use $m_e \ll m_i$. Some simple algebra shows that Equation (23) is equivalent to

$$\begin{aligned} \frac{\partial \mathbf{J}}{\partial t} = \frac{ne^2}{m_e} \left(\mathbf{E} + \mathbf{V}_p \times \mathbf{B} + \frac{\mathbf{j} \times \mathbf{B}}{en} \right) + e \left(\frac{\nabla \cdot \boldsymbol{\kappa}_e}{m_e} - \frac{\nabla \cdot \boldsymbol{\kappa}_i}{m_i} \right) \\ - (\mathbf{v}_{ei} + \mathbf{v}_{en} + \frac{m_e}{m_i} \frac{\mathbf{v}_{in}}{2})\mathbf{J} + en \left(\mathbf{v}_{en} - \frac{\mathbf{v}_{in}}{2} \right) (\mathbf{V}_p - \mathbf{V}_n) \end{aligned} \quad (25)$$

which is equivalent to the generalized Ohm's law presented in Vasyliūnas (2012), Equation (12), for a quasi-neutral plasma ($n_i = n_e$), though in that work the factor 1/2 is dropped from the \mathbf{v}_{in} terms.

It is worth deriving some initial quantities relevant to the electrodynamics at this point. The following magnetizations (the gyrofrequencies $\Omega_\alpha \equiv eB/m_\alpha$ divided by the collision frequencies $\nu_{\alpha\beta}$):

$$k_{in} = \frac{eB}{\frac{m_i}{2} \nu_{in}}, \quad (26)$$

$$k_{en} = \frac{eB}{m_e \nu_{en}}, \quad (27)$$

$$k_{ei} = \frac{eB}{m_e \nu_{ei}}, \quad (28)$$

$$\frac{1}{k_e} \equiv \frac{1}{k_{en}} + \frac{1}{k_{ei}}, \quad (29)$$

are measures of the ability of the ions and electrons to freely gyrate around the magnetic field. For example, if $k_e > 1$, then the gyration of the electrons around the magnetic field is largely unaffected by collisions with ions and neutrals. When $k_e < 1$, then the collisions decouple the electron from the field. The same situation applies to the ions. Note that ion-electron collisions hardly affect the gyration of the ions, so k_i , defined in the same way as k_e , is approximately k_{in} , and from hereon, we use k_{in} instead of k_i .

Multiplying Equation (23) by $\frac{m_e}{e^2 n}$, using the definitions of magnetizations above, noting that $k_{in}/k_{en} \sim \sqrt{m_e/m_i} \ll 1$, and neglecting terms of order $\sqrt{m_e/m_i}$ relative to terms of order 1, we obtain

$$\begin{aligned} \mathbf{E} + (\mathbf{V}_e \times \mathbf{B}) &= \left[\frac{1}{k_{ei}} + \frac{1}{k_{en}} \right] \frac{B}{en} \mathbf{J} - \frac{m_e B}{m_i en} \mathbf{J} \times \hat{\mathbf{b}} \\ &\quad - \frac{B}{k_{en}} \mathbf{W} - \frac{1}{en} \left(\nabla \cdot \boldsymbol{\kappa}_e - \frac{m_e}{m_i} \nabla \cdot \boldsymbol{\kappa}_i \right) + \frac{m_e}{e^2 n} \frac{\partial \mathbf{J}}{\partial t}. \end{aligned} \quad (30)$$

Later on we shall see how certain assumptions allow us to drop the term proportional to $\partial \mathbf{J} / \partial t$ to derive a low-frequency Ohm's law. This relates the electric field in a certain rest frame to the current density. Note that Equation (30) contains the electric field in the rest frame of the electrons $\mathbf{E} + (\mathbf{v}_e \times \mathbf{B})$. As we shall see later on in this section, there are other choices of rest frame which affect the interpretation of different terms in the equation.

To close the system of equations, an equation is needed for the difference between the ion and neutral velocities, $\mathbf{W} = \mathbf{V}_i - \mathbf{V}_n$. This is obtained by taking the sum of the ion and electron momentum equations (9+10) divided by the plasma density $m_i n$, and subtracting the neutral momentum equation (11) divided by the neutral density $m_i n_n$, again neglecting the ionization and recombination terms. This results in an equation for $d_i \mathbf{V}_i / dt - d_n \mathbf{V}_n / dt$, where $d_\alpha / dt = \partial / \partial t + \mathbf{V}_\alpha \cdot \nabla$ is the total Lagrangian derivative for a fluid of species α . This equation can be rearranged to express \mathbf{W} as:

$$\mathbf{W} = \frac{k_{in}}{k_{en} + k_{in}} \left\{ \frac{\mathbf{J}}{en} + k_{en} \left[\frac{\xi_n \mathbf{J} \times \hat{\mathbf{b}}}{en} + \frac{\xi_i \nabla \cdot \mathbb{P}_n}{eBn} - \frac{\xi_n \nabla \cdot \mathbb{P}_p}{eBn} - \frac{\xi_n m_i}{eB} \frac{d^* \mathbf{W}}{dt} \right] \right\} \quad (31)$$

where $\mathbb{P}_p = \mathbb{P}_e + \mathbb{P}_i$ and $d^* \mathbf{W} / dt \equiv \left(\frac{d_i \mathbf{V}_i}{dt} - \frac{d_n \mathbf{V}_n}{dt} \right)$. Using this equation for \mathbf{W} in Equation (30) yields {

$$\begin{aligned} \mathbf{E} + (\mathbf{V}_e \times \mathbf{B}) &= \left[\frac{1}{k_{ei}} + \frac{1}{k_{en} + k_{in}} \right] \frac{B}{en} \mathbf{J} - \left[\frac{\xi_n k_{in}}{k_{en} + k_{in}} \right] \frac{B}{en} \mathbf{J} \times \hat{\mathbf{b}} + \frac{m_e}{e^2 n} \frac{\partial \mathbf{J}}{\partial t} \\ &\quad + \frac{k_{in}}{k_{en} + k_{in}} \left(\frac{\xi_n \nabla \cdot \mathbb{P}_p - \xi_i \nabla \cdot \mathbb{P}_n}{en} \right) - \frac{1}{en} \left(\nabla \cdot \boldsymbol{\kappa}_e - \frac{m_e}{m_i} \nabla \cdot \boldsymbol{\kappa}_i \right) + \frac{\xi_n k_{in}}{k_{en} + k_{in}} \frac{m_i}{e} \frac{d^* \mathbf{W}}{dt} \end{aligned} \quad (32)$$

This is the generalized Ohm's law in the rest frame of the electrons. The first term that multiplies \mathbf{J} on the RHS is conventionally called the Ohmic resistivity. It describes the collisions of electrons and ions which act to dissipate electric current. By substituting the equation for \mathbf{W} (31) into the generalized Ohm's law, we introduced the effect of ion-neutral collisions into the Ohmic resistivity, this is because \mathbf{W} is linearly related to \mathbf{J} (for low frequency phenomena). Whereas in Equation (30), the term in front of \mathbf{J} only included electron collisions, now the Ohmic resistivity contains two terms. The first $1/k_{ei} \sim v_{ei}$ describes direct collisions of electrons and ions. The second $1/(k_{en} + k_{in}) \sim v_{en} v_{in} / (v_{en} + v_{in})$ describes

the combined effect of electron-neutral collisions (k_{en}) and ion-neutral (k_{in}) collisions. As the neutral density goes to zero, k_{en} and k_{in} tend to infinity and so the Ohmic resistivity becomes just direct electron-ion collisions.

The generalized Ohm's law can be recast in the rest frame of the plasma using $\mathbf{V}_e \approx \mathbf{V}_p - \mathbf{J}/en$:

$$\begin{aligned} \mathbf{E}^p \equiv \mathbf{E} + (\mathbf{V}_p \times \mathbf{B}) &\approx \left[\frac{1}{k_{ei}} + \frac{1}{k_{en} + k_{in}} \right] \frac{B}{en} \mathbf{J} + \left[1 - \frac{\xi_n k_{in}}{k_{en} + k_{in}} \right] \frac{B}{en} \mathbf{J} \times \hat{\mathbf{b}} + \frac{m_e}{e^2 n} \frac{\partial \mathbf{J}}{\partial t} \\ &+ \frac{k_{in}}{k_{en} + k_{in}} \left(\frac{\xi_n \nabla \cdot \mathbb{P}_p - \xi_i \nabla \cdot \mathbb{P}_n}{en} \right) - \frac{1}{en} \left(\nabla \cdot \boldsymbol{\kappa}_e - \frac{m_e}{m_i} \nabla \cdot \boldsymbol{\kappa}_i \right) + \frac{\xi_n k_{in}}{k_{en} + k_{in}} \frac{m_i}{e} \frac{d^* \mathbf{W}}{dt} \end{aligned} \quad (33)$$

The rest frame of the plasma generally is not the best choice for a frame of reference in a weakly ionized mixture. In the I/T, where the neutral fraction is so much greater than the ion fraction, the neutral rest frame is more commonly used. A discussion on the choice of rest frame and its consequences for the discussion of frictional heating is given in §6.2. Using

$$\mathbf{V}_n = \mathbf{V}_i - \mathbf{W} \approx \mathbf{V}_p + \frac{m_e}{m_i} \frac{\mathbf{J}}{en} - \mathbf{W} \quad (34)$$

and noting that when we substitute this into Equation (33), the resulting $\frac{m_e}{m_i} \frac{\mathbf{J} \times \hat{\mathbf{b}}}{en}$ can be neglected relative to $\frac{\mathbf{J} \times \hat{\mathbf{b}}}{en}$, gives

$$\begin{aligned} \mathbf{E}^* \equiv \mathbf{E} + (\mathbf{V}_n \times \mathbf{B}) &\approx \mathbf{E} + (\mathbf{V}_p \times \mathbf{B}) + \frac{m_e}{m_i} \frac{(\mathbf{J} \times \mathbf{B})}{en} - (\mathbf{W} \times \mathbf{B}) \\ &= \left[\frac{1}{k_{ei}} + \frac{1}{k_{en} + k_{in}} \right] \frac{B}{en} \mathbf{J} + \left[\frac{k_{en}}{k_{en} + k_{in}} - \frac{\xi_n k_{in}}{k_{en} + k_{in}} \right] \frac{B}{en} \mathbf{J} \times \hat{\mathbf{b}} + \frac{m_e}{e^2 n} \frac{\partial \mathbf{J}}{\partial t} \\ &- \frac{B}{en} \left[\frac{\xi_n k_{en} k_{in}}{k_{en} + k_{in}} \right] (\mathbf{J} \times \hat{\mathbf{b}}) \times \hat{\mathbf{b}} - \frac{1}{en} \left(\nabla \cdot \boldsymbol{\kappa}_e - \frac{m_e}{m_i} \nabla \cdot \boldsymbol{\kappa}_i \right) \\ &+ \frac{k_{in}}{k_{en} + k_{in}} \left(\frac{\xi_n \nabla \cdot \mathbb{P}_p - \xi_i \nabla \cdot \mathbb{P}_n}{en} \right) + \frac{\xi_n k_{in}}{k_{en} + k_{in}} \frac{m_i}{e} \frac{d\mathbf{W}}{dt} \\ &+ \frac{k_{en} k_{in}}{k_{en} + k_{in}} \frac{(\xi_n \nabla \cdot \mathbb{P}_p \times \hat{\mathbf{b}} - \xi_i \nabla \cdot \mathbb{P}_n \times \hat{\mathbf{b}})}{en} + \frac{\xi_n k_{en} k_{in}}{k_{en} + k_{in}} \frac{m_i}{e} \left(\frac{d^* \mathbf{W}}{dt} \right) \times \hat{\mathbf{b}}. \end{aligned} \quad (35)$$

We note that when $\xi_n \rightarrow 0$, the fully ionized generalized Ohm's law is recovered.

In the chromosphere, where the ion fraction can become comparable to the neutral fraction as the plasma is heated up to 10000 K, the center of mass frame is often used (see Mitchner and Kruger 1967). The center of mass velocity is defined by

$$\mathbf{V}_{CM} \equiv \xi_i \mathbf{V}_i + \xi_n \mathbf{V}_n = \mathbf{V}_i - \xi_n \mathbf{W} \approx \mathbf{V}_p + \frac{m_e}{m_i} \frac{\mathbf{J}}{en} - \xi_n \mathbf{W}. \quad (36)$$

Again, noting that when we substitute this into Equation (33), the resulting $\frac{m_e}{m_i} \frac{\mathbf{J} \times \hat{\mathbf{b}}}{en}$ can be neglected relative to $\frac{\mathbf{J} \times \hat{\mathbf{b}}}{en}$ gives

$$\begin{aligned} \mathbf{E}^{CM} \equiv \mathbf{E} + (\mathbf{V}_{CM} \times \mathbf{B}) &\approx \mathbf{E} + (\mathbf{V}_p \times \mathbf{B}) + \frac{m_e}{m_i} \frac{(\mathbf{J} \times \mathbf{B})}{en} - \xi_n (\mathbf{W} \times \mathbf{B}) \\ &= \left[\frac{1}{k_{ei}} + \frac{1}{k_{en} + k_{in}} \right] \frac{B}{en} \mathbf{J} + \left[1 - \frac{2\xi_n k_{in}}{k_{en} + k_{in}} \right] \frac{B}{en} \mathbf{J} \times \hat{\mathbf{b}} + \frac{m_e}{e^2 n} \frac{\partial \mathbf{J}}{\partial t} \end{aligned}$$

$$\begin{aligned}
& - \frac{B}{en} \left[\frac{\xi_n^2 k_{en} k_{in}}{k_{en} + k_{in}} \right] (\mathbf{J} \times \hat{\mathbf{b}}) \times \hat{\mathbf{b}} - \frac{1}{en} \left(\nabla \cdot \boldsymbol{\kappa}_e - \frac{m_e}{m_i} \nabla \cdot \boldsymbol{\kappa}_i \right) \\
& + \frac{k_{in}}{k_{en} + k_{in}} \left(\frac{\xi_n \nabla \cdot \mathbb{P}_p - \xi_i \nabla \cdot \mathbb{P}_n}{en} \right) + \frac{\xi_n k_{in}}{k_{en} + k_{in}} \frac{m_i}{e} \frac{d\mathbf{W}}{dt} \\
& + \frac{\xi_n k_{en} k_{in}}{k_{en} + k_{in}} \frac{(\xi_n \nabla \cdot \mathbb{P}_p \times \hat{\mathbf{b}} - \xi_i \nabla \cdot \mathbb{P}_n \times \hat{\mathbf{b}})}{en} + \frac{\xi_n^2 k_{en} k_{in}}{k_{en} + k_{in}} \frac{m_i}{e} \left(\frac{d^* \mathbf{W}}{dt} \right) \times \hat{\mathbf{b}}. \quad (37)
\end{aligned}$$

It is important to note the difference between the generalized Ohm's law for the center of mass frame (37) and the generalized Ohm's law for the neutral frame (35). The pre-factor in front of the $(\mathbf{J} \times \hat{\mathbf{b}}) \times \hat{\mathbf{b}}$ term, which will be discussed later in terms of the Pedersen conductivity or Pedersen resistivity, contains ξ_n for the neutral frame equation and a ξ_n^2 for the center of mass equation, which is purely a result of the choice of frame. To allow for a collaborative discussion of the chromosphere and I/T in the context of the generalized Ohm's law, we will use the neutral frame equation (35) from hereon, but will refer to other frames where necessary. As will be seen in §6.2, changing the reference frame leads to different terms appearing in the thermal energy equations for the species' temperatures, but cannot change the final values for these temperatures which determine the ionization fraction.

3.5.1 Low Frequency Approximation to the Ohm's Law

As stated above, the generalized Ohm's law (35) can be simplified to a linear equation relating \mathbf{E} and \mathbf{J} , under certain assumptions. Let us look at the competing terms in Equation (35), but first define the following resistivities:

$$\eta_{\parallel} \equiv \frac{B}{en} \left[\frac{1}{k_{ei}} + \frac{1}{k_{en} + k_{in}} \right], \quad (38)$$

$$\eta_C \equiv \frac{B}{en} \left[\frac{\xi_n k_{en} k_{in}}{k_{en} + k_{in}} \right], \quad (39)$$

$$\eta_P \equiv \eta_{\parallel} + \eta_C, \quad (40)$$

$$\eta_H \equiv \frac{B}{en} \left[\frac{k_{en} - \xi_n k_{in}}{k_{en} + k_{in}} \right], \quad (41)$$

then Equation (35) becomes

$$\begin{aligned}
\mathbf{E}^* &= \mathbf{E} + \mathbf{V}_n \times \mathbf{B} = \eta_{\parallel} \mathbf{J} + \eta_H \mathbf{J} \times \hat{\mathbf{b}} - \eta_C (\mathbf{J} \times \hat{\mathbf{b}}) \times \hat{\mathbf{b}} \\
& + \frac{m_e}{e^2 n} \frac{\partial \mathbf{J}}{\partial t} + \frac{\xi_n k_{in}}{k_{en} + k_{in}} \frac{m_i}{e} \frac{d^* \mathbf{W}}{dt} + \frac{\xi_n k_{en} k_{in}}{k_{en} + k_{in}} \frac{m_i}{e} \left(\frac{d^* \mathbf{W}}{dt} \right) \times \hat{\mathbf{b}} - \frac{1}{en} \left(\nabla \cdot \boldsymbol{\kappa}_e - \frac{m_e}{m_i} \nabla \cdot \boldsymbol{\kappa}_i \right) \\
& + \frac{k_{in}}{k_{en} + k_{in}} \left(\frac{\xi_n \nabla \cdot \mathbb{P}_p - \xi_i \nabla \cdot \mathbb{P}_n}{en} \right) + \frac{k_{en} k_{in}}{k_{en} + k_{in}} \frac{(\xi_n \nabla \cdot \mathbb{P}_p \times \hat{\mathbf{b}} - \xi_i \nabla \cdot \mathbb{P}_n \times \hat{\mathbf{b}})}{en}. \quad (42)
\end{aligned}$$

We can non-dimensionalize this equation by expressing each variable A as $A = A_0 \tilde{A}$ where \tilde{A} has no dimensions. The dimensional constants A_0 are related to each other. For example, if L_0 is the system length, B_0 is the system magnetic field strength, and n_0 is the system number density of plasma, then $v_0 = B_0 / \sqrt{(\mu_0 m_i n_0)}$ is the system velocity, $J_0 = B_0 / \mu_0 L_0$ is the system current density, and $f_0 = v_0 / L_0$ is the system frequency (or inverse time scale). We can then remove the dimensions from Equation (42) by dividing it by $v_0 B_0$. Using the

following definitions of Lundquist number (S), ion inertial scale length (d_i), ion plasma frequency ($\omega_{p,i}$), electron inertial scale length (d_e), and electron plasma frequency ($\omega_{p,e}$):

$$S = \frac{\mu_0 L_0 v_0}{\eta_{\parallel}}, \quad d_i = \frac{c}{\omega_{p,i}}, \quad \omega_{p,i}^2 = \frac{e^2 n_0}{m_i \epsilon_0}, \quad d_e = \frac{c}{\omega_{p,e}}, \quad \omega_{p,e}^2 = \frac{e^2 n_0}{m_e \epsilon_0} \quad (43)$$

yields the dimensionless equation

$$\begin{aligned} \tilde{\mathbf{E}} + (\tilde{\mathbf{V}}_n \times \tilde{\mathbf{B}}) &= \frac{1}{S} \tilde{\mathbf{J}} + \frac{d_i}{L_0} \tilde{\mathbf{J}} \times \hat{\mathbf{b}} - \frac{1}{S} \frac{\eta_C}{\eta_{\parallel}} (\tilde{\mathbf{J}} \times \hat{\mathbf{b}}) \times \hat{\mathbf{b}} \\ &+ \left(\frac{d_e}{L_0} \right)^2 \frac{\partial \tilde{\mathbf{J}}}{\partial \tilde{t}} + \frac{\xi_n k_{in}}{k_{en} + k_{in}} \frac{f_0}{\Omega_i} \frac{f_0}{v_{in}} \left[\frac{d^* \tilde{\mathbf{W}}}{d\tilde{t}} + k_{en} \frac{d^* \tilde{\mathbf{W}}}{d\tilde{t}} \times \hat{\mathbf{b}} \right] - \frac{d_i}{L_0} \left(\beta_e \tilde{\mathbf{V}} \cdot \tilde{\boldsymbol{\kappa}}_e - \beta_i \frac{m_e}{m_i} \tilde{\mathbf{V}} \cdot \tilde{\boldsymbol{\kappa}}_i \right) \\ &+ \frac{k_{in}}{k_{en} + k_{in}} \frac{d_i}{L_0} \left[(\xi_n \beta_p \tilde{\mathbf{V}} \cdot \tilde{\mathbb{P}}_p - \xi_i \beta_n \tilde{\mathbf{V}} \cdot \tilde{\mathbb{P}}_n) + k_{en} (\xi_n \beta_p \tilde{\mathbf{V}} \cdot \tilde{\mathbb{P}}_p - \xi_i \beta_n \tilde{\mathbf{V}} \cdot \tilde{\mathbb{P}}_n) \times \hat{\mathbf{b}} \right]. \end{aligned} \quad (44)$$

Assuming that $\tilde{\mathbf{E}} + (\tilde{\mathbf{V}}_n \times \tilde{\mathbf{B}})$ is of order 1, then we neglect terms on the RHS of Equation (44) which are much less than unity. For length scales longer than the electron inertial scale $L_0 \gg d_e$, the $\partial \tilde{\mathbf{J}} / \partial \tilde{t}$ term can be neglected. For the chromosphere, using the smallest density from Figure 2 of 10^{17} m^{-3} gives a maximum for d_e of 17 cm. For the ionosphere, using the smallest density from Figure 2 of 10^9 m^{-3} gives 170 m. Hence, it is safe to neglect the $\partial \tilde{\mathbf{J}} / \partial \tilde{t}$ term in the chromosphere, and appropriate in the I/T for lengths larger than a km.

The terms containing $d^* \tilde{\mathbf{W}} / d\tilde{t}$ can in general be neglected if the frequency of the system, f_0 , is much smaller than the minimum of the ion-neutral collisional frequency v_{in} and the ion gyrofrequency Ω_i .

$$f_0 \ll \min(\Omega_i, v_{in}). \quad (45)$$

This is the low frequency approximation mentioned above. This condition is nearly always true in the highly collisional chromosphere, and mostly true in local I/T models, except on the topside of the ionosphere and extending into the plasmasphere because the collision frequencies decrease rapidly with height. For frequencies comparable to the ion neutral frequency, the $d^* \tilde{\mathbf{W}} / d\tilde{t}$ terms cannot be neglected. Note that there is an additional factor $\xi_n k_{in} / (k_{en} + k_{in})$ in front of one of these $d^* \tilde{\mathbf{W}} / d\tilde{t}$ terms, and $\xi_n k_{en} k_{in} / (k_{en} + k_{in})$ in front of the other. Also, $k_{en} / k_{in} \sim m_i v_{in} / m_e v_{en}$ and as we shall see later, $m_i v_{in} \gg m_e v_{en}$ for both atmospheres, so that $k_{en} \gg k_{in}$ and so $k_{in} / (k_{en} + k_{in}) \ll 1$ and $k_{en} k_{in} / (k_{en} + k_{in}) \approx k_{in}$. Hence one must be careful in the regime where $k_{in} \gg 1$.

The last two terms in Equation (44) are pressure terms. The first, the electron and ion modified pressure term, $\frac{d_i}{L_0} \left(\beta_e \tilde{\mathbf{V}} \cdot \tilde{\boldsymbol{\kappa}}_e - \beta_i \frac{m_e}{m_i} \tilde{\mathbf{V}} \cdot \tilde{\boldsymbol{\kappa}}_i \right)$, can be neglected if $\frac{d_i}{L_0} \beta_e \ll 1$. The ion inertial scale d_i has a maximum value of about 1 m in the chromosphere, and β_e can be as large as 100 (see Figure 4), so for length scales $L_0 \gg 100$ m, this pressure term can be neglected. For the I/T, the ion inertial scale can be as large as 2 km, but β_e has a maximum of 10^{-4} so that length scales larger than 1 m are sufficient to neglect the electron pressure.

The last pressure related term can be neglected in general when $\frac{d_i}{L_0} \xi_i \beta_n$ and $\frac{d_i}{L_0} \xi_n \beta_p$ are much less than unity (again care must be taken when $k_{in} \gg 1$). The first of these two is satisfied easily as the ionization level ξ_i is very small in most of the two atmospheres, and the second is of the order of the electron pressure term (see above).

Under these approximations, and noting that $\eta_P = \eta_{\parallel} + \eta_C$, the low frequency Ohm's law is simply

$$\begin{aligned} \mathbf{E}^* &= \eta_{\parallel} \mathbf{J}_{\parallel} + \eta_P \mathbf{J}_{\perp} + \eta_H \mathbf{J} \times \hat{\mathbf{b}} \\ &+ \mathbf{G}_{\parallel} + \mathbf{G}_{\perp} + \mathbf{G}_{\perp} \times \hat{\mathbf{b}} \end{aligned} \quad (46)$$

Here $\mathbf{J}_{\perp} = \hat{\mathbf{b}} \times \mathbf{J} \times \hat{\mathbf{b}}$ is the component of the current density perpendicular to the magnetic field. The quantity $\eta_C = \eta_P - \eta_{\parallel}$ is also referred to as the Cowling resistivity (Cowling 1956). The terms \mathbf{G}_{\parallel} , \mathbf{G}_{\perp} , $\mathbf{G}_{\perp} \times \hat{\mathbf{b}}$ are the grouped neglected terms, and are kept to show that they do not enter into the conductivities when we invert Equation (46) to give $\mathbf{J} = \underline{\underline{\sigma}} \cdot \mathbf{E}^*$ in terms of the parallel, Hall and Pedersen conductivities:

$$\begin{aligned} \mathbf{J} &= \sigma_{\parallel} \mathbf{E}_{\parallel}^* + \sigma_P \mathbf{E}_{\perp}^* - \sigma_H \mathbf{E}_{\perp}^* \times \hat{\mathbf{b}} \\ &+ \sigma_{\parallel} \mathbf{G}_{\parallel} + (\sigma_H - \sigma_P)(\mathbf{G}_{\perp} + \mathbf{G}_{\perp} \times \hat{\mathbf{b}}), \end{aligned} \quad (47)$$

where

$$\sigma_{\parallel} = \frac{1}{\eta_{\parallel}}, \quad (48)$$

$$\sigma_P = \frac{\eta_P}{\eta_P^2 + \eta_H^2}, \quad (49)$$

$$\sigma_H = \frac{\eta_H}{\eta_P^2 + \eta_H^2}. \quad (50)$$

The neglected terms are terms which add to the electric field in the rest frame of the neutrals regardless of the presence of a current, and as such it is correct that they do not enter into the conductivities above.

Ohm's law, whether expressed in the form $\mathbf{E}^* = \underline{\underline{\eta}} \cdot \mathbf{J}$ or $\mathbf{J} = \underline{\underline{\sigma}} \cdot \mathbf{E}^*$, can be derived in a number of different ways (e.g., Song et al. 2001; Vasyliūnas 2012). Here, we have derived it from the first-principles governing equations of motion for the electrons, ions, and neutrals. In the next section, we discuss applications of these general relations to the chromosphere and the I/T. We note here that Song et al. (2005) and Vasyliūnas (2012) discuss the assumptions needed to reduce the generalized Ohm's law to a low-frequency Ohm's law equation which relates \mathbf{E} and \mathbf{J} . In these papers, they state that the current given by the conventional ionospheric Ohm's law (Equation (47) above), is a stress-balance current, determined by a balance between Lorentz force and plasma-neutral collisional friction. Then \mathbf{J} is physically related to $\mathbf{V}_p - \mathbf{V}_n$, and hence to \mathbf{E} (as \mathbf{E} is linearly related to $\mathbf{V}_p - \mathbf{V}_n$). Looking at the sum of the momentum equations for ions and electrons, then a balance of Lorentz force and plasma-neutral collisional friction is equivalent to the neglect of all inertial terms, as well as pressure and gravity terms. This is not exactly the same as our assumptions made here, as we neglect terms proportional to $\partial \mathbf{J} / \partial t$ and $d^* \mathbf{W} / dt$, based on length and frequency arguments, rather than neglecting $\partial(m_i n \mathbf{V}_i) / dt$ and $\partial(\min_n \mathbf{V}_n) / dt$ individually, a fact which allows us to retain individual inertial terms later during discussion of electromagnetic energy transfer into thermal and kinetic energy.

Note that in the limit of vanishing collisions, the resistive terms in the generalized Ohm's law (30) tend to zero, but that in the linear Ohm's law (46) the Pedersen resistivity tends to infinity. This behavior originates in our solution for \mathbf{W} in Equation (31), which assumes that collisions dominate over inertia. This cannot occur, of course, in the limit of vanishing collision frequency.

4 Magnetization, Mobility, and Resistive Properties

4.1 Magnetization Domains

Having derived Ohm's law in terms of the plasma magnetizations, it is useful to now compare and contrast these fundamental parameters in the two environments, as was originally done by Goodman (2000, 2004). Figure 5 shows the contributing collision frequencies (ν_{ei} , ν_{en} , $\nu_e \equiv \nu_{en} + \nu_{ei}$, ν_{in}) and the electron and ion gyrofrequencies (Ω_e, Ω_i) as functions of height in the chromosphere and I/T.

The frequencies of collisions of charged particles with neutrals are similar at the base of both environments, and are very high, in the range 10^8 – 10^{10} Hz. They decline to about 1 kHz at the top of the chromosphere, and much farther, to below 1 Hz, at the top of the I/T. The charged and neutral fluids may be considered to be strongly coupled in response to waves and transient phenomena whose frequencies fall well below these collision frequencies at any particular height. Independent motions of the charged particles and neutrals can occur at frequencies well above those thresholds. Some consequences of this frequency-varying coupling on the propagation of Alfvén waves, and the relative motions of plasma and magnetic field generally, are considered in more detail below in §5.1.

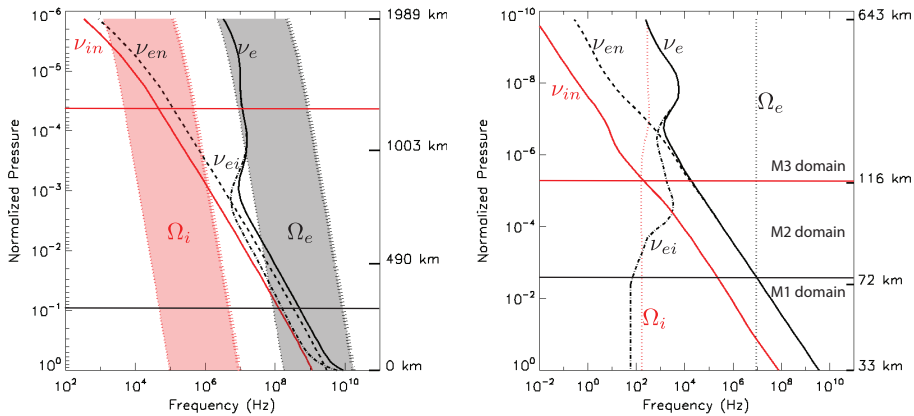


Fig. 5 Collision frequencies and gyrofrequencies (Hz) in the ALC7 chromosphere (left) and TIMEGCM I/T (right). The collision frequencies are shown as solid red lines (ν_{in}), dashed lines (ν_{en}), dot-dashed lines (ν_{ei}), and solid black lines (ν_e). The gyrofrequencies are shown as dotted lines for ions (Ω_i ; red) and electrons (Ω_e ; black). For the chromosphere, where gyrofrequencies depend on height and there is a choice of three surface field values, the lines for the two extreme values of $B_0 = 10$ G (thin dotted line) and $B_0 = 1000$ G (thick dotted line) in Equation (2) are shown, with a shaded area between them. In the I/T (right panel), the horizontal lines mark altitudes at which $\nu_e = \Omega_e$ (black line) and $\nu_{in} = \Omega_i$ (red line). In the chromosphere model (left panel), these heights do not have one single value, but a representative line is shown for these transitions.

In the I/T (right panel), the horizontal lines mark altitudes at which $\nu_e = \Omega_e$ (black line) and $\nu_{in} = \Omega_i$ (red line). These locations are where $k_e = 1$ and $k_{in} = 1$, respectively, and represent transitions from unmagnetized to magnetized. In the chromosphere model (left panel), these respective heights do not have one single value, but a representative line is shown for these transitions. The magnetizations, defined in Equations (26-29), associated

with these collision frequencies and gyrofrequencies are shown in Figures 6 and 7 for both the chromosphere and I/T. This analysis was originally conducted by Goodman (2000, 2004) using a different semi-implicit model for the chromosphere, and the profiles obtained in this review are quantitatively comparable to those of Goodman (2000, 2004) and those obtained in a more recent analysis by Vranjes and Krstic (2013). From Figure 7, one can define three distinct regions in the I/T:

M1 domain	both ions and electrons are unmagnetized	$k_{in}, k_e < 1$
M2 domain	ions are unmagnetized; electrons are magnetized	$k_{in} < 1, k_e > 1$
M3 domain	both ions and electrons are magnetized	$k_{in}, k_e > 1$

We point out that the magnetization domains are not directly related to the D, E, and F layers of the I/T, which are characterized by the dominant ion and neutral chemistry that occurs in the corresponding altitude bands. Our M1, M2, and M3 domains instead highlight commonalities in the charged-particle dynamics within the chromosphere and I/T. For the chromosphere, where there is a range of locations where these transitions occur, these three magnetization regions do not have specific heights. For example, for strong field strengths, e.g., above sunspots, the electrons can be magnetized $k_e > 1$ at all heights (solid black line in Figure 6), but for low field strengths (thin black line) they can be magnetized above about 500 km and unmagnetized beneath. For ions in the chromosphere, there is a range between about 600 and 1600 km where the ions can transition from being unmagnetized ($k_{in} < 1$) to magnetized ($k_{in} > 1$), depending on the field strength. In general, however, both the chromosphere and I/T are stratified, partially ionized mixtures in which the charged particles undergo a transition from completely unmagnetized (lower M1) to completely magnetized (upper M3), with a central region (M2) in which ions are unmagnetized and electrons are magnetized. Figure 7 also shows the function $\Gamma \equiv \xi_n k_e k_{in}$ (green line) which is equal to unity near the center of the M2 domain. As will be discussed later, the transition from $\Gamma < 1$ to $\Gamma > 1$ is a transition from isotropic transport processes to anisotropic. This transition can be important for both the electrodynamics and magnetohydrodynamics, and the heating of the chromosphere (if not the I/T). In the chromosphere, the locations of the M1, M2, and M3 domains change as the magnetic field strength changes, and so can be quite different over active regions compared to quiet regions of the Sun. In the I/T, in contrast, the magnetic field is nearly static and the collision frequencies are dictated by the vertical distribution of the neutral gas. Thus, the locations of the M1, M2 and M3 domains in the I/T change only slowly with respect to altitude and latitude.

Figure 5 shows that electron-ion collisions are much less frequent than electron-neutral collisions in the M1 and M2 domains of the I/T, but not so in the chromosphere. This is due to the much larger ionization fraction in the chromosphere relative to the I/T. In the M3 domains of both the chromosphere and I/T, on the other hand, electron-ion collisions dominate as the neutral density falls off. Nevertheless, a common assumption in ionospheric physics is that electron-ion collisions do not play a part in the electrodynamics (Song et al. 2001). We will discuss this assumption in relation to the mobility of charged particles below. When electron-ion collisions are negligible, then k_{ei} becomes very large (as is evident in Figure 6 in the lower I/T) and $k_e \approx k_{en}$ in Equations (26–29). Also, the neutral fraction ξ_n is very close to 1, which is valid for all of the I/T and all but the highest altitudes in the chromosphere. In this limit, the resistivities (38–41), simplify to

$$\eta_{\parallel} \approx \frac{B}{en} \frac{1}{k_{en} + k_{in}}, \quad (51)$$

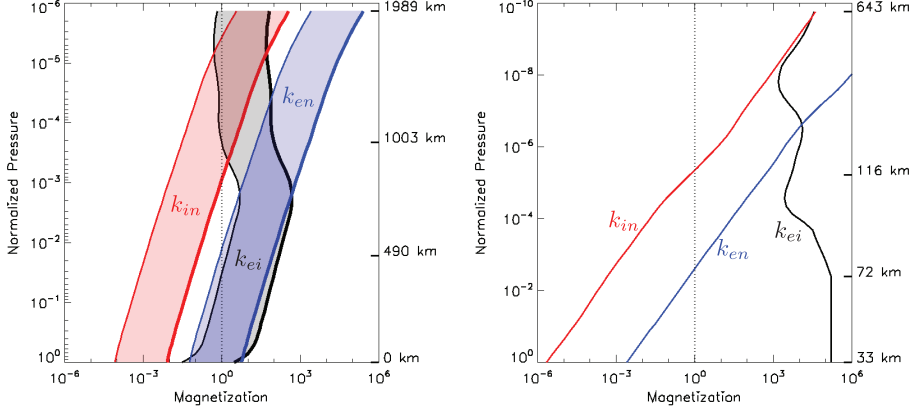


Fig. 6 Individual magnetizations in the chromosphere (left) and I/T (right). The magnetizations are shown as blue lines (k_{en}), red lines (k_{in}) and black lines (k_{ei}). For the chromosphere (left panel), where magnetizations depend on magnetic field strength, the lines for the two extreme values of $B_0 = 10$ G (thin lines) and $B_0 = 1000$ G (thick lines) in Equation (2) are shown, with a shaded area between them.

$$\eta_C \approx \frac{B}{en} \frac{k_{en} k_{in}}{k_{en} + k_{in}}, \quad (52)$$

$$\eta_P \approx \frac{B}{en} \frac{1 + k_{en} k_{in}}{k_{en} + k_{in}}, \quad (53)$$

$$\eta_H \approx \frac{B}{en} \frac{k_{en} - k_{in}}{k_{en} + k_{in}}. \quad (54)$$

Substituting these expressions into (48–50) and combining terms yields the corresponding conductivities

$$\sigma_{\parallel} \approx \frac{en}{B} (k_{en} + k_{in}), \quad (55)$$

$$\sigma_P \approx \frac{en}{B} \left(\frac{k_{in}}{1 + k_{in}^2} + \frac{k_{en}}{1 + k_{en}^2} \right), \quad (56)$$

$$\sigma_H \approx \frac{en}{B} \left(\frac{1}{1 + k_{in}^2} - \frac{1}{1 + k_{en}^2} \right). \quad (57)$$

These expressions (55–57) are identical to those in Equations (27–29) of Song et al. (2001), who derived them under the same assumptions: $v_{ei} \rightarrow 0$ and $\xi_n \rightarrow 1$.

4.2 Charged Particle Mobilities and Electrical Currents

We can extract the common pre-factor (en/B) from the conductivities (55–57):

$$\mu_{\parallel} \equiv \sigma_{\parallel} \frac{B}{en} \approx k_{en} + k_{in}, \quad (58)$$

$$\mu_P \equiv \sigma_P \frac{B}{en} \approx \frac{k_{en}}{1 + k_{en}^2} + \frac{k_{in}}{1 + k_{in}^2}, \quad (59)$$

$$\mu_H \equiv \sigma_H \frac{B}{en} \approx \frac{1}{1 + k_{in}^2} - \frac{1}{1 + k_{en}^2}. \quad (60)$$

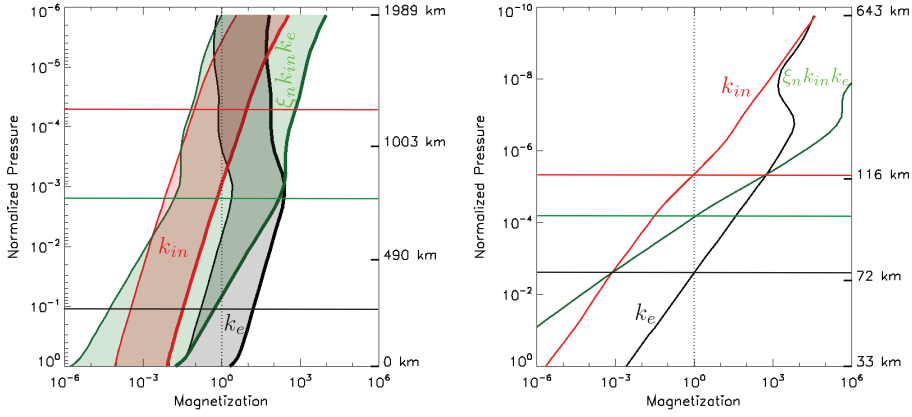


Fig. 7 Combined magnetizations in the chromosphere (left) and I/T (right). The magnetizations are shown as black lines (k_e), red lines (k_{in}) and green lines ($\xi_n k_{in} k_e$). For the chromosphere (left panel), where magnetizations depend on magnetic field strength, the lines for the two extreme values of $B_0 = 10$ G (thin lines) and $B_0 = 1000$ G (thick lines) in Equation (2) are shown, with a shaded area between them. In the I/T (right panel), the horizontal lines mark altitudes at which $k_e = 1$ (black line), $k_{in} = 1$ (red line), and $\xi_n k_{in} k_e = 1$ (green line). In the chromosphere model (left panel), these heights do not have one single value, but a representative line is shown for these transitions.

These definitions also were introduced by Song et al. (2001). The mobilities μ (58–60) are explicit functions of the magnetizations k (26–29) that show the relative contributions of electrons and ions to the electric current.

Figure 8 shows the mobilities μ_P and μ_H for the chromosphere and I/T. The plots for the full mobilities and those for the approximations assuming $v_{ei} = 0$ and $\xi_n = 1$ (58–60) overlay each other, validating the assumption that electron-ion collisions do not contribute to the electrodynamics. The overall shape of the mobility curves in the chromosphere and in the I/T is very similar, though the vertical extent of these curves in the chromosphere depends on the magnetic field model used. Three curves for each mobility are shown in the left panel, one for each of the three magnetic field surface strengths in Equation (2). In the chromosphere and I/T, the Pedersen mobility μ_P (red line in Figure 8) is double peaked, with maxima very near the transitions from domains M1 to M2 (where $k_e = 1$) and from M2 to M3 (where $k_{in} = 1$). The Hall mobility μ_H (green line) is single peaked, with its maximum between the two peaks in the Pedersen mobility. The lower peak for the weakest chromospheric magnetic field model is missing from the plot as it appears below the lower boundary of the atmosphere. We shall discuss the mobility of the ions and electrons and their contribution to currents below.

The conductivities (including the electron density and representative magnetic field strength for the chromosphere and I/T) are shown in Figure 9. The calculations using the full expressions are shown as solid lines, while those neglecting electron-ion collisions are shown as dashed lines. Convolving the electron density with the relative mobilities causes some of the structure with altitude in Figure 8 to be less obvious in Figure 9. In particular, for the I/T, the lower Pedersen conductivity peak is significantly reduced due to the strongly diminished electron density at those altitudes. The figure also reveals that the entire I/T above 70 km is subject to anisotropic electrodynamics ($\sigma_P \neq \sigma_{\parallel}$). In the chromosphere, for weak fields, σ_P can be equal to σ_{\parallel} up to about 500km before anisotropy develops, but for

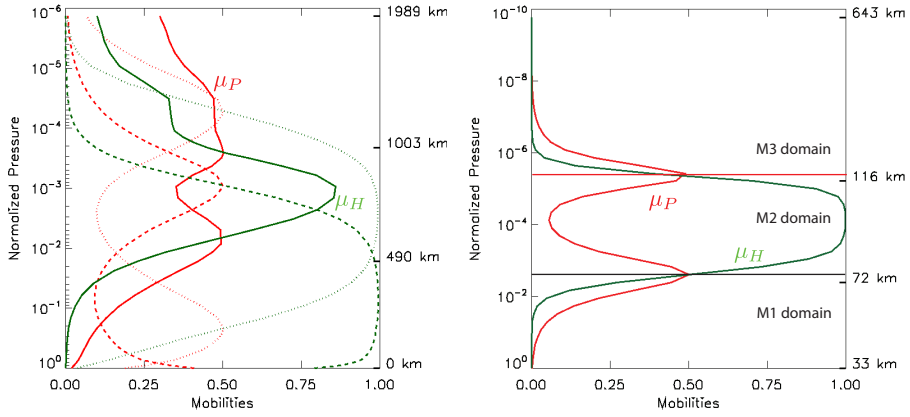


Fig. 8 Pedersen (μ_P ; red) and Hall (μ_H ; green) mobilities in the chromosphere (left) and I/T (right). For the chromosphere, the solid, dotted and dashed lines represent the profiles using the three different values of $B_0 = 10, 100, 1000$ G, respectively, in Equation (2) for the magnetic field.

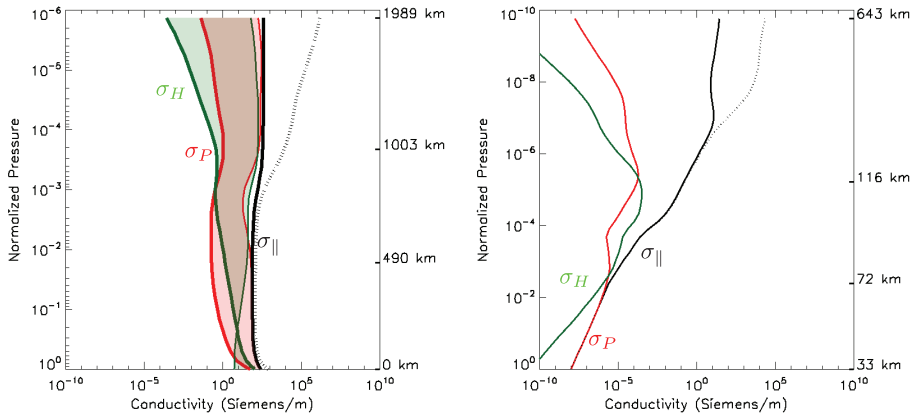


Fig. 9 Parallel (σ_{\parallel} ; black), Pedersen (σ_P ; red), and Hall (σ_H ; green) conductivities (in Siemens/m) in the chromosphere (left) and I/T (right). Dashed lines show the corresponding values when electron-ion collisions are ignored. For the chromosphere (left panel), where the Pedersen and Hall conductivity depend on magnetic field strength, the lines for the two extreme values of $B_0 = 10$ G (thin lines) and $B_0 = 1000$ G (thick lines) in Equation (2) are shown, with a shaded area between them. The parallel conductivity is the only conductivity that appears to be affected by the assumption that electron-ion collisions can be ignored.

strong fields, the anisotropy can be evident for the entire chromosphere. An important role of electron-ion collisions in limiting the parallel conductivity (σ_{\parallel}) is obvious at high altitudes (compare the solid and dashed black lines), throughout the upper half of the chromosphere and also above 120 km in the ionosphere, as can be seen in Figure 9. All three conductivities, especially the Pedersen and Hall conductivities, are far larger in the chromosphere than in the I/T.

It is worth further study of the contribution of electrons and ions to the Pedersen and Hall currents responding to a generic electric field in the rest frame of the neutrals \mathbf{E}^* , via the Pedersen and Hall mobilities. Examination of the curves for the I/T allows a simple discussion, but one must note that the chromosphere has a variable magnetic field, and so the transitions discussed here, such as unmagnetized to magnetized plasma, will vary with height depending on the field strength.

First recall the low frequency Ohm's law

$$\mathbf{J} = \sigma_{\parallel} \mathbf{E}_{\parallel} + \sigma_P \mathbf{E}_{\perp}^* - \sigma_H \mathbf{E}_{\perp}^* \times \hat{\mathbf{b}} \quad (61)$$

and so the current perpendicular to the magnetic field vector (\mathbf{J}_{\perp}) is a combination of Hall ($\sigma_H \mathbf{E}_{\perp}^* \times \hat{\mathbf{b}}$) and Pedersen ($\sigma_P \mathbf{E}_{\perp}^*$) currents. We shall see later how the relative contribution of these two currents affects the efficiency of heating due to plasma-neutral collisions. Let us first consider the variation with altitude of these mobilities, conductivities, and currents. A complete description would involve examining the momentum equations for ions and electrons, and solving for velocity, and then using $\mathbf{J} = en(\mathbf{V}_i - \mathbf{V}_e)$ to define the current. For brevity, we discuss the motions of the ions and electrons and do not present such a derivation, though the results are consistent with such a method.

- At the lowest altitudes in the I/T, and near the solar surface in weak field regions, collisions with neutrals are high, and the mobility of electrons and ions are low and they are unmagnetized, $k_{en}, k_{in} \ll 1$ (see Figure 6). Thus $\mu_P \approx \mu_H \approx 0$, and $\mathbf{J}_{\perp} \approx 0$.
- With increasing altitude, just below the lower peak in the Pedersen mobility (Figure 8), electrons become more mobile $k_{en} > k_{in}$ and drive a Pedersen current in the \mathbf{E}_{\perp}^* direction. Here $\mu_P > \sigma_H$ and $\sigma_P \sim \sigma_{\parallel} > \sigma_H$ (see Figure 9).
- There is a height at which $k_{en} \approx 1$, while $k_{in} \ll 1$. This is the lower peak in the Pedersen mobility in Figure 8. Here $\mu_P \approx \mu_H \approx 1/2$ and the perpendicular current is equally contributed to by the Hall and Pedersen currents. At this point, there is still isotropy in the conductivity: $\sigma_P \approx \sigma_H \approx \sigma_{\parallel}$, as seen in Figure 9.
- At higher altitudes, the electrons become completely magnetized, but the ions remain unmagnetized. Here $k_{en} \gg 1$ while $k_{in} \ll 1$, and $\mu_H \approx 1$, while $\mu_P < \mu_H$ and $\sigma_P < \sigma_H < \sigma_{\parallel}$. This is the peak in the Hall mobility in Figure 8). The electron motion drives a current predominantly in the Hall direction $-\sigma_H \mathbf{E}_{\perp}^* \times \hat{\mathbf{b}}$.
- The next altitude of interest is where ions start to become mobile and $k_{in} \approx 1$ and $k_{en} \ll 1$. This is the higher peak in the Pedersen mobility, where $\mu_P = \mu_H = 1/2$, and the perpendicular current is equally Pedersen and Hall current. However, unlike at the lower peak in the Pedersen mobility, at this upper peak $\sigma_P \approx \sigma_H \ll \sigma_{\parallel}$ and there is significant anisotropy in the conductivities (this will be important for plasma-neutral heating, as discussed in later sections).
- Just above the upper Pedersen mobility peak, $\mu_P > \mu_H$, $\sigma_P > \sigma_H$, and the perpendicular current is mainly the Pedersen current in the \mathbf{E}_{\perp}^* direction and $\sigma_H < \sigma_P \ll \sigma_{\parallel}$.
- Finally, at the highest altitudes where collisions with neutrals have fallen sufficiently, the electrons and ions are completely magnetized, and $k_{en}, k_{in} \gg 1$. In this region $\mu_P \sim \mu_H \sim 0$, $\mathbf{J}_{\perp} \approx 0$ and $\sigma_H < \sigma_P < \sigma_{\parallel}$.

This discussion of currents not only highlights the similarities between the two atmospheres, but allows for a discussion of the conversion of electromagnetic energy into thermal and kinetic energy, via the $\mathbf{E} \cdot \mathbf{J}$ term, as will be discussed in a later section on energy transfer.

4.3 Perpendicular vs. Parallel Current Resistivity

As we have discussed in some detail, collisional drag between the charged-particle and neutral fluids introduces a substantial anisotropy in the resistivities and conductivities of a partially ionized mixture. At high altitudes of the chromosphere and I/T, the parallel and Pedersen conductivities increasingly diverge from one another, with $\sigma_P < \sigma_{\parallel}$, or equivalently $\eta_P > \eta_{\parallel}$. This reveals a preference in both atmospheres toward relatively fast dissipation of currents that are directed perpendicular to the magnetic field and so contribute to magnetic forces, but relatively slow dissipation of currents that are directed along the magnetic field and so are force-free. On the Sun, during the emergence of magnetic flux from below the photosphere into the overlying atmosphere, the anisotropic resistivities in the chromosphere reshape the current profile and transition the magnetic field to the essentially force-free configuration ($\mathbf{J}_{\perp} \approx 0$) that it must assume in the very low-beta corona (Leake and Arber 2006; Arber et al. 2007, 2009; Leake and Linton 2013). Goodman (2000, 2004) discusses the relationship between anisotropy and the force-free nature of the field for current dissipation driven by wave motions in the chromosphere. At Earth, the anisotropic conductivities in the I/T enable magnetic-field-aligned currents to neutralize the parallel electric field ($\mathbf{E}_{\parallel} = \mathbf{b} \cdot \mathbf{E} \approx 0$) while perpendicular currents and electric fields can be sustained when driven by, for example, cross-field neutral winds. As mentioned earlier, a slowly evolving electric field can be written as the gradient of a scalar potential, $\mathbf{E} = -\nabla\Phi$. Then $\mathbf{E}_{\parallel} \approx 0 \Rightarrow \mathbf{b} \cdot \nabla\Phi \approx 0$, and magnetic field lines are equipotential paths through the I/T if it is not coupled to the magnetosphere.

Another way of expressing this anisotropy in the resistivities is to use the magnetizations. In general, one would expect that $m_e v_{en} \ll m_i v_{in}$, since $m_{\alpha} v_{\alpha n} \propto \sqrt{m_{\alpha} T_{\alpha}}$. However, this approximation may not hold throughout the I/T at all times (Song et al. 2001). Assuming that $m_e v_{en} \ll m_i v_{in}$, and noting that this implies $k_{in} \ll k_{en}$, the resistivities (38–41) in Ohm’s law (46) become

$$\eta_{\parallel} \approx \frac{B}{en} \frac{1}{k_e}, \quad (62)$$

$$\eta_C \approx \frac{B}{en} \xi_n k_{in}, \quad (63)$$

$$\eta_P \approx \frac{B}{en} \frac{1 + \xi_n k_e k_{in}}{k_e}, \quad (64)$$

$$\eta_H \approx \frac{B}{en}. \quad (65)$$

The corresponding expressions for σ_{\parallel} , σ_P and σ_H , after using Equations (48–50), are exactly the same as Equations (23–25) in Song et al. (2001), derived under the same assumptions. The parallel, Pedersen, and Hall resistivities for the chromosphere and I/T are shown in Figure 10. The plots calculated under the assumption $m_e v_{en} \ll m_i v_{in}$ overlay the full calculations, verifying the assumption.

An important quantity that sets the anisotropy of the resistivities is the ratio of the Cowling to parallel resistivity:

$$\frac{\eta_C}{\eta_{\parallel}} \approx \xi_n k_e k_{in}. \quad (66)$$

Note that this was denoted Γ in Goodman (2004), where the Ohm’s law was cast in the center of mass frame and thus had the form $\xi_n^2 k_e k_{in}$. Figure 7 shows the product $\xi_n k_e k_{in}$ in the chromosphere and I/T. Increasing with height from the bottom, the electrons become

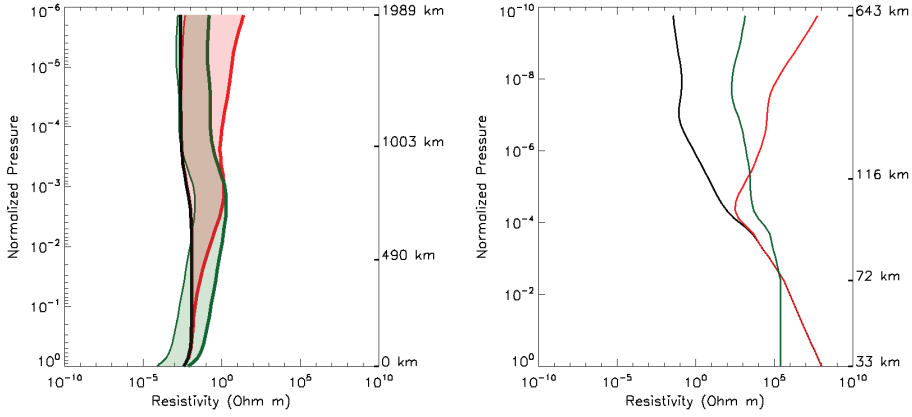


Fig. 10 Parallel (black), Pedersen (red), and Hall (green) resistivities in the chromosphere (left) and I/T (right). For the chromosphere (left panel), where the resistivities depend on magnetic field strength, the lines for the two extreme values of $B_0 = 10$ G (thin lines) and $B_0 = 1000$ G (thick lines) in Equation (2) are shown, with a shaded area between them.

magnetized first ($k_e > 1$), then the ions do so ($k_{in} > 1$). Between these two points, $\xi_n k_e k_{in} = 1$ within the M2 domain. At lesser heights, the current density is isotropic, $\eta_c / \eta_{\parallel} \ll 1$, or $\eta_{\parallel} \approx \eta_p$ and $\mathbf{E}^* \approx \eta_{\parallel} \mathbf{J}$, while at greater heights it is anisotropic, $\eta_p \gg \eta_{\parallel}$ and $\mathbf{E}^* = \eta_{\parallel} \mathbf{J}_{\parallel} + \eta_p \mathbf{J}_{\perp} + \eta_H \mathbf{J} \wedge \hat{\mathbf{b}}$. As will be discussed later in this paper, this transition is believed to be important with respect to the heating of the chromosphere.

4.4 Summary

Despite a large disparity in electron number density between the chromosphere and I/T, the governing physics of the two regions display some remarkable similarities. These similarities are mainly related to the transition from unmagnetized to magnetized plasma, and the variation of the electron and ion mobilities with altitude. The decrease in collisional frequency with height in both environments causes a change in magnetization with altitude, such that a central region is created where the ions are unmagnetized and electrons are magnetized. This is characterized by the region $\Gamma \equiv \xi_n k_e k_{in} \approx 1$. As Γ increases with altitude, the ions become more magnetized and can drive Pedersen currents. These dissipative currents are perpendicular to the field, and are a possible source of heating via the $\mathbf{E} \cdot \mathbf{J}$ term (frictional heating, of which some is Joule heating, see the discussion in the following section).

However, a large electron number density difference between the two regions leads to a large difference in the magnitudes of the conductivities and resistivities. As we shall see in the next section this leads to the I/T being resistively dominated, while the chromosphere is only resistive for scales less than a km. Also, the nature of the drivers in the two environments is also very different. The drivers of the low frequency (relative to the collision frequency) electric fields in the I/T are mainly neutral winds colliding with ions and electrons, and externally imposed electric fields from the magnetosphere. In the chromosphere, the drivers exist on a large range of time scales, as long as weeks (sunspot and prominence

formation and persistence) and as short as seconds (magnetic reconnection events such as jets and flares, and high-frequency waves).

5 Magnetohydrodynamic and Electrodynamic Processes

5.1 Frozen-In vs. Resistive-Slip Evolution

A key parameter governing the coupling of a fully ionized plasma to the magnetic field is the Lundquist number (Lundquist 1952),

$$S \equiv \frac{\mu_0^{1/2} B_0 \ell}{\rho_0^{1/2} \eta_{\parallel}} = \frac{\mu_0 V_{A0} \ell}{\eta_{\parallel}}, \quad (67)$$

where $\rho_0 = m_i n$ is the mass density, η_{\parallel} is the resistivity, ℓ is a characteristic length scale of variation, and $V_{A0} = B_0 / (\mu_0 \rho_0)^{1/2}$ is the Alfvén speed. This dimensionless ratio measures the relative importance of convection and resistive diffusion in the evolution of the magnetic field. Where it is large, convection dominates, and the plasma moves with the magnetic field so that the field lines are “frozen” into the fluid (Alfvén and Fälthammar 1963); where it is small, resistivity dominates, and the plasma slips through the magnetic field lines. A derivation of the Lundquist number demonstrating this fundamental property is instructive and guides its generalization to multi-fluid situations with plasma-neutral coupling.

The motion of the fully ionized plasma induced by fluctuations in the magnetic field is estimated by balancing inertia against Lorentz forces in the equation of motion,

$$\rho_0 \frac{\partial \mathbf{V}_p}{\partial t} \approx \frac{1}{\mu_0} (\nabla \times \delta \mathbf{B}) \times \mathbf{B}_0, \quad (68)$$

whence

$$\omega \rho_0 V_p \approx \frac{B_0 \delta B}{\mu_0 \ell}, \quad (69)$$

where ω is the frequency associated with the length ℓ . The evolution of the magnetic field \mathbf{B} is governed by Faraday’s law, which requires Ohm’s law. In the limit of a fully ionized plasma, and for low frequency phenomena ($f_0 \ll v_{in}, \Omega_i$), the Ohm’s law is

$$\mathbf{E} + (\mathbf{V}_p \times \mathbf{B}) = \eta_{\parallel} \mathbf{J} = \frac{\eta_{\parallel}}{\mu_0} \nabla \times \mathbf{B}, \quad (70)$$

consistent with Alfvén and Fälthammar (1963), where we have also assumed that the length scale of interest is larger than the ion and electron inertial scales $l \gg d_e, d_i$, as discussed in §3.5.

Faradays law then yields the standard MHD induction equation:

$$\frac{\partial \mathbf{B}}{\partial t} = \nabla \times (\mathbf{V}_p \times \mathbf{B}) + \frac{\eta_{\parallel}}{\mu_0} \nabla^2 \mathbf{B}. \quad (71)$$

Balancing the time derivative of the fluctuating field against the convection of the ambient field, which is assumed to dominate the effects of resistivity acting on the fluctuating field, we find

$$\omega \delta B \approx \frac{1}{\ell} V_p B_0 \gg \frac{\eta_{\parallel}}{\mu_0 \ell^2} \delta B. \quad (72)$$

Using Equation (72) to eliminate ω from Equation (69) and solving for V_p gives

$$V_p^2 \approx \frac{\delta B^2}{\mu_0 \rho_0}, \quad (73)$$

so that the velocity V_p is just the Alfvén speed evaluated at the perturbed field strength δB . The ratio of the retained convection term to the neglected resistivity term in Equation (72) then becomes

$$\frac{\mu_0 \ell B_0}{\eta_{\parallel}} \frac{V_p}{\delta B} = \frac{\mu_0^{1/2} B_0 \ell}{\rho_0^{1/2} \eta_{\parallel}} = S, \quad (74)$$

the Lundquist number. Thus, as claimed, convection dominates resistivity if $S \gg 1$. Reversing the inequality in Equation (72) and carrying through the rest of the analysis, the unimportance of the convection term relative to the resistivity term in that case is measured by the ratio

$$\frac{\mu_0 \ell B_0}{\eta_{\parallel}} \frac{V_p}{\delta B} = \frac{\mu_0 B_0^2 \ell^2}{\rho_0 \eta_{\parallel}^2} = S^2. \quad (75)$$

Therefore, again as claimed, resistivity dominates convection if $S \ll 1$.

Now we generalize these considerations to a partially ionized mixture. First we note that the Lundquist number is directly proportional to the characteristic length ℓ of the variations in the magnetic and velocity fields. By combining Equations (69) and (72), we find in the convection-dominated case that ℓ is just the reciprocal wavenumber of an Alfvén wave at frequency ω ,

$$\ell = \frac{B_0}{\mu_0^{1/2} \rho_0^{1/2} \omega} = \frac{V_{A0}}{\omega}. \quad (76)$$

In a fully ionized plasma, the waves span a continuum of frequencies and wavenumbers whose character changes from frozen-in, oscillatory motions at large S (large ℓ , small ω) to resistive-slip, damped motions at small S (small ℓ , large ω). In a partially ionized mixture, the collisions between plasma particles and neutrals modify the response of the gas to the magnetic field and also raise the resistivity acting on perpendicular currents \mathbf{J}_{\perp} from the parallel value η_{\parallel} to the Pedersen value η_P , as in Equation (46). Two limiting frequency ranges are particularly illustrative. At high frequencies $\omega > v_{in}$, the plasma-neutral coupling is weak, and the waves propagate at the Alfvén speed V_{Ap0} determined by the plasma mass density ρ_{p0} alone. We note here that the low frequency Ohm's law may not exactly apply in this high frequency situation, and there will be a term related to $d^* \mathbf{W}/dt$ that contributes to the electric field in the rest frame of the plasma, as in Equation (33). As discussed in §3.5.1 the importance of this $d^* \mathbf{W}/dt$ term depends on the product of the three ratios ω/v_{in} , ω/Ω_i and k_{in}/k_{en} , the first of which is large in this high frequency regime, and the last of which is always small. Choosing a magnetized regime where $v_{in} < \Omega_i$, we can still have $\omega > v_{in}$ but be able to apply the low frequency limit of the Ohm's law (46). Using the transition frequency $\omega = v_{in}$ in Equation (76) to set ℓ , the Lundquist number in Equation (67) then takes the value

$$S'_{in} \equiv \frac{\mu_0 V_{Ap0}^2}{\eta_P v_{in}}. \quad (77)$$

At low frequencies $\omega < v_{in}$, on the other hand, the plasma-neutral coupling is strong, and the waves propagate at the Alfvén speed V_{A0} determined by the total (plasma+neutral) mass

density $\rho_{t0} = \rho_{p0} + \rho_{n0}$ (e.g., Song et al. 2005). Using the transition frequency $\omega = \nu_{ni}$ for these waves, we obtain the Lundquist number

$$S'_{ni} \equiv \frac{\mu_0 V_{At0}^2}{\eta_P \nu_{ni}}. \quad (78)$$

The ratio of the convection to the resistivity terms in the plasma-neutral-modified MHD induction equation at the transition frequency ν_{in} (ν_{ni}) is S'_{in} (S'_{ni}). Thus, the motions of the plasma in response to magnetic field fluctuations at that frequency are frozen-in or resistive-slip, respectively, according to whether $S' \gg 1$ or $S' \ll 1$. We point out that the values of S'_{in} and S'_{ni} are nearly equal, since they are inversely proportional to the products $n_{p0}n_{n0}$ and $(n_{n0} + n_{p0})n_{p0}$, respectively, whereas $n_{p0} \ll n_{n0}$ through much of both atmospheres (Figure 2).

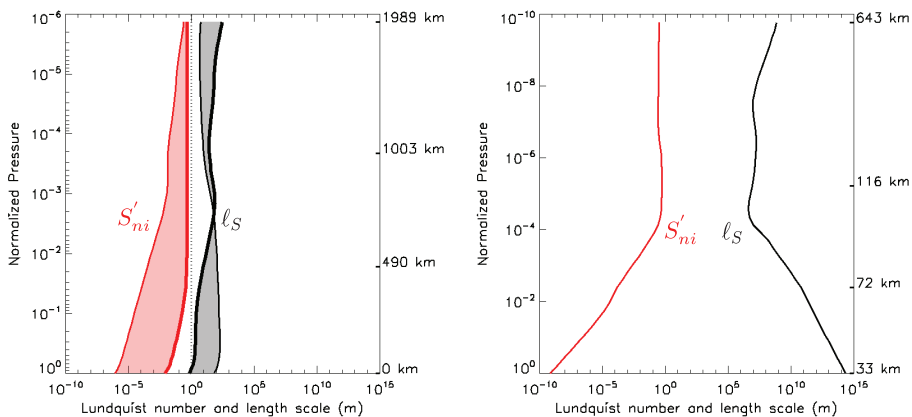


Fig. 11 Values of the Lundquist number S'_{ni} (red line), Equation (78), for Alfvén waves at the neutral/ion collision frequency ν_{ni} , and of the Lundquist scale (black line) ℓ_S , in m, Equation (79), using the Pedersen resistivities in the ALC7 chromosphere (left) and the TIMEGCM I/T (right). For the chromosphere (left panel), where the values depend on magnetic field strength, the lines for the two extreme values of $B_0 = 10$ G (thin lines) and $B_0 = 1000$ G (thick lines) in Equation (2) are shown, with a shaded area between them.

The values of the Lundquist number S'_{ni} at the lower transition frequency ν_{ni} are shown (red dashed curves) for the ALC7 chromosphere (left) and TIMEGCM I/T (right) in Figure 11. For the chromosphere (left panel), where the values depend on magnetic field strength, the lines for the two extreme values of $B_0 = 10$ G (thin lines) and $B_0 = 1000$ G (thick lines) in Equation (2) are shown, with a shaded area between them. The numbers are very small at low altitudes and approach, but do not quite attain, unity at high altitudes, in both cases. Consequently, the field lines resistively slip through the gas very readily at low altitudes, and they are not well frozen-in to the gas motions anywhere in the two atmospheres, for frequencies at or above the neutral/ion collision frequency ν_{ni} . Flux-freezing will occur only at still lower frequencies $\omega \leq \nu_{ni} S'_{ni}$, where the condition $S \geq 1$ can, in principle, be met. This is mostly likely to happen at high altitudes. The condition $S = 1$ is met at the Lundquist scale ℓ_S , defined using Equations (67) and then (78) as

$$\ell_S \equiv \frac{\eta_P}{\mu_0 V_{At0}} = \frac{V_{At0}}{\nu_{ni}} \frac{1}{S'_{ni}}. \quad (79)$$

The values of the Lundquist scale ℓ_S (in m) also are shown (black solid curves) for the ALC7 chromosphere (left) and TIMEGCM I/T (right) in Figure 11. We emphasize the very sharp contrast in the Lundquist scales for the two environments. In the chromosphere, in quiet average conditions, ℓ_S is everywhere below 1 km; only shorter-wavelength disturbances are resistivity-dominated, whereas an extended range of longer-wavelength disturbances on the Sun is convection-dominated, with increasingly frozen-in motions of gas and magnetic field. In the I/T, on the other hand, ℓ_S everywhere exceeds 9×10^4 km, or $15 R_E$; therefore, *all* Alfvénic disturbances at Earth are resistivity-dominated, with easy slippage of the partially ionized mixture relative to the magnetic field. This implies that any fluctuations in the geomagnetic field of significant amplitude must be driven by some external agent, rather than from within the I/T itself. Thus, excepting disturbances incident from the overlying magnetosphere, Earth’s magnetic field is approximately static. Meanwhile, both the photosphere and chromosphere serve as very active sources of strong magnetic-field fluctuations on the Sun. This confluence of circumstances – the disparate small/large Lundquist scales and the dynamic/static character of the chromospheric/ionospheric magnetic field – is responsible for the prevalence of magnetohydrodynamics in conceptualizing and quantifying processes in the chromosphere, on the one hand, and of electrodynamics in the I/T, on the other.

5.2 Neutral-Wind Driven Dynamos: An example of the E-J and v-B paradigms

In this section we discuss the phenomena of neutral-wind driven dynamos, and use it as an example of how the I/T and chromospheric communities use two different paradigms to explain the same phenomena. Another example will be given in §7.

At Earth, hydrodynamic forcing of the thermosphere neutral gas through pressure-gradient forces generated by differential solar radiative heating, Coriolis forces, and ion-drag forces create a global circulation of neutral winds. Additional forces on the neutral gas from Joule, collisional, and particle heating and from vertically propagating waves complicate the circulation. This neutral circulation is impressed upon the ionospheric plasma through collisions, causing the ions and electrons to undergo differential motion and leading to the production of currents and electric fields (e.g., Richmond and Thayer 2000).

Neutral winds on the Sun that, in principle, might drive I/T-like dynamo action through collisional coupling to the plasma originate in (1) the randomly shifting near-surface convection cells in the neutral-dominated photosphere and (2) the global atmospheric oscillations produced by acoustic and gravity waves. Hence, both the chromosphere and I/T may be subject to dynamo action in which inhomogeneous flows of neutrals couple to the plasma and drive persistent electric currents.

For clarity, we point out that the usual usage of the term “dynamo” in solar physics refers to amplification of seed magnetic fields to greater strengths by convective turnover, twisting, and differential shearing of the plasma alone. Such dynamo action is widely accepted to occur deep in the Sun’s fully ionized convective zone, producing the sunspot cycle of strong magnetic fields (e.g., Charbonneau 2010), and also may occur within the near-surface convective layers to produce flux concentrations at much smaller scales (e.g., Stein 2012). Neither of these dynamos relies upon plasma-neutral coupling to generate magnetic fields; indeed, neutrals generally are not considered in these models, especially in the deep Sun.

Below is a discussion of the neutral wind driven dynamo action from two points of view, dynamic and static electrostatics, which highlights the differing approaches of the chromospheric and I/T communities to common phenomena.

Proceeding from the full time-dependent equations of electromagnetics and plasma physics, Vasylūnas (2012) describes the sequence of events that establishes the distributed neutral-wind driven dynamo as follows:

1. Plasma motions \mathbf{V}_p are induced locally by collisions with the neutral wind \mathbf{V}_n ;
2. The resultant bulk plasma flow \mathbf{V}_p produces a persistent electric field, $\mathbf{E}_\perp = -\mathbf{V}_p \times \mathbf{B}_0$;
3. Gradients in \mathbf{E}_\perp along and across \mathbf{B}_0 generate magnetic perturbations $\delta\mathbf{B}$;
4. Electric currents \mathbf{J} arise due to gradients in the magnetic perturbations $\delta\mathbf{B}$;
5. Lorentz forces $\mathbf{J} \times \mathbf{B}_0$ drive MHD waves propagating away from the dynamo region, propagating flows and currents;

From the perspective of solar chromospheric physics, this chain of processes is intuitively appealing and non-controversial, although the details undoubtedly would be debated and additional study would be warranted to confirm its essential correctness. The chromosphere exhibits unceasing vigorous flows and strong magnetic variability. Therefore, explaining any chromospheric phenomenon based on a neutral-wind driven dynamo demands consistency with the full time-dependent equations and their implications from the outset. Exploratory work in this direction has been done on the quasi-static structuring of so-called network magnetic fields in the lanes of chromospheric convection cells by Henoux and Somov (1991), who call this process a “photospheric dynamo” (see also Henoux and Somov 1997). In addition, Kropotkin (2011) has proposed that the highly intermittent, collimated chromospheric upflows known as spicules, which are ubiquitous in the inter-cellular lanes, are powered by Alfvén waves driven by neutral-wind dynamo action. One of the necessary conditions for this “photospheric dynamo” is that the electrons are magnetized but the ions are not. This condition is realized in the 1D static model used here at about 500 km above the solar surface; for stronger background fields, this critical height is reduced due to the increase in the electron gyrofrequency. Krasnoselskikh et al. (2010) recently suggested that intense currents can be generated when magnetized electrons drift under the action of electric and magnetic fields induced in the reference frame of ions moving with the neutral gas, and that the resistive dissipation of these currents may be important for chromospheric heating.

From the perspective of ionospheric electrodynamics, Ohm’s law works very well on time scales longer than the ion-neutral collision time, which for the ionospheric M2 and M3 domains where primary dynamo activity occurs is only a few hundredths of a second to a few seconds. For periods exceeding this time scale, steady-state electrodynamic behavior results and electrostatic electric fields and divergence-free current densities can be assumed. Consequently, a static approach is often applied to describing the I/T’s neutral wind dynamo process:

1. Collisions with neutrals create plasma motions \mathbf{V}_p along \mathbf{V}_n . At the same time, oppositely directed $\mathbf{R}_i^{in} \times \mathbf{B}$ and $\mathbf{R}_e^{en} \times \mathbf{B}$ ion and electron drifts are created;
2. Electric currents \mathbf{J} resulting from the drifts drive charge separation between the ions and electrons;
3. An electric field \mathbf{E} is established in the dynamo region due to the charge separation;
4. Potential mapping along magnetic field lines due to rapid electron motions along \mathbf{B}_0 extends the electric field to increasingly remote regions;
5. $\mathbf{E} \times \mathbf{B}$ drifts create bulk plasma flows \mathbf{V}_p outside the dynamo region;

The first sequence above asserts that bulk plasma flows drive the electric field and distribute the dynamo along magnetic field lines through the intermediary of magnetic fluctuations having associated currents; thus, \mathbf{B} and \mathbf{V} have primary roles, while \mathbf{E} and \mathbf{J} are

secondary. The second sequence, on the other hand, states that current-generated electric fields distribute the dynamo along magnetic field lines and drive the bulk plasma flows; thus, \mathbf{E} and \mathbf{J} have primary roles, while \mathbf{B} and \mathbf{V} are secondary.

Vasyliūnas (2011, 2012) criticizes the electrodynamic interpretation as originating from extending intuition developed from the simple steady-state relations among the four variables – \mathbf{E} , \mathbf{J} , \mathbf{B} , \mathbf{V} – into time-varying situations, without due regard for the causal relationships implied by the dynamical equations. At scales long compared to the electron plasma oscillation period and large compared to the electron Debye length, the displacement current can be neglected in Ampères law and the time derivative of the particle current can be neglected in the generalized Ohms law, so there are no dynamical equations for $d\mathbf{E}/dt$ and $d\mathbf{J}/dt$ to be solved (Vasyliūnas 2005a). Instead, \mathbf{J} is related to \mathbf{B} through Ampères law, and \mathbf{E} is related to \mathbf{B} , \mathbf{V} , and \mathbf{J} through Ohms law. The dynamical equations that remain then contain only $d\mathbf{B}/dt$ and $d\mathbf{V}/dt$ among the four variables.

These dynamical issues also have been addressed more broadly and in several specific applications by Parker (1996a,b, 2007). He emphasizes that the converse procedure, eliminating \mathbf{B} and \mathbf{V} from the dynamical relations in favor of \mathbf{E} and \mathbf{J} , culminates in nonlinear integrodifferential equations that are nearly intractable to solve and obscure the underlying physical processes. The two alternatives are characterized as the B-V vs. E-J paradigms. He concludes that applying insights from laboratory experimental configurations – in which electric fields drive currents and generate magnetic fields – to anything beyond symmetric, static situations in the solar and terrestrial atmospheres is fraught with difficulty. The result has been much misunderstanding, and even misdirection of effort, in the two communities, according to Parker.

For the application to wind driven dynamos discussed here, we find that the difference in perspectives between the solar and ionospheric approach is driven by a difference in the plasma parameters. The chromosphere is ideal (non-resistive) on length scales much larger than a km, and so the electric field in the rest frame of the neutrals $\mathbf{E} + (\mathbf{V}_n \times \mathbf{B})$ is small. This leads to a magnetic perturbation and wave-propagation interpretation of the dynamo. In the resistive I/T however, there is an electric field in the rest frame of the neutrals created by charge separation due to ion electron drifts. This locally generated electric field propagates electrostatically along the field leading to a different interpretation of the phenomena.

The disparate perspectives imparted by these frameworks raise substantial barriers to communication and to making collaborative progress on otherwise similar phenomena. An explicit example of the challenges posed is provided in §7 on the Rayleigh-Taylor instability, which we analyze from both magnetohydrodynamic (chromospheric) and electrodynamic (ionospheric) perspectives.

5.3 Farley-Buneman Instability

As mentioned above, in the M2 domains of the chromosphere and I/T neutral flows perpendicular to the magnetic field can drive ions along with them but not electrons, and this produces currents. In the I/T, these currents comprise the electrojet current systems that occur in equatorial and auroral regions (Kelley and Hellis 1989; Schunk and Nagy 2000). The equatorial current system is driven by tidal E-layer neutral winds generated by daytime solar heating (the electric field is radial and the current is azimuthal). It peaks near the magnetic equator as a consequence of the nearly horizontal field lines. The auroral current system is associated with field-aligned, high-latitude currents driven by the solar-wind/magnetosphere interaction, as well as by precipitating energetic particles (Kamide 1982).

The M2 domains in both the I/T and chromosphere environments are an ideal place for the occurrence of the Farley-Buneman instability (Dimant and Sudan 1995; Fontenla 2005; Otani and Oppenheim 2006; Fontenla et al. 2008; Oppenheim and Dimant 2013; Madsen et al. 2013), which is a two-stream kinetic instability in which the ions are unmagnetized while the electrons are tied to the magnetic field (Farley 1963; Buneman 1963). Its thermodynamic consequences may not be very important compared to frictional heating, especially in the chromosphere where the spatial scales associated with the currents are so small that Joule heating outweighs the instability-related heating (Gogoberidze et al. 2009). However, there may be transient situations, such as the exhaust regions of magnetic reconnection in the chromosphere, where electron and ion fluids separate on small scales and the Farley-Buneman instability could be thermodynamically important. In the Earth's electrojet current systems, the plasma waves generated by the Farley-Buneman instability can provide an anomalous resistivity, which in turn modifies the ambient current systems and electric fields (e.g. Hamza and St.-Maurice 1995). When plasma waves are excited, the low frequency Ohm's law is incorrect, and as in the work of Hamza and St.-Maurice (1995), terms such as the electron and ion inertia should be included in the model.

5.4 Summary

Factors such as the resistive nature and the static magnetic field of the I/T have lead to a common approach where the electric field (\mathbf{E}) and electric current (\mathbf{J}) are the primary variables, and these are often used to describe how the I/T is driven (the E-J paradigm). An example was performed in our previous discussion of mobility of ions and electrons in an electric field. However, only very slow changes in the I/T can be accommodated by an electrostatic field. Furthermore, while for long time scales we can remove the dynamical equations for $d\mathbf{E}/dt$ and $d\mathbf{J}/dt$ and have \mathbf{B} and \mathbf{V} be the primary variables (V-B paradigm), the converse is not true.

At the same time, using the E-J paradigm may allow one to arrive at an equivalent result as the V-B paradigm. This was achieved in a general sense for wind-driven dynamos and will be shown to be possible for the Rayleigh-Taylor instability in a following section.

6 Energy Transfer

In this section we first discuss the major contributions to the energy balance in both the chromosphere and I/T, then go on to discuss the general process of conversion of electromagnetic energy to thermal and kinetic energy. Then we present ideas on the flux and dissipation of electromagnetic energy in the two environments, and the role of plasma-neutral collisions in this process.

6.1 Major Contributions to Energy Balance

6.1.1 Chromosphere

The bulk of the chromosphere is a few thousand degrees hotter than the underlying photosphere. It also is far cooler than the corona above, but is so much denser that it requires roughly ten times more heat input than the corona (when measured as a height-integrated

rate of change of energy density) to maintain its elevated temperature. Hydrogen ionization in the chromosphere acts to balance heating even as the density drops with height. This is because the large abundance and ionization energy of hydrogen allows the ionization of hydrogen to absorb energy, while this ionization creates free electrons which excite heavier species such as iron, magnesium and calcium, resulting in steady radiative cooling. The heating of the chromosphere, which must account for these radiative losses, comes from a combination of collisional effects (Joule, frictional, and viscous heating) and compressional heating. The Joule and viscous heating mechanisms become relatively more important on progressively smaller scales, such as those associated with current sheets, shocks, or wave motions. The first of these phenomena is a DC mechanism, while the last two are AC in nature.

A large class of potential heating mechanisms for the chromosphere is derived from the fact that the turbulent convection zone below is capable of supplying a flux of wave energy into the chromosphere. Previously suggested heating mechanisms for the chromosphere have included acoustic wave dissipation, though it is unclear if acoustic waves can propagate high enough to deposit their energy in the chromosphere (Biermann 1946; Schwarzschild 1948; Ulmschneider 1990; Fossum and Carlsson 2005a,b, 2006; Kalkofen 2007). MHD waves have more recently been investigated, particularly Alfvén waves as they can propagate upwards along magnetic fieldlines into the upper chromosphere (e.g. De Pontieu et al. 2007b; Tomczyk et al. 2007). However, although plasma-neutral collisions and viscous effects can potentially dissipate wave energy in the chromosphere, it is not fully understood whether the dissipation and heating of the waves provided by the convection zone is sufficient to counter the radiative losses (De Pontieu 1999; Leake et al. 2005; De Pontieu et al. 2007a; Hasan and van Ballegoijen 2008; Goodman 2011; Song and Vasylūnas 2011), although recent simulations of Joule-dissipated reflected Alfvén waves in the lower chromosphere (below 400 km) by Tu and Song (2013) suggest that the dissipated wave energy can account for the losses there.

Recently, the dissipation of Alfvén wave energy by other mechanisms has been considered, such as non-linear interactions, mode conversion, and resonant heating. Narain and Ulmschneider (1990) present a more comprehensive literature review of these types of investigations. Low frequency mechanisms, such as the dissipation of currents perpendicular to the magnetic field by Pedersen resistivity (Leake and Arber 2006; Arber et al. 2007, 2009; Khomenko and Collados 2012; Martínez-Sykora et al. 2012; Leake and Linton 2013), magnetic reconnection (Parker 1983, 1988; Dahlburg et al. 2003; Dahlburg et al. 2005; Klimchuk 2006; Goodman and Judge 2012), and neutral-wind dynamos (Krasnoselskikh et al. 2010), have also been investigated. Clearly, there is a “zoo” of possible chromospheric heating mechanisms, and a complete review of the chromospheric heating problem is one which is outside the scope of this review. What is also clear is that this heating is occurring in a region of highly coupled ionized plasma and neutral gas, and that plasma-neutral interactions are vital to heating of the chromosphere by bulk motions.

6.1.2 Ionosphere

The contributions to the energy transfer in the ionosphere/thermosphere are better understood than those in the chromosphere. However, the large variability in time and space of these mechanisms and the relative contributions to the overall heating and cooling remain challenges to understanding the thermal properties of the system. The lower amount of plasma-neutral and electron-ion coupling in the I/T (based on the collision frequencies), compared to the chromosphere, means that the individual heating of the constituents and

their thermal coupling must be considered. The dominant heating term for the neutral gas is absorption of UV/EUV radiation. The UV/EUV energy flux from the Sun is ~ 4 orders of magnitude less than at visible wavelengths (e.g., Tobiska et al. 2000), but is of sufficient energy to form the ionosphere through photoionization (by contrast, ionization is predominantly collisional excitation in the chromosphere), produce secondary ionization, energize gas emissions in airglow, and raise neutral and plasma temperatures to more than one thousand degrees. The UV/EUV flux is nearly completely absorbed between 80 and 200 km altitude. However, the most dynamic term of the energy equation given in Equation (13) is the collisional exchange term between ions and neutrals. This frictional heating of the neutral gas by collisions with ions can be as significant as solar heating during geomagnetic storms and represents the most variable source of energy to quantify in the I/T energy equation. Other internal processes within the weakly ionized mixture, such as thermal exchange between the plasma and neutral gas, lead to differing thermal structure with height for the plasma and neutral gas, as indicated in Figure 1.

It is worth examining high latitude heating further as it is central to the aims of this paper. It has been recognized for some time that the observed thermal structure of the I/T is only adequately represented when energy resulting from solar wind interactions with the Earth's magnetosphere is included in the I/T energy budget. This energy to the I/T is manifested in the form of Poynting flux (see below) and particle kinetic energy flux. The partitioning of auroral kinetic energy (KE) flux in the 80-200 km altitude range is roughly 50 % heating, 45 % ionization, and 5 % optical production (e.g., Thayer and Semeter 2004). Typically the energy flux by particles is less than that due to electromagnetic processes. Electromagnetic fields transfer energy from the plasma to the neutral gas on the neutral-ion collisional timescale. Other processes, at times, prove important in the energy balance of the plasma or neutral gas in the I/T. Ion frictional heating at high latitudes is an effective process that can lead to high ion temperatures in the M2 region. This heat is transferred to the neutral gas by thermal differences between the neutrals and ions, contributing to the heating of the neutral gas. Farley-Buneman (F-B) instability in the M2 region is a common occurrence in the I/T. At high latitudes, where strong electric fields are present, the F-B instability can lead to very efficient plasma wave heating of electrons in the M2 region with temperatures exceeding 2000 K. However, this does not lead to any significant change in the ion and neutral temperature as they have much greater thermal heat capacity.

6.2 Frictional Heating

One important contribution to the energy balance in both environments is the conversion of electromagnetic energy to thermal and kinetic energy, $\mathbf{E} \cdot \mathbf{J} > 0$. This is commonly expressed as the sum of two terms: frictional (including Joule) heating and work done (e.g. Lu et al. 1995; Thayer et al. 1995; Fujii et al. 1999; Thayer 2000; Richmond and Thayer 2000; Goodman 2000, 2004; Vasylūnas and Song 2005). In a non-relativistic, quasi-neutral plasma, \mathbf{E} is frame-dependent while \mathbf{J} is not, hence the relationship between \mathbf{E} and \mathbf{J} is frame-dependent. The electric field in a frame moving with velocity \mathbf{V} is $\mathbf{E}^V \equiv \mathbf{E} + (\mathbf{V} \times \mathbf{B})$ and

$$\mathbf{E} \cdot \mathbf{J} = \mathbf{E}^V \cdot \mathbf{J} - (\mathbf{V} \times \mathbf{B}) \cdot \mathbf{J} = \mathbf{E}^V \cdot \mathbf{J} + (\mathbf{J} \times \mathbf{B}) \cdot \mathbf{V} \quad (80)$$

thus, the electromagnetic energy conversion rate $\mathbf{E} \cdot \mathbf{J}$ is the sum of a heating term $\mathbf{E}^V \cdot \mathbf{J}$ and a term which is the rate work is done by the Lorentz force on the flow \mathbf{V} .

However, the choice of rest frame (\mathbf{V}) for the term $\mathbf{E}^V \cdot \mathbf{J}$ can alter the interpretation of frictional heating in the energy equation. As shown in §3.5, the equation for \mathbf{E}^V contains

different terms depending on the choice of rest frame (plasma, neutral, or center of mass). One should also note that in the upper chromosphere where the ionization level increases, the center of mass frame differs significantly from the neutral frame, which changes the equation for \mathbf{E}^V . Hence the term frictional heating can have physically different meanings depending on the rest frame chosen. For example, choosing the rest frame of the plasma, and using the low-frequency approximation to the generalized Ohm's law in §3.5, Equation (33), the frictional heating is

$$\mathbf{E}^P \cdot \mathbf{J} = (\mathbf{E} + \mathbf{V}_p \times \mathbf{B}) \cdot \mathbf{J} = \eta_{\parallel} \mathbf{J}^2, \quad (81)$$

and is just the Ohmic *Joule heating* term, related to the parallel resistivity (electron-ion collisions plus coupled electron-neutral and ion-neutral collisions). It should be noted that care must be taken to ensure that the assumptions made to obtain the low frequency limit are not violated when discussing frictional heating for a particular phenomena, e.g., wave propagation and dissipation (where the frequency must be smaller than the ion-neutral collision frequency). Choosing the rest frame of the neutrals the frictional heating is (using Equation (35) this time)

$$\mathbf{E}^* \cdot \mathbf{J} = (\mathbf{E} + \mathbf{V}_n \times \mathbf{B}) \cdot \mathbf{J} = \eta_{\parallel} \mathbf{J}^2 + \eta_C \mathbf{J}_{\perp}^2. \quad (82)$$

This $\mathbf{E}^* \cdot \mathbf{J}$, often called Joule heating by I/T researchers, is related to the Ohmic Joule heating (in the rest frame of the plasma), \mathbf{E}^P , by

$$\begin{aligned} \mathbf{E}^* \cdot \mathbf{J} &= \mathbf{E}^P \cdot \mathbf{J} - [(\mathbf{V}_p - \mathbf{V}_n) \times \mathbf{B}] \cdot \mathbf{J} = \mathbf{E}^P \cdot \mathbf{J} + (\mathbf{J} \times \mathbf{B}) \cdot (\mathbf{V}_p - \mathbf{V}_n) \\ &\approx \mathbf{E}^P \cdot \mathbf{J} + \rho_i v_{in} |\mathbf{V}_p - \mathbf{V}_n|^2 \end{aligned} \quad (83)$$

which assumes that Lorentz and plasma-neutral drag forces dominate in the plasma (ion + electron) equation of motion ($\mathbf{J} \times \mathbf{B} \approx \mathbf{R}_{in}$), and inertial, pressure and gravity terms can be neglected, as discussed in Vasyliūnas and Song (2005). Hence the conventional ionospheric Joule heating, in the rest frame of the neutrals, is the heating in the rest frame of the plasma plus heating due to plasma-neutral collisions. The first term, the plasma Joule heating, is strictly *Ohmic* Joule heating in the sense that the electric field in the rest frame of the plasma accelerates electrons and ions, creating a current proportional to the electric field, and this current is limited mainly by electron-neutral collisions. Vasyliūnas and Song (2005) explain that this Ohmic Joule heating goes into the thermal energy of the plasma, while the term due to plasma-neutral collisions distributes energy between the plasma and neutrals equally. The last term in Equation (83) can also be thought of as a term proportional to the difference in work done by the Lorentz force on the plasma relative to work done by the Lorentz force on the neutrals.

In addition to the frame-dependence issue stated above, care must be taken when discussing energy exchange (thermal and kinetic) between the electron, ion and neutral components, and the energy balance of the mass-averaged plasma-neutral mixture. This is discussed in detail in Vasyliūnas and Song (2005).

Figure 10 shows that $\eta_C \gg \eta_{\parallel}$ for most of the ionosphere, and for a reasonable proportion of the chromosphere. Using this fact, and comparing Equations (81) and (82), tells us that for most of the ionosphere and much of the chromosphere, the frictional heating has only a tiny contribution from the Ohmic Joule heating, and is dominated by the contribution from collisions of plasma with neutrals. The relationship of ionospheric Joule heating to neutral gas frictional heating was demonstrated in descriptions put forward by St. Maurice and Schunk (1981).

A common approach in chromospheric physics is to assume a single-fluid model. Recall the individual species (α) total energy equation:

$$\frac{\partial \mathcal{E}_\alpha}{\partial t} + \nabla \cdot (\boldsymbol{\varepsilon}_\alpha \mathbf{V}_\alpha + \mathbf{V}_\alpha \cdot \mathbb{P}_\alpha + \mathbf{h}_\alpha) = \mathbf{V}_\alpha \cdot \left(q_\alpha n_\alpha \mathbf{E} + \mathbf{R}_\alpha^{\alpha\beta} + m_\alpha n_\alpha \mathbf{g} \right) + \sum_{\beta \neq \alpha} Q_\alpha^{\alpha\beta} + S_\alpha + U_\alpha \quad (84)$$

where $Q_\alpha^{\alpha\beta}$ is the rate of change of total energy of the species α due to collisions with species β , and $\boldsymbol{\varepsilon}_\alpha = \rho_\alpha v_\alpha^2 / 2 + P_\alpha / (\gamma - 1)$. Summing over all species α gives the total energy equation for the mixture:

$$\frac{\partial \mathcal{E}_{CM}}{\partial t} + \nabla \cdot (\boldsymbol{\varepsilon}_{CM} \mathbf{V}_{CM} + \mathbf{V}_{CM} \cdot \mathbb{P}_{CM} + \mathbf{h}_{CM}) = \mathbf{E} \cdot \mathbf{J} + \rho_{CM} \mathbf{V}_{CM} \cdot \mathbf{g} + S_{CM} + U_{CM} \quad (85)$$

where the following mass-averaged quantities are defined in a similar vein as Vasyliūnas and Song (2005):

$$\begin{aligned} \rho_{CM} &= \sum_\alpha \rho_\alpha, \quad \mathbf{V}_{CM} = \frac{\sum_\alpha \rho_\alpha \mathbf{V}_\alpha}{\sum_\alpha \rho_\alpha} \\ \boldsymbol{\varepsilon}_{CM} &= \frac{\rho_{CM} V_{CM}^2}{2} + \frac{P_{CM}}{\gamma - 1} + \frac{\rho_{CM} \xi_n (1 - \xi_n) W^2}{2}, \quad P_{CM} = \sum_\alpha P_\alpha \\ \mathbb{P}_{CM} &= \sum_\alpha \mathbb{P}_\alpha + \rho_{CM} \xi_n (1 - \xi_n) \mathbf{W} \mathbf{W} \\ h_{CM} &= \sum_\alpha h_\alpha + \xi_n \mathbf{W} \cdot \left[\left(\frac{1}{\xi_n} - 1 \right) P_n - (P_i + P_e) - (1 - \xi_n) \frac{\rho_{CM}^2 \mathbf{W}^2}{2} \right] \\ &\quad - \xi_n \mathbf{W} \cdot \left[\left(\frac{1}{\xi_n} - 1 \right) \mathbb{P}_n - (\mathbb{P}_i + \mathbb{P}_e) \right] \end{aligned}$$

All the terms in the single-fluid equations reflect the total description of the plasma-neutral mixture. However, the individual species equations contain terms that reflect the species description within the mixture, which may not affect the behavior of the mixture as a whole. Thus, terms such as the collisional terms $\mathbf{V}_\alpha \cdot \mathbf{R}_\alpha^{\alpha\beta}$ and $Q_\alpha^{\alpha\beta}$ cancel when summed over the whole mixture. The individual species approach is a path-dependent system that accounts for the processes between the different species that lead to macroscopic changes in the system. The single-fluid approach is independent of the path by which energy is transferred amongst the species in its description of the macroscopic behavior of the mixture.

The term $\mathbf{E} \cdot \mathbf{J}$ comes from $\sum_\alpha \mathbf{V}_\alpha \cdot (q_\alpha n_\alpha \mathbf{E})$. As discussed above, the term $\mathbf{E} \cdot \mathbf{J}$ can be written as

$$\mathbf{E} \cdot \mathbf{J} = \mathbf{E}^{CM} \cdot \mathbf{J} + (\mathbf{J} \times \mathbf{B}) \cdot \mathbf{V}_{CM} \quad (86)$$

where $\mathbf{E}^{CM} = \mathbf{E} + (\mathbf{V}_{CM} \times \mathbf{B})$ is the electric field in the rest frame of the mass-averaged plasma-neutral mixture. The term $\mathbf{E} \cdot \mathbf{J}$, valid for any frame of reference, goes into the mass-averaged total (kinetic + thermal) energy of the plasma-neutral mixture. In the typical analysis of the total energy of a fluid, one can generally remove the kinetic part by subtracting the momentum equation dotted into the velocity to obtain the thermal energy equation. Looking at Equation (86) above, one may think that $\mathbf{E} \cdot \mathbf{J}$ can be split into a heating term $\mathbf{E}^{CM} \cdot \mathbf{J}$ which goes into the thermal energy of the center of mass fluid, and a work term $(\mathbf{J} \times \mathbf{B}) \cdot \mathbf{V}_{CM}$, which goes into the kinetic energy. However, as was discussed by Vasyliūnas and Song (2005), and looking at Equation (85) and the mass averaged energy, pressure, and heat flux defined above, one can see that the single-fluid has a thermal energy density that

includes a contribution from kinetic energy of relative motion between plasma and neutrals. It also has a non-isotropic pressure and a non-zero heat flux even if these are absent in the individual plasma and neutral fluids.

As we did for the Joule heating in the rest frame of the neutrals, we can write the heating term $\mathbf{E}^{CM} \cdot \mathbf{J}$ as the sum of the Ohmic Joule heating term and frictional heating due to the relative flow velocity of the mass-averaged mixture and the ionized plasma

$$\mathbf{E}^{CM} \cdot \mathbf{J} = \mathbf{E}^P \cdot \mathbf{J} - [(\mathbf{V}_p - \mathbf{V}_{CM}) \times \mathbf{B}] \cdot \mathbf{J} = \mathbf{E}^P \cdot \mathbf{J} + (\mathbf{J} \times \mathbf{B}) \cdot (\mathbf{V}_p - \mathbf{V}_{CM}). \quad (87)$$

Due to the low ionization level in the I/T and the lower and middle chromosphere, this is approximately the same as Equation (83) as $\mathbf{V}_{CM} \approx \mathbf{V}_n$ in these regions. Hence the frictional heating of the plasma-neutral mixture is dominated by collisions between plasma and neutrals, with a very small contribution from electron collisions (Ohmic) Joule heating.

Having seen how the electromagnetic energy is converted into thermal and kinetic energy, we can now examine the evolution of this energy. The use of Poyntings theorem, derived directly from Maxwells equations, can relate the total energy equation with the equation for electromagnetic energy when written in the form

$$\frac{\partial}{\partial t} \left(\frac{B^2 + E^2/c^2}{2\mu_0} \right) + \nabla \cdot \left(\frac{\mathbf{E} \times \mathbf{B}}{\mu_0} \right) + \mathbf{E} \cdot \mathbf{J} = 0 \quad (88)$$

The first term is the time-rate-of-change of electromagnetic energy density. The second term is the divergence in the Poynting vector $\mathbf{S}_p \equiv \mathbf{E} \times \mathbf{B}/\mu_0$, or the electromagnetic energy flux, and the last term is the rate of electromagnetic energy transferred to the medium. Clearly the last term couples this equation with the single fluid total energy equation described above, and connects electromagnetic energy changes with changes in the total energy of the gas mixture. Poyntings theorem applies to all types of electromagnetic interactions, ranging from electromagnetic waves to steady-state fields. It is this electromagnetic exchange between the fields and the gas mixture that is of interest in contrasting the chromosphere and the I/T.

6.3 The Role of Plasma-neutral Coupling in Energy Transfer

As mentioned above, heating $Q \equiv \mathbf{E}^V \cdot \mathbf{J}$ where \mathbf{E}^V is in the neutral or center of mass frame of the chromosphere and I/T contains a component due to plasma-neutral collisions. This component can dominate over Ohmic Joule heating when $\eta_P > \eta_{\parallel}$, or $\sigma_P < \sigma_{\parallel}$. Hence plasma-neutral collisions could play a major role in the conversion of electromagnetic energy into thermal energy.

We can discuss the efficiency of this heating without referring to a particular mechanism for the generation of currents. In §4.2 we presented a description of the altitude variation of electrical currents of a given electric field. In particular, we looked at how the contributions to the current perpendicular to the magnetic field \mathbf{J}_{\perp} by Pedersen ($\mathbf{J}_P \equiv \sigma_P \mathbf{E}_{\perp}^*$) and Hall ($\mathbf{J}_H \equiv -\sigma_H \mathbf{E}_{\perp}^* \times \hat{\mathbf{b}}$) currents varied as the mobilities of the electrons and ions varied. Let us now look at the contributions to the heating ($\mathbf{E}^* \cdot \mathbf{J}$). Goodman (2004) showed that when the heating is written as

$$Q \equiv \mathbf{E}^* \cdot \mathbf{J} = \frac{J_{\parallel}^2}{\sigma_{\parallel}} + \frac{\sigma_P J_{\perp}^2}{\sigma_P^2 + \sigma_H^2} \equiv Q_{\parallel} + Q_P \quad (89)$$

then the efficiency of Pedersen heating Q_P , the ratio of Pedersen heating to its maximal value, obtained when the perpendicular current \mathbf{J}_\perp is all Pedersen current and no Hall current, can be expressed as

$$R_Q \equiv Q_P/Q_{P,max} = \frac{\sigma_P^2}{\sigma_P^2 + \sigma_H^2}. \quad (90)$$

This tells us how efficiently the mechanism that generates \mathbf{E}_\perp^* heats the atmosphere. We discuss the general nature of R_Q here and return to such mechanisms later in this section.

Figure 12 shows this efficiency for both chromosphere and I/T, including the results for the three different magnetic field models for the chromosphere. Also shown is the temperature (we show the neutral temperature only for the I/T).

Due to the above definition of R_Q , when $\mathbf{J}_\perp \approx 0$, $R_Q \approx 1$. Otherwise, R_Q is close to 1 when the perpendicular current is dominated by Pedersen current. Recall from §4.2 that this occurs just below the lower peak, and just above the upper peak, in the Pedersen mobility. Near the lower peak, the conductivity (and resistivity) is isotropic and Joule heating and Pedersen heating are the same. Near the upper peak, $\eta_P > \eta_\parallel$ and Pedersen heating dominates over Joule heating. Between these two regions of $R_Q \approx 1$ is a region where the Hall current dominates the perpendicular current and so R_Q is minimal. Thus the transition of interest is from the minimal efficiency near the Hall mobility peak up to the region above the upper peak in the Pedersen resistivity. This transition altitude occurs somewhere around the temperature minimum. In fact, the efficiency increases from its minimum to 1 with altitude as the term $\Gamma \equiv \xi_n k_e k_{in}$ increases from below to above 1. This can be observed by comparing Figure 12 and Figure 7.

Goodman (2000, 2004) proposed that the increase in Pedersen heating as Γ undergoes the transition from much less than 1 to much more than 1 may explain the source of chromospheric heating that has so puzzled solar physicists. Moreover, theoretical work by Song and Vasylūnas (2011) and numerical simulations by Tu and Song (2013) have found that given an atmospheric profile similar to the one used here, the heating due to damping of propagating Alfvén waves is predominantly Ohmic Joule heating below the temperature minimum, and plasma-neutral frictional (or Pedersen) heating above. These recent simulations suggest a possible explanation for the presence of the temperature minimum. However, such simulations, which contain no energy equation and thus no self-consistent heating, do not produce the observed temperature structure of the chromosphere, but use an initial condition which is designed to look like observationally inferred 1D profiles. The physics of thermal conduction from the hot corona, as well as radiative processes, must be included for the simulations to obtain self-consistent heating rates. Future simulations that investigate heating mechanisms must be able to create the correct temperature profile self-consistently (for example of attempts to do so see the papers of Carlsson and Leenarts (2012) and Abbett (2007)) as well as including well-resolved physical mechanisms (such as Alfvén wave heating). This is the largest obstacle to identifying chromospheric heating mechanisms through numerical and theoretical investigations.

Pedersen current dissipation is a general mechanism for dissipating the energy in electric currents which are orthogonal to the magnetic field. Therefore any process which drives such currents is damped by this mechanism. To actually estimate Q_P and not just R_Q , a process must first be identified and a physical model of the process must then be created. The degree of the damping of the process which drives perpendicular currents depends on two things: the reservoir of energy to drive the currents, and the amount of energy which is used to generate and maintain electric fields to support the currents. In the I/T, the actual value of Q_P is small compared to the dominant processes of heating. Thus, we just consider the

chromosphere in this discussion. In the chromosphere transient electric fields are created by general time-dependent flows, such as convection zone flows, wave motions, and magnetic reconnection sites.

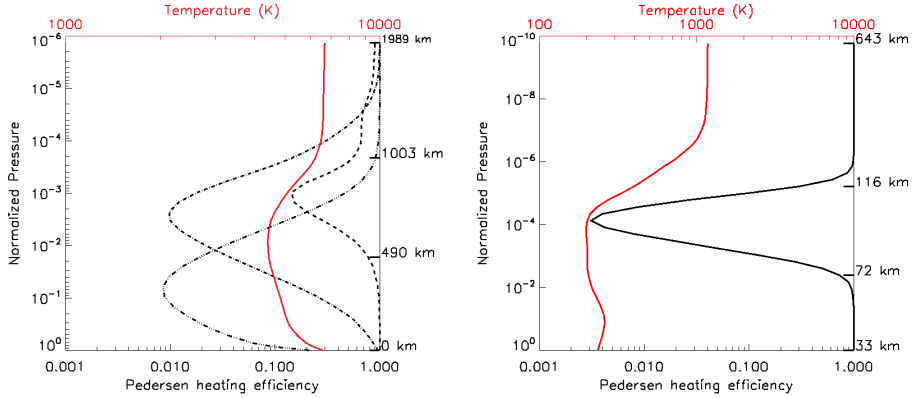


Fig. 12 Pedersen heating efficiencies (black lines) in the ALC7 chromosphere (left) and in the TIMEGCM I/T (right). Also shown is the electron temperature (red line). For the chromosphere, the three black lines show the heating efficiencies for the three magnetic field strengths of 10 G (dashed), 100 G (dot-dashed), and 1000 G (dot-dot-dashed).

The chromosphere and I/T are atmosphere regions commonly characterized as weakly ionized mixtures permeated by magnetic field lines. These regions are subject to electromagnetic energy flux from neighboring regions of electrical energy generation. On the Sun, the turbulent convection zone beneath the chromosphere creates a spectrum of oscillations, in the range 0.5 to 1000 minutes, or 10^{-5} to 0.03 Hz (e.g., Cranmer and van Ballegoijen 2005). In the high plasma β_p , highly ionized convection zone there are three types of fluid (non-kinetic) waves: Alfvén waves, isotropic sound waves, and magneto-acoustic waves that are guided by the magnetic field (Zaqarashvili et al. 2011). The last two of these types are compressional and most likely do not propagate into the upper chromosphere. However, the changing conditions with height change the nature of these waves as they propagate into the chromosphere. Alfvén waves from the convection zone cause the oscillation of ionized plasma in the presence of a magnetic field which provides a mechanism for the conversion of the kinetic energy of convection into electrical energy in a manner equivalent to a magnetohydrodynamic (MHD) electrical generator. In this case, $\mathbf{E} \cdot \mathbf{J}$ is negative and mechanical energy is converted to electromagnetic energy which propagates with the waves into the chromosphere. Thus there is an influx of electromagnetic energy from the convection zone into the chromosphere. Much work has been done on the propagation and dissipation of Alfvén waves into the chromosphere from the convection zone (e.g. De Pontieu 1999; Leake et al. 2005; De Pontieu et al. 2007a; Hasan and van Ballegoijen 2008; Goodman 2011; Song and Vasyliūnas 2011; Tu and Song 2013).

A similar situation occurs above the I/T. The Earth's magnetosphere undergoes convection due to the interaction of the solar wind with the magnetosphere. There is a net downflow of energetic particles and Alfvén waves. Thus the Earth's magnetosphere can also be considered an MHD electrical generator converting solar wind mechanical energy to electri-

cal energy that is transferred to the I/T along highly conducting magnetic field lines (Thayer and Semeter 2004; Song and Vasyliūnas 2011; Tu et al. 2011).

Both atmospheres exhibit an inflow of electromagnetic energy in the form of waves from outside regions. The chromosphere experiences a large drop in density, and this implies that for a given field strength, the Alfvén speed rapidly increases. If the length scale of the increase is comparable to the wavelength of an upwardly propagating wave then reflection can occur, similar to the situation in the Ionospheric Alfvén Resonator (see Poliakov and Rapoport 1981, and references therein). Thus the chromosphere has downwardly propagating reflected waves. High frequency (1-100 Hz) Alfvén waves generated from coronal reconnection sites (e.g. Voitenko and Goossens 2002; Kigure et al. 2010; Edmondson et al. 2011) may also propagate downward into the chromosphere, as well as leaking coronal loop oscillations caused by disturbances in the corona (e.g. Nakariakov et al. 1999; Ofman 2002). In the I/T, Alfvén waves and quasi-static fields imposed by the magnetosphere are manifested in the form of auroral arcs, field-aligned currents and electric fields that constitute the electromagnetic energy flux into the region (e.g. Erlandson et al. 1994; Tung et al. 2001; Keiling et al. 2003; Drob et al. 2013)

The chromosphere and Earth's I/T are conductors (the M2-domain in particular) and can convert the electrical energy of the waves to thermal and mechanical energy of the neutral gas ($\mathbf{E} \cdot \mathbf{J} > 0$). As shown previously, the plasma-neutral collisions dominate over electron-ion Ohmic Joule heating, and must play a vital role in the dissipation of EM wave energy in both environments. For a finite superposition of waves with commensurate frequencies, one can use Poynting's theorem, Equation (88), averaged over a wave period, to give

$$\langle \nabla \cdot \mathbf{S}_p \rangle = \langle \mathbf{E} \cdot \mathbf{J} \rangle . \quad (91)$$

Integrating over a volume of atmosphere (be it chromosphere or I/T), one can use the integral divergence theorem to express the rate at which electromagnetic energy is converted into both thermal energy and bulk flow kinetic energy in the volume as

$$Q \equiv \int_V \langle \mathbf{E} \cdot \mathbf{J} \rangle dV = \int_S \langle \mathbf{S}_p \cdot \hat{\mathbf{n}} \rangle \quad (92)$$

i.e., the surface integral of the Poynting vector normal to the surface of the volume. Thus the convergence of Poynting flux into the volume can tell us something about the frictional heating rate inside the volume. Examples of this have been performed in polar regions of the Earth's atmosphere (e.g. Kelley et al 1991; Thayer and Semeter 2004) and for simple models of the Sun's chromosphere (Leake et al. 2005; Goodman 2011; Song and Vasyliūnas 2011; Tu and Song 2013).

Looking at the volume integral of the thermal energy equation (85), one can see other terms other than frictional heating which add to the thermal energy in the volume V. The terms represent processes such as the thermal flux through the boundary S of V due to work done by compressive and viscous forces acting at S on the fluid in V. This is in addition to the dissipative mechanisms which are resistive, viscous and compressive, such as the shock absorption of magneto-acoustic waves that are created by conversion of Alfvén waves, and viscous dissipation of non-linearly interacting Alfvén waves, are also important in the chromosphere, if not for the I/T (Narain and Ulmschneider 1990). The various forcing and dissipation mechanisms and the scales on which they operate present a significant challenge for the use of convergence of the Poynting flux to understand the heating of the two environments. In addition there are exchange processes for other quantities, such as particle kinetic energy (from the magnetosphere into the I/T and from flares in the corona

into the chromosphere), which complicate matters further. However, even if plasma-neutral collisions are not a main contributor to the heating in the chromosphere and I/T, they significantly affect the propagation of waves (e.g. Song et al. 2005; Zaqarashvili et al. 2011), and thus must be included in theoretical and numerical investigations into wave heating.

7 Rayleigh-Taylor Instability

7.1 Occurrence in the Sun's and Earth's atmospheres

The unsteady transfer of energy and mass in the dynamic atmospheres of both the Earth and the Sun often creates configurations in which dense matter overlies tenuous matter. In the presence of gravity, such configurations can be unstable to disturbances that exchange the overlying heavy fluid with the light fluid below. This evolution produces falling spikes of the former and rising bubbles of the latter, and the atmosphere evolves toward a state of lower gravitational potential energy. The linear stability of such unstable hydrostatic equilibria has been examined both for broadly distributed layers of continuously upward-increasing mass density, in which the characteristic wavelength of the disturbances is comparable to or smaller than the layer thickness (Rayleigh 1882), and for very narrow layers of effectively discontinuous upward jumps in mass density, in which the characteristic wavelength of the disturbances is much larger than the thickness of the layer (Taylor 1950).

At Earth, a continuously distributed negative gradient in density of charged plasma is created by the nonuniform production and loss of ions. At high altitudes, relatively few atoms are available to be ionized by the absorption of EUV energy from the Sun, so low-density plasma is created; at low altitudes, more ions are created because of the higher neutral density, but rapid recombination with electrons again yields low-density plasma. The result is a plasma density that peaks at an intermediate height of about 300 km (see Figure 2), and at altitudes below that it can be unstable to the Rayleigh-Taylor instability. Typically this occurs after sunset. Disturbances generate large-scale density depletions in the lower I/T that can rise to high altitudes (over 1000 km). Severe disruptions in the radio transmission characteristics of Earth's atmosphere are one consequence of onset of this phenomenon, commonly known as "spread-F" (see review by Woodman 2009). Additional fine structure is induced at the sides of the rising bubbles by non-uniformities in the winds of the coexisting neutral component of the atmosphere.

On the Sun, negative density gradients can be produced by the plasma pressure deficit present in regions of strong magnetic field, which compensates for the magnetic pressure enhancement there and maintains an overall balance of the total pressure force across the magnetic region. The magnetic Rayleigh-Taylor instability creates filamentary structures in newly emerged flux regions that are long parallel to the field lines (to avoid bending them) and short perpendicular to the field (to grow as fast as possible); see Isobe et al. (2005) and Isobe et al. (2006) for these results and applications to arch filament systems on the Sun, and Arber et al. (2007) for an application to the dynamic emergence of a new active region. The Rayleigh-Taylor instability also has been invoked in observations and modeling of hedgerow solar prominences (Berger et al. 2010; Hillier et al. 2011, 2012a,b). Prominences (e.g., Tandberg-Hanssen 1995) are large-scale clouds of relatively cold and dense material, consisting mostly of neutral hydrogen atoms, suspended on magnetic field lines within the surrounding hot and tenuous coronal plasma, comprised primarily of fully ionized hydrogen. In these observations and models of hedgerow solar prominences, bubbles

of low-density, high-temperature coronal plasma well up from below and intrude into the high-density, low-temperature body of the prominence above.

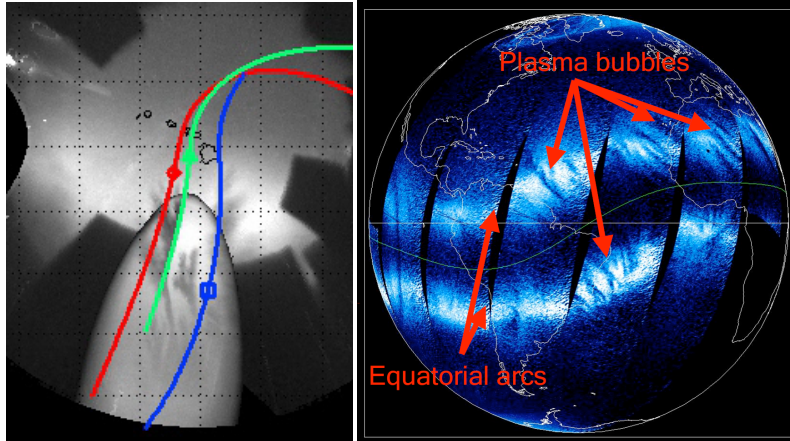


Fig. 13 Left: Rayleigh-Taylor instabilities in the heliosphere. Airglow measurements showing evidence of the Rayleigh-Taylor instability in the terrestrial I/T. The dark shapes in the gray color-scale are expanding bubbles of plasma due to the instability. Colored tracks (red/green/blue) are paths of Global Positioning System (GPS) satellites. Figure is reprinted courtesy of J. Makela and *Annales Geophysicae*. Right: Global 135.6 nm brightness map indicating plasma depletions. Figure is reprinted courtesy of F. Kamalabadi and *Annales Geophysicae*

The qualitative similarities in these phenomena at the Earth and Sun are illustrated by the images in Figures 13 and 14. The left panel in Figure 13 shows data from airglow measurements made at Haleakala, Hawaii during the interval 29-30 September 2002 of spread-F bubbles in the I/T (Makela et al. 2004). Colored tracks (red/green/blue) are paths of Global Positioning System (GPS) satellites. Notice the intricate fingering of the dark bubbles, which are regions of very low electron density. This image is taken from a movie (Sep29_30_GPS_7774.mov) that illustrates more completely the dynamics of these features. The left panel in Figure 14 shows data from the *Hinode* Solar Optical Telescope on 30 November 2006 of a solar hedgerow prominence at the solar limb (Berger et al. 2010, Figure 1). The dashed white box outlines a region of a dark bubble forming, rising, fingering, and fragmenting among the shimmering strands of the prominence gas. Note that this measured emission originates in the Balmer series of neutral hydrogen atoms, marking cool material; the dark bubble is hot material in which the hydrogen is fully ionized and so does not radiate in this line (Berger et al. 2011). The inset image at the upper right shows the prominence as a dark feature on the otherwise bright solar disk three days earlier. The *Hinode* image is part of a movie (Berger et al. 2010, ApJ330604F1.mov) that shows the full evolution of this bubble and many others. Both the terrestrial and solar movies are included in this paper as supplementary material.

Another apparent consequence of Rayleigh-Taylor instability in solar prominences is the organization of the cool material into long, thin threads that are extended along magnetic field lines. A striking example of this structure (Lin et al. 2007, Figure 1c) is shown in Figure 14, as observed at high resolution with the Swedish Solar Telescope on 22 August 2004. The measured thread diameter is comparable to the resolution limit (~ 200 km) of

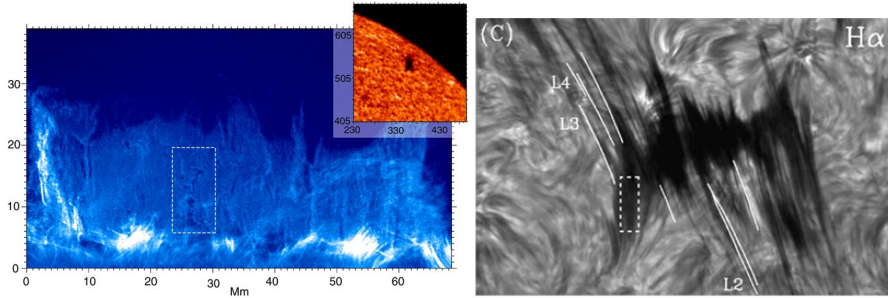


Fig. 14 Left: Magneto-convection in a solar hedgerow prominence (blue/white color shading, right panel). Figure and movies are reprinted courtesy of T. E. Berger and the *Astrophysical Journal*. Right: Filamentary structure in a quiescent solar prominence, a possible consequence of Rayleigh-Taylor instability in the corona. Figure is reprinted courtesy of Y. Lin and *Solar Physics*.

the telescope's adaptive optics, while the thread lengths range up to at least 10 Mm. The excellent thermal insulation across the prominence magnetic field implies that the cross-thread scale length separating the cool (10^4 K) prominence and hot (10^6 K) corona is very small (~ 10 km or less) compared to the thread diameter. During the onset of the instability, the horizontal magnetic field exerts a stabilizing force that favors long wavelengths parallel to the field, while the motion feeding the growth favors short wavelengths perpendicular to the field (Chandrasekhar 1961). This implies a predisposition toward long, thin, field-aligned threads, like those observed. Similar features have been found in simulations of magnetized Rayleigh-Taylor instability in astrophysical contexts (e.g., Stone and Gardiner 2007a,b). The implications of the instability for understanding the observed thread structure in solar prominences are now being investigated (e.g., DeVore 2013).

Images of the Rayleigh-Taylor instability at Earth similarly show elongation along the magnetic field. In this case it is the plasma density depletions that appear as dark features in EUV images (see Figure 13 and Kamalabadi et al. 2009) such as produced by the Global Ultraviolet Imager (GUVI) on the NASA TIMED satellite (Christensen et al. 2003). The elongation occurs because, in the I/T, the instability is governed by an electrostatic potential that varies across but not along the geomagnetic field (Haerendel et al. 1992). This potential produces $\mathbf{E} \times \mathbf{B}$ drifts that act everywhere along a given geomagnetic flux tube, moving low-density plasma upward and outward, to higher altitudes and latitudes. Ion dynamics within these field-aligned plasma density bubbles has only recently been simulated (Huba et al. 2009a,b; Krall et al. 2010).

7.2 Stability Analysis

The occurrence of Rayleigh-Taylor instabilities is important in both the chromospheric and ionospheric contexts and has a common physical origin in the negative density stratification of a fluid in the presence of gravity, as discussed above. However, the mathematical manipulations performed and the language used to describe the underlying physics are quite different in the two communities of investigators. In the following subsections, we present simple derivations of the dispersion relation for unstable Rayleigh-Taylor disturbances within the contexts of chromospheric magnetohydrodynamics (§7.2.1) and ionospheric electrodynamics (§7.2.2). The first uses \mathbf{B} and \mathbf{V} as primary variables, while the second uses \mathbf{E} and \mathbf{J} . In

the end, however, the approaches are complementary, and the same dispersion relation is obtained irrespective of how the analysis is framed. In the concluding subsection (§7.2.3), we simplify the general dispersion equation for regimes in which the plasma is strongly coupled to the neutrals by collisions. This is the case in the solar chromosphere and prominences, and in the I/T. This example illustrates an important physical process that is common to the two environments, but is conceptualized and analyzed in very different ways, therefore, in our experience, impeding mutual understanding across disciplines.

7.2.1 Magnetohydrodynamic (Chromospheric) Context

The basic equations used in the analysis are those for continuity and momentum of the neutral gas and the one-fluid plasma. The plasma equations are the mass-weighted sum of the ion and electron continuity equations (5 and 6) and the sum of the momentum equations for the ions and electrons (9 and 10). Ionization and recombination terms are ignored, as are electron inertia effects; in particular, we assume that $m_e v_{en} \ll m_i v_{in}$ (see §4.3). Consider a simple neutral-plasma configuration in a slab geometry, $\mathbf{B} = B_0 \hat{\mathbf{e}}_z$, $\mathbf{g} = g \hat{\mathbf{e}}_x$, $\mathbf{V}_{n0} = \mathbf{V}_{p0} = 0$, $\rho_n(x) = m_n n_n(x)$, and $\rho_p(x) = m_p n_p(x)$, where the subscript 0 indicates an equilibrium value. Perturbed variables \tilde{q} are assumed to vary as $\tilde{q} \exp(iky - i\omega t)$, where $\omega = \omega_r + i\gamma$ and the disturbances propagate in the y direction. The neutral and plasma flows are assumed to be incompressible, $\nabla \cdot \mathbf{V} = 0$. For the uniform equilibrium magnetic field assumed, the ideal MHD induction equation, Equation (71) with $\eta = 0$, then yields $\tilde{\mathbf{B}} = 0$, so the magnetic field remains undisturbed. Since we neglect the x dependence of the perturbed quantities, incompressibility requires $\tilde{V}_{ny} = \tilde{V}_{py} = 0$. Physically, the time scale associated with the instability is required to be much longer than those associated with compressive acoustic or magnetosonic waves.

The linearized continuity equation (7) and the x component of the linearized momentum equation (11) for the neutrals then take the forms

$$-i\omega \tilde{n}_n = -\tilde{V}_{nx} \frac{dn_{n0}}{dx}, \quad (93)$$

$$-i\omega n_{n0} m_n \tilde{V}_{nx} = +\tilde{n}_n m_n g - n_{n0} m_n v_{ni} (\tilde{V}_{nx} - \tilde{V}_{px}). \quad (94)$$

The corresponding equations for the plasma, from (5–6) and (9–10), are

$$-i\omega \tilde{n}_p = -\tilde{V}_{px} \frac{dn_{p0}}{dx}, \quad (95)$$

$$-i\omega n_{p0} m_p \tilde{V}_{px} = +\tilde{n}_p m_p g - n_{p0} m_p v_{in} (\tilde{V}_{px} - \tilde{V}_{nx}). \quad (96)$$

Solving for \tilde{n}_n and \tilde{n}_p in Equations (93) and (95) and substituting into Equations (94) and (96), respectively, yields, after some rearrangement,

$$\left(\omega^2 + i\omega v_{ni} - \frac{g}{L_n} \right) \tilde{V}_{nx} = i\omega v_{ni} \tilde{V}_{px}, \quad (97)$$

$$\left(\omega^2 + i\omega v_{in} - \frac{g}{L_p} \right) \tilde{V}_{px} = i\omega v_{in} \tilde{V}_{nx}, \quad (98)$$

where $L_n^{-1} = d \ln n_{n0} / dx$ and $L_p^{-1} = d \ln n_{p0} / dx$ are the local neutral and plasma density scale heights. Combining Equations (97) and (98), we arrive at the dispersion equation

$$\left(\omega^2 + i\omega v_{ni} - \frac{g}{L_n} \right) \left(\omega^2 + i\omega v_{in} - \frac{g}{L_p} \right) + \omega^2 v_{ni} v_{in} = 0, \quad (99)$$

which can be expanded to read

$$\omega^4 + i\omega^3 (v_{in} + v_{ni}) - \omega^2 \left(\frac{g}{L_p} + \frac{g}{L_n} \right) - i\omega \left(\frac{v_{ni}g}{L_p} + \frac{v_{in}g}{L_n} \right) + \frac{g^2}{L_n L_p} = 0. \quad (100)$$

Rewritten in terms of the Brunt-Väisälä frequencies N_n and N_p , Equation (1), the dispersion relation (100) becomes

$$\omega^4 + i\omega^3 (v_{in} + v_{ni}) - \omega^2 (N_p^2 + N_n^2) - i\omega (v_{ni}N_p^2 + v_{in}N_n^2) + N_n^2 N_p^2 = 0. \quad (101)$$

Approximate solutions to this equation in the strong-coupling limit reveal the instability growth rates, as discussed in §7.2.3 below.

7.2.2 Electrostatic (Ionospheric) Context

The set of three-fluid equations used to analyze the Rayleigh-Taylor instability in the F layer of the Earth's I/T consists of those for electron continuity and current conservation, electron and ion momentum, and neutral continuity and momentum (Ossakow 1981). The equilibrium state has $n_{e0}(x) = n_{i0}(x)$, $\mathbf{E}_0 = 0$, $\mathbf{B} = B_0 \hat{\mathbf{e}}_z$, and $\mathbf{V}_{e0} = \mathbf{V}_{i0} = \mathbf{V}_{n0} = 0$. The equilibrium is perturbed such that all disturbances are proportional to $\exp(iky - i\omega t)$. We invoke the local approximation that $\partial/\partial x \ll k$ with regard to the perturbed variables. In conjunction with Faraday's law, this implies that $\tilde{E}_x = 0$ in order for $\tilde{\mathbf{B}} = 0$ to be maintained.

Neglecting inertia, gravity, and collisional coupling due to the small electron mass, the perturbed electron velocity from the linearized Equation (10) is simply the $\mathbf{E} \times \mathbf{B}$ drift due to the instability,

$$\tilde{V}_{ex} = \frac{\tilde{E}_y}{B_0}, \quad \tilde{V}_{ey} = 0. \quad (102)$$

Applying the local approximation to the current conservation constraint, Equation (22), we find that it must be the case that $\tilde{J}_y = 0$. Hence,

$$\tilde{V}_{iy} = \tilde{V}_{ey} = 0, \quad (103)$$

where the second equality follows from Equation (102). In the y component of the ion momentum equation (9), only the drag term due to collisions with neutrals now remains. Thus, we also must have that

$$\tilde{V}_{ny} = \tilde{V}_{iy} = 0. \quad (104)$$

The three conditions (102–104) imply that $\nabla \cdot \mathbf{V}_e = \nabla \cdot \mathbf{V}_i = \nabla \cdot \mathbf{V}_n = 0$, i.e., the flows of all three fluids are incompressible in this approximation. This demonstration justifies *a posteriori* the incompressibility assumption that we made at the outset of §7.2.1.

A second deduction that follows from the current conservation constraint and $\tilde{J}_y = 0$ is that \tilde{J}_x must be uniform along x ,

$$\frac{\partial \tilde{J}_x}{\partial x} = (\tilde{V}_{ix} - \tilde{V}_{ex}) e \frac{dn_e}{dx} = 0. \quad (105)$$

Consequently, we also must have that

$$\tilde{V}_{ix} = \tilde{V}_{ex} = \frac{\tilde{E}_y}{B_0}. \quad (106)$$

The bulk flows of the electrons and ions due to the instability are, therefore, identical, $\tilde{\mathbf{V}}_e = \tilde{\mathbf{V}}_i = \tilde{\mathbf{E}} \times \mathbf{B}$. This is consistent with a vanishing electric field in the frame of the electrons, $\tilde{\mathbf{E}} + \tilde{\mathbf{V}}_e \times \mathbf{B}_0 = 0$, which was tacitly assumed in the magnetohydrodynamic analysis in §7.2.1, where $\tilde{\mathbf{E}}$ plays no explicit role. In addition, the total perturbed current vanishes, $\tilde{\mathbf{J}} = 0$, consistent with $\tilde{\mathbf{B}} = 0$ and with the earlier analysis.

From the linearized electron continuity equation (6), the perturbed electron density satisfies

$$-i\omega\tilde{n}_e = \frac{dn_{e0}}{dx}\tilde{V}_{ex} = -\frac{dn_{i0}}{dx}\tilde{V}_{ix} = i\omega\tilde{n}_i, \quad (107)$$

after using first $n_{i0} = n_{e0}$ and $\tilde{V}_{ix} = \tilde{V}_{ex}$, and then the ion continuity equation (5). Substituting the definition $L_p = d \ln n_{i0} / dx = d \ln n_{e0} / dx$, and the $\mathbf{E} \times \mathbf{B}$ drift velocity from Equation (106), we obtain the (equal) electron and ion density perturbations

$$\frac{\tilde{n}_e}{n_{e0}} = \frac{\tilde{n}_i}{n_{i0}} = \frac{i}{\omega} \frac{1}{L_p} \tilde{V}_{ex} = \frac{i}{\omega} \frac{1}{L_p} \tilde{V}_{ix} = -\frac{i}{\omega} \frac{1}{L_p} \frac{\tilde{E}_y}{B_0}. \quad (108)$$

Equations (107) and (108) are equivalent to Equation (95) in §7.2.2, since $n_e = n_i = n_p/2$ and $\mathbf{V}_e = \mathbf{V}_i = \mathbf{V}_p$.

Finally, after recalling that $\tilde{E}_x = 0$ and $\tilde{V}_{iy} = 0$, the x component of the linearized ion momentum equation (9) yields

$$v_{in}\tilde{V}_{nx} = (-i\omega + v_{in})\tilde{V}_{ix} - g\frac{\tilde{n}_i}{n_{i0}} \quad (109)$$

$$= \left(-i\omega + v_{in} + \frac{i}{\omega} \frac{g}{L_p}\right)\tilde{V}_{ix} \quad (110)$$

$$= \left(-i\omega + v_{in} + \frac{i}{\omega} \frac{g}{L_p}\right)\frac{\tilde{E}_y}{B_0}. \quad (111)$$

The linearized continuity and momentum equations for the neutrals are combined as in §7.2.1 to obtain (cf. Equation 97)

$$\left(-i\omega + v_{ni} + \frac{i}{\omega} \frac{g}{L_n}\right)\tilde{V}_{nx} = v_{ni}\tilde{V}_{ix} = v_{ni}\frac{\tilde{E}_y}{B_0}. \quad (112)$$

Eliminating \tilde{V}_{nx} from Equations (111) and (112) leads to the desired dispersion equation,

$$\left(\omega^2 + i\omega v_{ni} - \frac{g}{L_n}\right)\left(\omega^2 + i\omega v_{in} - \frac{g}{L_p}\right) + \omega^2 v_{ni} v_{in} = 0. \quad (113)$$

This is identical to the magnetohydrodynamic result, Equation (99), and will be analyzed further in the next section.

Our derivations of the dispersion equation in the electrodynamic and magnetohydrodynamic contexts culminate in the same result, albeit by following different paths. The principal difference is the role assigned to the electric field, which is primary in the ionospheric context and in the literature of the *I/T* community, but is all but invisible in the chromospheric context and in much of the literature of the solar community (excepting situations of rapidly changing magnetic fields associated with flares and other transient behavior). As the derivations highlight, it is commonly said about the *I/T* that the electric field gives rise to $\mathbf{E} \times \mathbf{B}$ drifts, implying that \mathbf{E} drives \mathbf{V} . In contrast, the same is rarely, if ever, said about the chromosphere or corona, where \mathbf{E} is principally a consequence of plasma flow \mathbf{V} across

the magnetic field \mathbf{B} , so \mathbf{V} drives \mathbf{E} . The normal mode analysis performed here does not distinguish between these two perspectives; only an initial value analysis can do that.

For completeness, we note that this analysis of the Rayleigh-Taylor instability in the ionospheric context is predicated on a local evaluation of plasma and neutral variables, i.e., it applies in a restricted region in space. In this limit, as we have seen, the dispersion equation is the same as in the solar context. However, in the I/T, as discussed in §3.4, the magnetic field lines are assumed to be equipotentials and the electric field generated by the instability extends along the entire magnetic flux tube. Thus, the instability is affected by the plasma on the flux tube that encompasses both the E and F layers of the I/T and a “flux-tube integrated” analysis of the instability is required. A discussion of this type of analysis as it applies to Rayleigh-Taylor instability in the I/T is given by Sultan (1996). The result is a growth rate averaged all along an equipotential field line, which in order of magnitude has a growth time of about 15 min. In contrast, the Alfvén travel time is only about 10 s. Thus, as argued by Vasyliūnas (2012) (see our §5.2), the non-potential component of the electric field is small, and the electrostatic approximation is quite good. A similar conclusion follows from a more complete electromagnetic analysis of the Rayleigh-Taylor instability, including Alfvén waves and the Pedersen resistivity of the I/T, performed by Basu (2005). The result found is that the magnetic field perturbations are very small due to resistive slip between the plasma and magnetic field (see our §5.1), so that, again, the electrostatic approximation is well justified.

7.2.3 Strong-coupling Limit

The general dispersion equation (99) or (113) trivially factors into distinct neutral and plasma modes in the limit of weak collisions, $\nu_{\alpha\beta} \rightarrow 0$:

$$\omega^2 = N_n^2 = \frac{g}{L_n}; \quad \omega^2 = N_p^2 = \frac{g}{L_p}. \quad (114)$$

In §2, Figure 3, on the other hand, we noted that the characteristic Brunt-Väisälä frequencies $N \equiv (g/L)^{1/2}$ in the solar and terrestrial atmospheres are much smaller than the ion-neutral collision frequencies ν_{in} . We can scale these quantities by setting $\nu_{in} = \mathcal{O}(1)$, and $N_p, N_n = \mathcal{O}(\varepsilon)$ where $\varepsilon \ll 1$. We also have $\nu_{ni} = \mathcal{O}(\varepsilon)$ in a weakly ionized plasma. We can now look for strongly-coupled solutions to the general quartic dispersion relation given in Equation (101), i.e. $\omega_r \ll \nu_{in}$ where $\omega = \omega_r + i\gamma$. Note that this regime justifies the use of the low frequency Ohm’s law, where $|\omega| \ll \min(\nu_{in}, \Omega_i)$ is required. Let us first consider high frequency solutions $\omega_r \gg N_p, N_n$, of which $\omega_r = 0$, $\gamma = \mathcal{O}(1)$ is one. Balancing the largest terms in the dispersion relation (101) for this scaling, the quartic and cubic terms, yields Equation (115) below. Next we consider intermediate solutions, where $|\omega| \sim N_p, N_n$, of which $\omega_r = \mathcal{O}(\varepsilon)$, $\gamma = \mathcal{O}(\varepsilon)$ is one. Then the largest terms in the dispersion relation (101) are the cubic and linear terms, and balancing these yields Equation (116) below. Finally we consider low-frequency solutions, where $|\omega| \ll N_p, N_n$, of which $\omega_r = 0$, $\gamma = \mathcal{O}(\varepsilon^2)$ is one. Then the largest terms in the dispersion relation (101) are the linear and constant terms, and balancing these yields Equation (117) below:

$$\omega \approx -i(\nu_{in} + \nu_{ni}); \quad (115)$$

$$\omega^2 \approx (\nu_{in}N_n^2 + \nu_{ni}N_p^2) / (\nu_{in} + \nu_{ni}); \quad (116)$$

$$\omega \approx -iN_n^2N_p^2 / (\nu_{in}N_n^2 + \nu_{ni}N_p^2). \quad (117)$$

The high-frequency solution in Equation (115) is a strongly damped inter-penetrating mode in which the two fluid velocities are 180° out of phase. It is always stable.

The pair of intermediate-frequency solutions in Equation (116) are a weighted average of the classical single-fluid Rayleigh-Taylor growth rates (or Brunt-Väisälä frequencies) of the neutral gas and plasma. Due to the preponderance of neutrals over ions (i.e., $n_n \gg n_i$, hence $v_{in} \gg v_{ni}$; see Fig. 3) these solutions simplify to

$$\omega^2 \approx N_n^2 = \frac{g}{L_n}. \quad (118)$$

They are oscillatory in the chromosphere and the I/T where the neutrals are stably stratified, $gL_n > 0$. On the other hand, in a cool, dense, partially neutral prominence suspended within the ionized solar corona, $gL_n < 0$, and one of these modes is a growing Rayleigh-Taylor instability. A two-fluid (electrically neutral ionized plasma plus neutral gas) numerical simulation of such an unstable configuration is presented below in §7.3.1. Due to the strong collisional coupling of the neutral gas and plasma, their velocities are essentially equal,

$$\mathbf{V}_n \approx \mathbf{V}_p. \quad (119)$$

This can be deduced readily from Equations (97) and (98).

A second potentially unstable solution is the low-frequency mode in Equation (117). It also is a weighted average of the plasma and neutral contributions, and as $v_{in} \gg v_{ni}$, simplifies to

$$\omega \approx -i \frac{N_p^2}{v_{in}} = -i \frac{g}{v_{in} L_p}. \quad (120)$$

This is the classical collision-dominated Rayleigh-Taylor instability in the I/T (e.g., Osakow 1981), driven by the upward-increasing plasma density, $gL_p < 0$. A similar instability should occur in the ALC7 solar chromosphere where the ionization fraction increases sufficiently rapidly with height above the surface (cf. Fig. 2). A multi-fluid simulation of this low-frequency mode is presented below in §7.3.2. In this case, due to the approximate balance between gravity and collisional coupling to neutrals on the part of the ions, Equation (98), and to the very low frequency and the weak collisional coupling to ions on the part of the neutrals, Equation (97), the velocities satisfy

$$|\mathbf{V}_p| \gg |\mathbf{V}_n|. \quad (121)$$

All of these features represented by Equations (118–121) are evident in the simulation results described next.

7.3 Simulation Study

We now present a simulation study applicable to both the solar and ionospheric case performed within the HiFi spectral-element multi-fluid modeling framework (Lukin 2008). The calculations use an implementation of the partial differential equations describing self-consistent, nonlinear evolution of a partially ionized, three-fluid hydrogen mixture of ions, electrons and neutrals (Leake et al. 2013, and references therein). The set of equations solved are (5–13), but neglecting the electron momentum, and with Equation (122), neglecting the last two terms in the low-frequency approximation, and neglecting the plasma and neutral pressure term (third term on the RHS). The electron pressure terms is kept, because, in some cases, when there are small variations of out-of-plane B-field from the uniform $\mathcal{O}(1)$ guide

field, as is the case for the I/T simulation, it isn't quite so clear that this term can always be ignored. Hence the Ohm's law used is:

$$\mathbf{E}^p \equiv \mathbf{E} + (\mathbf{V}_p \times \mathbf{B}) = \left[\frac{1}{k_{ei}} + \frac{1}{k_{en} + k_{in}} \right] \frac{B}{en} \mathbf{J} + \left[1 - \frac{\xi_n k_{in}}{k_{en} + k_{in}} \right] \frac{B}{en} \mathbf{J} \times \hat{\mathbf{b}} - \frac{\nabla \cdot \mathbb{P}_e}{en} \quad (122)$$

We point out that using a hydrogen fluid is not truly appropriate for the F-layer I/T, which is dominated by oxygen ions. However, the significance of our study is that we can capture the essential physics of both situations within the framework of a single model, using parameters appropriate to the two different environments. The boundary conditions are periodic on the sides, and are closed and reflecting on the top and bottom, respectively.

In the subsections below, we describe the basic parameters and show the key figures for the two cases studied. Some mathematical details are relegated to the Appendix to streamline the presentation of the essential results.

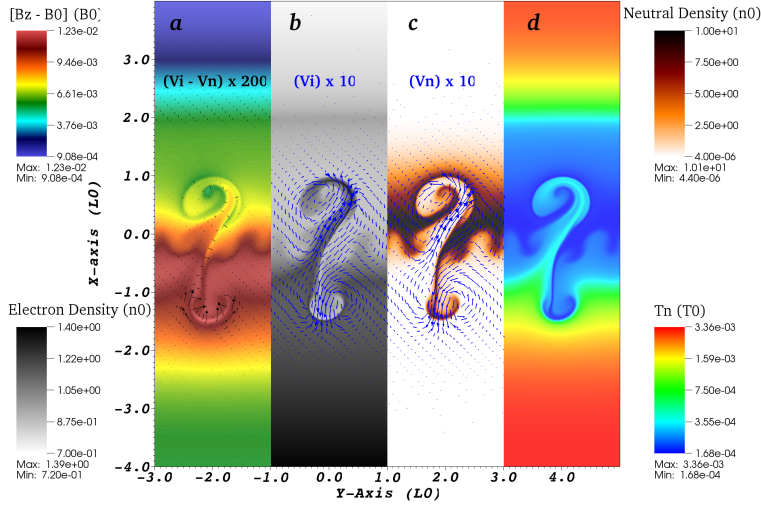


Fig. 15 Two-fluid numerical simulation of Rayleigh-Taylor instability in a solar prominence: (a) magnetic field $[B_z - B_0]/B_0$; (b) electron or ion density $n_e/n_0 = n_i/n_0$; (c) neutral density n_n/n_0 ; (d) neutral temperature T_n/T_0 . Vector velocities for the neutrals (\mathbf{V}_n) and ions (\mathbf{V}_i), and their difference ($\mathbf{V}_i - \mathbf{V}_n$), are shown in panels (c), (b), and (a) respectively.

7.3.1 Solar Prominence

Our first case is a model for the Rayleigh-Taylor instability in a solar prominence. We adopt a two-dimensional slab equilibrium for the prominence structure, showing the result of the simulation at a time when the instability is already well-developed in Figure 15. In the initial equilibrium, the electron (and ion) density n_e of the background corona (Fig. 15b) is exponentially stratified, attaining a value $n_0 = 1 \times 10^{15} \text{ m}^{-3}$ at height $x = 0$ in the Cartesian coordinate system scaled to a typical prominence size, $L_0 = 1 \times 10^6 \text{ m}$. The neutral density $n_n(x)$ within the prominence slab (Fig. 15c) is an order of magnitude larger, reaching $10n_0 =$

$1 \times 10^{16} \text{ m}^{-3}$ at its central height, $x = 0.5$. The characteristic temperatures of the fluids are $T = 2 \times 10^5 \text{ K}$ in the corona and $T = 1 \times 10^4 \text{ K}$ in the prominence; the neutral temperature is shown in Figure 15d, scaled to a normalization temperature $T_0 = 5.8 \times 10^7 \text{ K}$. The electron and ion temperatures are very similar, due to the fast thermal exchange between the fluids. Finally, the deviation of the out-of-plane magnetic field $B_z(x)$ from a uniform value $B_0 = 1 \times 10^{-3} \text{ T}$ is displayed in Figure 15a. As detailed in the Appendix, B_z is vertically stratified to balance the initial pressure and gravity forces in magnetohydrostatic equilibrium. Because beta is low for both the plasma and neutral gas, the associated magnetic-field deviations are relatively small.

This unstable neutral-plasma system is initialized with small-amplitude neutral-density perturbations centered at $x = 0$, on the bottom side of the prominence slab. The resulting evolved solution at time $t = 4.0 \times 10^2 \text{ s}$ is shown in Figure 15. Velocity vectors are shown in panels a, b, and c that correspond to the differential ion-neutral velocity, ion velocity, and neutral velocity, respectively. We observe that all contours have the same shape, and the plasma and neutrals track each other quite closely. The neutral gas is unstable and, due to the collisional coupling to the plasma, the plasma follows the neutrals. We determined the e-folding growth time τ of the flow velocity and the resulting growth rate is $\tau^{-1} \sim 2 \times 10^{-2} \text{ s}^{-1}$. For solar gravity and the chosen neutral density profile, the Brunt-Väisälä frequency, which is the analytic growth rate for the strong-coupling limit, see Equation (118), is $N_n \approx 2.6 \times 10^{-2} \text{ s}^{-1}$, which is in very good agreement with the numerically determined growth rate, given the simplicity of the derivation compared to the complexity of the simulation model. An evaluation of the collision frequencies at $x = 0$ gives $\nu_{in} = 2.2 \times 10^2 \text{ s}^{-1}$ and $\nu_{ni} = 5.2 \times 10^1 \text{ s}^{-1}$. Thus, this calculation lies in the strong-coupling regime of §7.2.3, and Equations (118) and (119) apply.

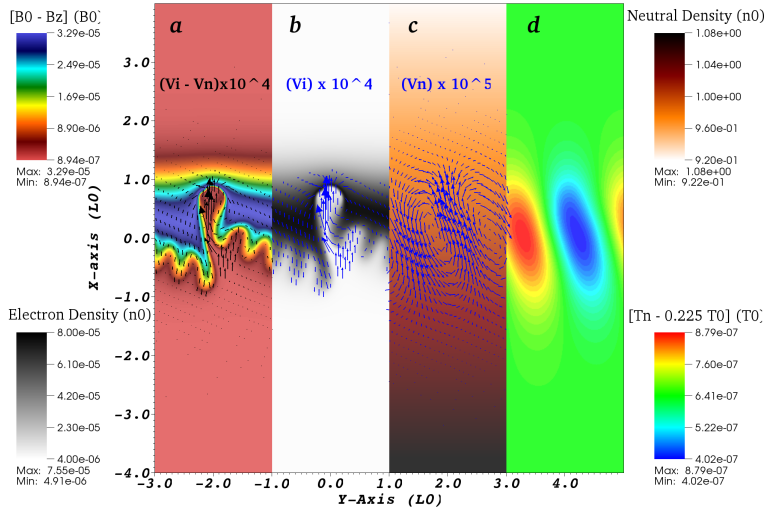


Fig. 16 Three-fluid numerical simulation of Rayleigh-Taylor instability in the Earth's I/T: (a) magnetic field $[B_0 - B_z]/B_0$; (b) electron or ion density $n_e/n_0 = n_i/n_0$; (c) neutral density n_n/n_0 ; (d) neutral temperature $[T_n - T_b]/T_0$. Vector velocities for the neutrals (\mathbf{V}_n) and ions (\mathbf{V}_i), and their difference ($\mathbf{V}_i - \mathbf{V}_n$), are shown in panels (c), (b), and (a) respectively.

7.3.2 Terrestrial Ionosphere

Our second case is a model for the Rayleigh-Taylor instability in the I/T. The well-developed instability in the simulation initialized with a two-dimensional slab equilibrium is shown in Figure 16. In this case, the neutral density $n_n(x)$ of the background atmosphere (Figure 16c) is exponentially stratified, attaining a value $n_0 = 1 \times 10^{16} \text{ m}^{-3}$ at height $x = 0$ in the Cartesian coordinate system scaled to a typical F-layer size, $L_0 = 2 \times 10^4 \text{ m}$. The electron (and ion) density $n_e(x)$ within the I/T (Figure 16b) is four orders of magnitude smaller, reaching $10^{-4}n_0 = 1 \times 10^{12} \text{ m}^{-3}$ at its central height, $x = 0.5$. The temperatures of the fluids are all uniform and equal, at $T_b = 1.2 \times 10^3 \text{ K}$; the deviation of the neutral temperature from this value is shown in Figure 16d, scaled to a normalization temperature $T_0 = 5.3 \times 10^3 \text{ K}$. Finally, the deviation of the out-of-plane magnetic field $B_z(x)$ from a uniform value $B_0 = 3 \times 10^{-5} \text{ T}$ is displayed in Figure 16a. Here, B_z is vertically stratified to balance the plasma pressure and gravity forces in magnetohydrostatic equilibrium. Because the plasma beta is far smaller in the I/T than in the chromosphere and corona, the resulting ionospheric magnetic-field deviations are similarly smaller, by comparison.

This unstable neutral-plasma system is initialized with small-amplitude electron-density perturbations centered at $x = 0$, on the bottom side of the ionization layer. The resulting evolved solution at time $t = 4.6 \times 10^5 \text{ s}$ is shown in Figure 16. Velocity vectors again are shown in panels a, b, and c that correspond to the differential ion-neutral velocity, ion velocity, and neutral velocity, respectively. In this case, we observe that the plasma and neutrals do not track each other very well. The plasma is unstable and develops a low-density bubble that rises through the plasma layer, as is observed in the I/T (Fig. 13). The contours of perturbed magnetic field closely resemble those of the plasma density. The formation of the bubble and the generation of the ion flows are strongly affected by drag exerted by the neutrals. Because the collisional coupling to the neutrals by the plasma is very weak, however, the neutrals move only slowly and somewhat independently, as shown by the neutral density, velocity, and temperature. The numerically calculated growth rate is $\tau^{-1} \sim 1.3 \times 10^{-5} \text{ s}^{-1}$. For terrestrial gravity and the chosen plasma density profile, the Brunt-Väisälä frequency is $N_p = 3.7 \times 10^{-2} \text{ s}^{-1}$, which is much smaller than the ion-neutral collision frequency $\nu_{in} = 1.1 \times 10^2 \text{ s}^{-1}$. This calculation also lies in the strong-coupling regime of §7.2.3, but here Equations (120) and (121) are the relevant solutions. The low-frequency growth rate calculated from Equation (120) is $\gamma \approx 1.3 \times 10^{-5} \text{ s}^{-1}$, in excellent agreement with the numerically determined rate. We point out that the growth rate for an O^+ plasma in the real I/T would be about ten times greater than the rate for our simulated H^+ plasma, with a resulting e-folding time of about 2 hrs, in reasonable agreement with observations.

7.4 Summary

These simulations show how a common framework has been used to describe the Rayleigh-Taylor instability in both the chromosphere and I/T, even though historically, the phenomena has been approached in two very different ways. There are many other common phenomena between the chromosphere and I/T, and much knowledge can be gained from applying this universal approach.

8 Conclusions

In this paper we have compared the Sun's chromosphere and Earth's ionosphere/thermosphere (I/T). Both are weakly ionized, stratified mixtures of plasma and neutral gas with an increasing ionization fraction with height (altitude). Both have typical plasma β less than one, and a neutral (or total) β which transitions from above to less than one. Thus plasma motions alone are not capable of creating large perturbations in magnetic field, but if the coupling between plasma and neutrals is strong enough, the average motions of neutrals and plasma can potentially create large perturbations in the field. For the chromosphere, where the neutral-ion collision frequency is larger than 10^3 Hz, then for phenomena with timescales longer than 10^{-3} s, the coupling is strong enough. For the I/T the neutral-ion collision frequency is larger than 10^{-6} Hz, so most timescales of interest (e.g. minutes to hours, or 60-3600 s) are too quick for the coupling to be sufficient. This difference is brought about by the much lower ionization level in the I/T compared to the chromosphere, something which creates many important difference between the two atmospheres, such as neutral-plasma collision rates and conductivity. It also affects fluid instabilities, as demonstrated by our discussion of the Brunt-Väisälä frequency. In both environments, this frequency N_p is smaller than the ion-neutral collision frequency, so that the Brunt-Väisälä oscillations (or Rayleigh-Taylor instabilities) of the plasma are affected by coupling to the neutrals. In the chromosphere, the oscillations and instabilities of the neutrals are similarly strongly affected by coupling to the plasma, since there the neutral Brunt-Väisälä frequency is less than the neutral-ion collision frequency. However, the opposite is true in the I/T, and so the oscillations of the stably stratified neutral gas are unaffected by the plasma, and neutral motion is essentially undisturbed by the evolution of unstably stratified plasma.

Both environments exhibit a variation of the magnetization of the ions and electrons with altitude, with magnetization being defined by the ratio of collision frequency to gyrofrequency. The magnetization is also a measure of how mobile the ions and electrons are in the presence of neutrals. As the magnetization depends on magnetic field, we found a range of behavior in the chromosphere, but for certain magnetic field cases we found a similar behavior of the magnetization and mobility in both the chromosphere and the I/T. In general, at low heights, the electrons and ions are unmagnetized due to high collision rates with neutrals. With increasing altitude, the electrons become mobile first, driving first mainly Pedersen currents, then Hall and Pedersen currents. Higher up still, the ions become magnetized and drive Pedersen currents also. We found that for the 1D I/T model, there are three regions, representing unmagnetized plasma (M1), magnetized electrons and unmagnetized ions (M2), and magnetized plasma (M3). In the middle of the M2 region is a height at which the conductivity became anisotropic (this is where $\Gamma = \xi_n k_e k_{in}$ become larger than unity, and is also the height at which Pedersen heating becomes important see below). Similar transitions were seen in the chromosphere, with a variation of the altitude of these transitions for different magnetic field models. This anisotropy can also be seen in the relative contribution of current dissipation by perpendicular currents and parallel currents, and is a factor in the location at which the field becomes force-free.

The large disparity in plasma density between the chromosphere and I/T also creates differences in the modeling and analysis of phenomena in the two atmospheres. We showed that the chromosphere is ideal (non-resistive) on length scales much larger than a km, such that the evolution of the magnetic field is dominated by advection by coupled plasma-neutral flows, but resistive below these lengths, where the field becomes decoupled from the average flow. However, because the conductivity is so much lower in the I/T, the Earth's atmosphere is essentially resistive such that the field is always decoupled from the average flow

and coupled to electron flow. This generally leads to the treatment of I/T phenomena with electrodynamics, where \mathbf{E} and \mathbf{J} are considered primary variables and drivers, while in the chromosphere \mathbf{B} and \mathbf{V} are the primary variables. An example of this was applied to the phenomena of wind driven dynamos in §5.2. Parker (2007), Vasyliūnas (2001), Vasyliūnas (2011), and Vasyliūnas (2012) criticize the E-J paradigm, stating that for long time scales we can remove the dynamical equations for $\partial\mathbf{E}/\partial t$ and $\partial\mathbf{J}/\partial t$ and have \mathbf{B} and \mathbf{V} be the primary variables (V-B paradigm), but the converse is not true, and the E-J paradigm is not tractable. Despite these facts, we find that using the E-J paradigm may allow one to arrive at the same result as the V-B paradigm, as was achieved in a general sense for wind-driven dynamos and the Rayleigh-Taylor instability in this review. However, in general this may not always be the case.

The two atmospheres of the Earth and the Sun have different mechanisms that contribute to the heating. We know more about the heating mechanisms in the I/T compared to the chromosphere. In the I/T the dominant heating term for the neutral gas is absorption of UV/EUV radiation, which forms the ionosphere through photoionization and raises neutral and plasma temperatures to more than one thousand degrees. However, frictional heating of the neutral gas by collisions with ions can be as significant as solar heating during geomagnetic storms and represents the most variable source of energy to quantify in the I/T energy equation. Other processes, such as ion friction and the Farley-Buneman instability can also contribute to energy transfer. In the chromosphere, the presence of a temperature minimum and temperature gradient reversal is a major challenge for solar physics. The observed average chromospheric temperature profile is created by a balance of a few major processes. Radiation in the chromosphere is optically thick, due to both spectra and line emission, and formed in non-LTE. The downward conduction of energy from the much hotter corona (the heating of which is also a major open question in solar physics) is important in the upper chromosphere, but in the lower chromosphere, the radiation must be balanced by some heating mechanism. In fact the chromosphere requires roughly ten times more heat input than the corona to maintain its elevated temperature, due to a much larger density (Narain and Ulmschneider 1990).

In §6.2, we showed how frictional heating provides a mechanism for the conversion of electromagnetic energy into thermal and kinetic energy of the plasma-neutral gas mix, via the term $\mathbf{E} \cdot \mathbf{J}$. This frictional heating includes the well known “Joule heating” term due to ion-electron collisions, and a plasma-neutral frictional term, the latter of which dominates when the ions start to become mobile in the presence of neutrals, i.e. when they start to become magnetized. We showed that when this occurs the currents perpendicular to the magnetic field become dominated by Pedersen currents, driven by ion motions. As shown in Goodman (2000, 2004) the efficiency of Pedersen current heating $\mathbf{E}_\perp \cdot \mathbf{J}_\perp = \eta_\perp J_\perp^2$ increases as $\Gamma k_e k_{in}$ starts to become large, which is when the conductivity (and resistivity) tensor becomes anisotropic. Below this region, the heating is mainly Ohmic Joule heating (electron-ion collisions). This analysis applies to a general dissipation mechanism, and to derive the actual heating term one must model the generation of such currents in the atmosphere. Goodman (2000, 2001), Song and Vasyliūnas (2011), and Tu and Song (2013) considered the propagation of MHD waves into the chromosphere. The center of mass flow due to the wave motion has a component perpendicular to \mathbf{B} which drives a center of mass electric field, which in turn drives the Pedersen current. Future simulations with self-consistent thermodynamics and resolved non-linear wave interactions and reflections are key to confirming the hypothesis that wave damping by Pedersen current dissipation is responsible for the required chromospheric heating.

In reviewing the two atmospheres in terms of plasma-neutral coupling, we have brought to light some of the many open questions and issues. We review here some of those issues, and suggest what future studies should address, and what are the main challenges.

As mentioned, one of the main unanswered questions in the chromosphere is the mechanism which maintains its elevated temperature. Over the last 60 or so years there have been many proposed mechanisms, and reviews of such mechanisms can be found in Narain and Ulmschneider (1990). These include dissipation of acoustic, magneto acoustic and Alfvén wave which originate at the turbulent convection zone, which is capable of creating a spectrum of waves. Other mechanisms include magnetic reconnection, the Farley-Buneman instability, and low frequency current dissipation. The majority of these proposed mechanisms are only efficient at small scales, which creates one of the main challenges in modeling them. A numerical model must be able to sufficiently resolve the scales on which processes such as magnetic reconnection and wave dissipation operate (down to 10m or smaller), but it must also cover the spatial scales of interest, namely the extent of the chromosphere which is ~ 2 Mm. The other major problem when modeling proposed heating mechanisms is that to self-consistently model the heating, the model must include the complicated radiation in the chromosphere. Recent advances in modeling the chromosphere have included the coupling of the 3D non-LTE radiative physics to the MHD physics (see e.g., Carlsson and Leenarts 2012, and references therein) on regions of small extent. The approach of using such detailed simulations to parameterize the radiation physics in terms of MHD variables (total density, temperature) and model chromospheric proposed heating mechanisms, is a possibly fruitful approach to solving the chromospheric heating problem. However, care must be taken to ensure the correct mechanism are resolved sufficiently, and that on the length and time scales of interest, the correct equations are used, particularly when it comes to the generalized Ohm's law. The problems in understanding the thermodynamic structure of the chromosphere also apply to prominences, which as mentioned are structures of chromospheric material suspended in the corona. The cause of fine structure in prominences is also an open issue, as well as fine structure in the chromosphere such as fibrils, jets, and surges. In addition to explaining the emission in the average, or quiet chromosphere, the increase of emission during flares is also an interesting issue, and has been newly investigated with simulations (e.g. Russell and Fletcher 2013). As with the generic chromospheric heating problem, this issue is an example of the need for well-resolved self-consistent simulations with all of the MHD and radiative physics and with the ability to reproduce high fidelity observations of the atmosphere.

The relatively lesser amount of knowledge of the chromosphere is surely due to the fact that we can only remotely sample the plasma in the chromosphere, and this part of the solar atmosphere is optically thick in some lines, which makes for a difficult interpretation of the spectra obtained. The recently launched Interface Region Imaging Spectrograph (IRIS, De Pontieu et al. 2013) will be valuable in the effort to identify chromospheric heating mechanisms, using relatively high resolution (0.33 arcsec) spectra and line emissions from plasma at temperatures between 5,000 K and 10 MK. These observations will also be used to constrain improved chromospheric simulations which couple the non-LTE radiation that occurs in the chromosphere to the MHD evolution of the plasma (e.g., Carlsson and Leenarts 2012). These simulations are not currently able to resolve all chromospheric physics, but are valuable in the ongoing effort to test proposed heating mechanisms.

The Earth's I/T system is better understood than the chromosphere because it is easier to make a wide range of measurements in the former domain. Despite this there are many challenges remaining to I/T science. Rishbeth (2007) outlined a number of them including: semiannual variations, and the annual asymmetry in both the ionosphere and thermo-

sphere; why the I/T survives at night; day-to-day atmospheric and ionospheric variability, its forcing mechanisms and the I/Ts apparent predilection for certain time scales; and ionospheric memory and preconditioning. Other challenges include the solar cycle change in the winter anomaly (Torr and Torr 1973) and the way that high latitude forcing apparently drives changes in the low latitude I/T (Wang et al. 2008). Understanding these phenomena is difficult because the I/T system is driven from below and above. The Earth's ionosphere is affected by both tropospheric/stratospheric dynamic through modification of the neutral composition/temperature/winds, and the magnetosphere through high-latitude currents and heating, so one must have a good understanding of these other regions as well as the ability to incorporate these effects self-consistently into an ionosphere model. Moreover, ionospheric dynamics spans an enormous range of spatial and temporal scales and different physical processes are important in different regions. It is difficult to bring all of this together in a single, coherent model (this is also a generic issue with most geospace and solar regions).

Virtually all ionosphere models assume the magnetic field lines are equipotentials. This reduces the potential equation to 2D and is readily solvable. However, it is clear that this is an approximation and should be relaxed. Recently, Aveiro and Hysell (2010, 2012); Aveiro and Huba (2013) developed a 3D electrostatic model of the ionosphere and applied it to the development of equatorial spread F. Although, in a general sense, the results are similar to the 2D results there are differences which could be important. Huba and Joyce (2013) have been able to embed a very high resolution grid (.06 degrees over a 60 degree sector) within the context of a global model. They were able to simulate for the first time the onset and evolution of equatorial bubbles (scale sizes 10s km) in a global model. Such coupled simulations are one possible solution to deal with the multi-scale problem of I/T physics. This approach could also be applied to traveling ionospheric disturbances and gravity waves.

The recently selected NASA I/T missions ICON (Ionospheric Connection) and GOLD (Global-scale Observations of the Limb and Disk) will also address some of the key I/T issues. In particular, ICON will obtain the baseline characterization of the internally driven non-linear coupling between the neutral atmospheric drivers of winds, composition changes and the ionospheric responses of plasma densities and ion drifts. During periods of enhanced solar and geomagnetic activity ICON will determine how these parameters deviate from their baseline and will relate them to the strength of the solar wind electrical forcing that is externally applied to the global ionosphere-magnetosphere system. The GOLD mission will investigate the significance of atmospheric waves and tides propagating from below on the temperature structure of the thermosphere, and it will resolve how the structure of the equatorial ionosphere influences the formation and evolution of equatorial plasma density irregularities.

One of the goals of this review paper is to highlight how considering the commonalities of two different atmospheres can shed light on what can be learnt from one about the other. We have found a lot of commonalities, and have been able to talk about the two atmospheres within a common framework, but the differences between the two atmospheres create barriers to common studies. The main difference is the plasma density, which affects neutral-ion collisions frequencies, conductivity, and resistive vs convective magnetic field nature. However, the Rayleigh-Taylor instability is one particular phenomena that we were able to simulate in both atmospheres using the same equations and model (§7). Rather than search for common phenomena that exist in both atmospheres, the key to future collaboration is to identify common fundamental partially ionized plasma physics problems such as the Rayleigh-Taylor instability. Other common fundamental partially ionized plasma physics studies include the development of two stream instabilities in regions where ions are unmagnetized but electrons are magnetized, and the subsequent generation of turbulence (e.g.

the Farley-Buneman instability). Also the neutral wind-driven dynamo is a common problem that can occur in the chromosphere and I/T. The use of the V-B paradigm to describe I/T phenomena that were previously described in the E-J paradigm, as was done for the neutral wind dynamo by Vasylūnas (2012), will help shed light on the fundamental physics. The use of detailed simulations based on these fundamental studies is also a possible route to better understanding. Previous examples include the work by (e.g. Tu and Song 2008) on driving by electric fields. Future studies could also involve numerical experiments of a localized neutral wind in a static, uniform background magnetic field, plasma, and neutral gas, using a three-fluid model (neutrals, electrons, and ions) that retains the displacement current in Ampère's law, which would help test the magnetohydrodynamic interpretation of the neutral wind-driven dynamo. Simpler experiments could use a two-fluid model (neutrals and charge-balanced plasma) to determine whether charge separation in the electrodynamic description truly is required to generate the dynamo or, instead, is transient and merely incidental to the process.

A Appendix

The two-dimensional simulation results shown in Figures 15 and 16 were performed with the HiFi spectral-element multi-fluid model (Lukin 2008). Effective grid sizes of 480×1920 and 180×720 were used in the solar-prominence and ionosphere cases, respectively, along the horizontal (y) and vertical (x) directions. Periodic conditions were applied at the side boundaries (y), while closed, reflecting, free-slip, perfect-conductor conditions were applied at the top and bottom boundaries (x), which were placed sufficiently far from the unstable layer to have negligible effect on the Rayleigh-Taylor evolution. Details of the plasma and neutral profiles and parameters used in the simulations are given below.

A.1 Prominence

Normalization constants for this case are number density $n_0 = 1 \times 10^{15} \text{ m}^{-3}$, length scale $L_0 = 1 \times 10^6 \text{ m}$, and magnetic field $B_0 = 1 \times 10^{-3} \text{ T}$. Using these in a hydrogen plasma, normalization values for the time $t_0 = 1.45 \text{ s}$ and temperature $T_0 = 5.76 \times 10^7 \text{ K}$ can be derived. The ion inertial scale is so much smaller than any scale of interest that, in this case, its value has been set explicitly to zero, $d_i = (c/\omega_{pi0})/L_0 = 0$. This is equivalent to neglecting the Hall term in the Ohm's law. Using the ratio of Hall term to Pedersen in the center of mass Ohm's law (37), and the simplifications used in §4.3, this is equivalent to $\xi_n^2 k_{in} \gg 1$, which is valid for these simulations.

The electron and ion density profiles are given by atmospheric stratification,

$$n_i(x) = n_e(x) = n_0 \exp\left(-\frac{x}{x_0}\right). \quad (123)$$

The scale height x_0 is set by the solar gravitational acceleration, $g_S = 2.74 \times 10^2 \text{ m s}^{-2}$, and the assumed background temperature of the corona, $T_b = 3.5 \times 10^{-3} T_0 = 2.02 \times 10^5 \text{ K}$, scaled to the normalization length L_0 ; its value is $x_0 = 12.2$. The density profile of the neutral fluid that constitutes the prominence is given by a prescribed function of x plus a very low uniform background value,

$$n_n(x) = n_{n0} \text{sech}^2(2x - 1) + n_{nb}. \quad (124)$$

The peak neutral number density enhancement is taken to be $n_{n0} = 1 \times 10^{16} \text{ m}^{-3} = 10n_0$, while $n_{nb} = 3.5 \times 10^{-7} n_{n0}$, corresponding to the neutral fraction obtained in the HiFi ionization/recombination equilibrium at the background temperature T_b . We chose an artificially low value of T_b (compared to a typical coronal temperature of about $2 \times 10^6 \text{ K}$) in order to prevent the background neutral density n_{nb} from being far smaller still.

The electron, ion, and neutral temperatures are all assumed to be equal to each other initially. The temperature profile is given by a prescribed function $f(x)$,

$$T(x) = T_b f(x) = T_b \frac{\cosh^2(x - 0.5)}{\cosh^2(x - 0.5) + \lambda}, \quad (125)$$

which approaches T_b away from the prominence and attains a minimum value $T_p = T_b / (1 + \lambda)$ within the prominence. To obtain a temperature approximately corresponding to that observed on the Sun, with an associated low ionization fraction $(n_{e0} / (n_{e0} + n_{n0})) = 0.091$, we set the parameter $\lambda = 20$. The resulting prominence temperature $T_p = 9.60 \times 10^3$ K.

The magnetic field is initialized to lie in the out-of-plane direction \hat{e}_z , so that it is perpendicular to both gravity in the $-\hat{e}_x$ direction and the instability wavenumber k in the \hat{e}_y direction. It is given by

$$\mathbf{B} = B_0 \hat{e}_z \left[1 + \beta \left\{ \frac{n_e(x)}{n_0} [1 - f(x)] - \frac{n_n(x)}{2n_0} f(x) - \frac{1}{x_0} \frac{n_{n0}}{2n_0} [\tanh(2x - 1) - 1] \right\} \right]^{1/2}, \quad (126)$$

where $\beta = 1.4 \times 10^{-2}$ is the plasma beta evaluated using the background plasma pressure at $x = 0$ and B_0 . The magnetic field profile so constructed accommodates (1) the plasma pressure change from the isothermal hydrostatic profile (2) the neutral pressure, and (3) the gravitational force exerted on the bulk of the neutral fluid (neglecting the small background contribution n_{nb}) throughout the atmosphere.

This initial condition is not an exact solution to the multi-fluid model, including ionization and recombination, with no flow. It is close enough to the solution, however, that any flows created by pressure gradients driven by ionization/recombination of the initial condition are small compared to the flows initiated by the instability. The instability is initiated by introducing a small neutral density perturbation localized in x on the bottom side of the prominence,

$$\Delta n_n(x, y) = \delta n_n(x) \exp[-4x^2] \frac{1}{5} \sum_{j=1}^5 \sin[j\pi y], \quad (127)$$

where we chose $\delta = 10^{-2}$, and y is the normalized distance along the gravitational equipotential surface.

A.2 Ionosphere

The normalization constants are number density $n_0 = 1 \times 10^{16} \text{m}^{-3}$, length scale $L_0 = 2 \times 10^4$ m, and magnetic field $B_0 = 3 \times 10^{-5}$ T. Using these in a hydrogen plasma, normalization values for the time $t_0 = 3.06$ s, temperature $T_0 = 5.19 \times 10^3$ K, and ion inertial scale length $d_i = (c / \omega_{pi0}) / L_0 = 1.14 \times 10^{-4}$ can be derived.

The neutral density profile is given by atmospheric stratification,

$$n_n(x) = n_0 \exp\left(-\frac{x}{x_0}\right). \quad (128)$$

The scale height x_0 is set by Earth's gravitational acceleration, $g_E = 9.81 \text{m s}^{-2}$, and the assumed background temperature of the ionosphere, $T_b = 0.225T_0 = 1.17 \times 10^3$ K, scaled to the normalization length L_0 ; its value is $x_0 = 49.1$. The electron/ion density profile of the plasma is given by a prescribed function of x plus a low uniform background value,

$$n_e(x) = n_i(x) = n_{e0} \text{sech}^2(2x - 1) + n_{eb}. \quad (129)$$

The peak electron number density is taken to be $n_{e0} = 1 \times 10^{12} \text{m}^{-3} = 10^{-4} n_0$, while $n_{eb} = 0.05 n_{e0}$. The electron, ion, and neutral temperatures are all assumed to be equal and uniform initially, at $T_b = 1.17 \times 10^3$ K.

As before, the magnetic field is initialized to lie in the out-of-plane direction. It is given by

$$\mathbf{B} = B_0 \hat{e}_z \left[1 - \beta \left\{ \frac{2n_e(x)}{n_0} + \frac{1}{2x_0} [\tanh(2x - 1) - 1] \right\} \right]^{1/2}, \quad (130)$$

where $\beta = 0.450$ is the neutral beta calculated using the background neutral pressure at $x = 0$ and B_0 . The magnetic field profile so constructed accommodates (1) the plasma pressure and (2) the gravitational force exerted on the bulk of the plasma (neglecting the small background contribution n_{eb}) throughout the atmosphere.

The instability is initiated with a small electron density perturbation localized in x on the bottom side of the ionization layer,

$$\Delta n_e(x, y) = -\delta n_e(x) \exp[-4x^2] \frac{1}{5} \sum_{j=1}^5 \sin[j\pi y], \quad (131)$$

where again we chose $\delta = 10^{-2}$, and y is the normalized distance along the gravitational equipotential surface.

Acknowledgements This work was funded by NASA's "Living with a Star" Targeted Research and Technology program "Plasma-Neutral Gas Coupling in the Chromosphere and Ionosphere". Numerical simulations were performed using a grant of computer time from the DoD High Performance Computing Program. NCAR is sponsored by the National Science Foundation.

References

- W.P. Abbett, The Magnetic Connection between the Convection Zone and Corona in the Quiet Sun. *Astrophys. J.* **665**, 1469–1488 (2007). doi:10.1086/519788
- H. Alfvén, C.-G. Fälthammar, *Cosmical Electrodynamics* (Oxford University Press, Clarendon, 1963)
- T.D. Arber, G.J.J. Botha, C.S. Brady, Effect of solar chromospheric neutrals on equilibrium field structures. *Astrophys. J.* **705**, 1183–1188 (2009). doi:10.1088/0004-637X/705/2/1183
- T.D. Arber, M. Haynes, J.E. Leake, Emergence of a flux tube through a partially ionized solar atmosphere. *Astrophys. J.* **666**, 541–546 (2007). doi:10.1086/520046
- H.C. Aveiro, J.D. Huba, Equatorial spread F studies using SAMI3 with two-dimensional and three-dimensional electrostatics. *Annales Geophysicae* **31**, 2157-2162 (2013). doi:10.5194/angeo-31-2157-2013
- H.C. Aveiro, D.L. Hysell, Three-dimensional numerical simulation of equatorial F region plasma irregularities with bottomside shear flow. *Journal of Geophysical Research (Space Physics)* **115**, 11321 (2010). doi:10.1029/2010JA015602
- H.C. Aveiro, D.L. Hysell, Implications of the equipotential field line approximation for equatorial spread F analysis. *Geophys. Res. Lett.* **39**, 11106 (2012). doi:10.1029/2012GL051971
- E.H. Avrett, R. Loeser, Models of the solar chromosphere and transition region from SUMER and HRTS observations: Formation of the extreme-ultraviolet spectrum of hydrogen, carbon, and oxygen. *Astrophys. J. Suppl. Ser.* **175**, 229–276 (2008). doi:10.1086/523671
- B. Basu, Characteristics of electromagnetic Rayleigh-Taylor modes in nighttime equatorial plasma. *J. Geophys. Res.* **110**, 2303 (2005). doi:10.1029/2004JA010659
- T.E. Berger, G. Slater, N. Hurlburt, R. Shine, T. Tarbell, A. Title, B.W. Lites, T.J. Okamoto, K. Ichimoto, Y. Katsukawa, T. Magara, Y. Suematsu, T. Shimizu, Quiescent prominence dynamics observed with the Hinode Solar Optical Telescope. I. Turbulent upflow plumes. *Astrophys. J.* **716**, 1288–1307 (2010). doi:10.1088/0004-637X/716/2/1288
- T. Berger, P. Testa, A. Hillier, P. Boerner, B.C. Low, K. Shibata, C. Schrijver, T. Tarbell, A. Title, Magnetothermal convection in solar prominences. *Nat.* **472**, 197–200 (2011). doi:10.1038/nature09925
- L. Biermann, Zur Deutung der chromosphärischen Turbulenz und des Exzesses der UV-Strahlung der Sonne. *Naturwissenschaften* **33**, 118–119 (1946). doi:10.1007/BF00738265
- S.I. Braginskii, Transport Processes in a Plasma. *Reviews of Plasma Physics* **1**, 205 (1965).
- D. Brunt, The period of simple vertical oscillations in the atmosphere. *Q. J. R. Meteorol. Soc.* **53**, 30–32 (1927)
- O. Buneman, Excitation of field-aligned sound waves by electron streams. *Phys. Rev. Lett.* **10**, 285–287 (1963). doi:10.1103/PhysRevLett.10.285
- M. Carlsson, J. Leenaarts, Approximations for radiative cooling and heating in the solar chromosphere. *Astron. Astrophys.* **539**, A39 (2012). doi:10.1051/0004-6361/201118366
- S. Chandrasekhar, *Hydrodynamic and Hydromagnetic Stability* (Clarendon, Oxford, 1961)
- P. Charbonneau, Dynamo models of the solar cycle. *Living Rev. Sol. Phys.* **7**, 3 (2010). doi:10.12942/lrsp-2010-3
- A.B. Christensen, L.J. Paxton, S. Avery, J. Craven, G. Crowley, D.C. Humm, H. Kil, R.R. Meier, C.-I. Meng, D. Morrison, B.S. Ogorzalek, P. Straus, D.J. Strickland, R.M. Swenson, R.L. Walterscheid, B. Wolven, Y. Zhang, Initial observations with the global ultraviolet imager (guvi) in the nasa timed satellite mission. *Journal of Geophysical Research: Space Physics* **108**(A12), (2003). doi:10.1029/2003JA009918. <http://dx.doi.org/10.1029/2003JA009918>
- T.G. Cowling, The dissipation of magnetic energy in an ionized gas. *Mon. Not. R. Astron. Soc.* **116**, 114–124 (1956)
- S.R. Cranmer, S.R. van Ballegoijen, On the Generation, Propagation, and Reflection of Alfvén Waves from the Solar Photosphere to the Distant Heliosphere. *Mon. Not. R. Astron. Soc.* **156**, 265–293 (2005)
- R.B. Dahlburg, J.A. Klimchuk, S.K. Antiochos, Coronal energy release via ideal three-dimensional instability. *Adv. Space Res.* **32**, 1029–1034 (2003). doi:10.1016/S0273-1177(03)00305-3
- R.B. Dahlburg, J.A. Klimchuk, S.K. Antiochos, An explanation for the "switch-on" nature of magnetic energy release and its application to coronal heating. *Astrophys. J.* **622**, 1191 (2005)

- B. De Pontieu, Numerical simulations of spicules driven by weakly-damped Alfvén waves. I. WKB approach. *Astron. Astrophys.* **347**, 696–710 (1999)
- B. De Pontieu, P.C.H. Martens, H.S. Hudson, Chromospheric Damping of Alfvén Waves. *Astrophys. J.* **558**, 859–871 (2001). doi:10.1086/322408
- B. De Pontieu, S.W. McIntosh, M. Carlsson, V.H. Hansteen, T.D. Tarbell, C.J. Schrijver, A.M. Title, R.A. Shine, S. Tsuneta, Y. Katsukawa, K. Ichimoto, Y. Suematsu, T. Shimizu, S. Nagata, Chromospheric Alfvénic waves strong enough to power the solar wind. *Sci.* **318**, 1574 (2007a). doi:10.1126/science.1151747
- B. De Pontieu, S.W. McIntosh, M. Carlsson, V.H. Hansteen, C.J. Schrijver, T.D. Tarbell, A. Title, SOT Team, Observational evidence for the ubiquity of strong Alfvén waves in the magnetized chromosphere, in *American Astronomical Society Meeting Abstracts #210*. *Bull. Am. Astron. Soc.*, vol. 39, 2007b, p. 219
- B. De Pontieu, A.M. Title, J. Lemen, J. Wuelser, T.D. Tarbell, C.J. Schrijver, L. Golub, C. Kankelborg, M. Carlsson, V.H. Hansteen, S. Worden, IRIS team, The Interface Region Imaging Spectrograph (IRIS), in *AAS/Solar Physics Division Meeting*. *AAS/Solar Physics Division Meeting*, vol. 44, 2013, p. 03
- C.R. DeVore, Prominence fine structure due to magnetized Rayleigh-Taylor instability, in *AAS/Solar Physics Division Meeting*. *AAS/Solar Physics Division Meeting*, vol. 44, 2013, p. 41
- Y.S. Dimant, R.N. Sudan, Kinetic theory of the Farley-Buneman instability in the E region of the ionosphere. *J. Geophys. Res.* **100**, 14605–14624 (1995). doi:10.1029/95JA00794
- D.P. Drob, D. Broutman, M.A. Hedlin, N.W. Winslow, R.G. Gibson, A method for specifying atmospheric gravity wavefields for long-range infrasound propagation calculations. *Journal of Geophysical Research (Atmospheres)* **118**, 3933–3943 (2013). doi:10.1029/2012JD018077
- J.K. Edmondson, B.J. Lynch, C.R. DeVore, M. Velli, Reconnection-Driven Alfvén (RDA) Waves in the Solar Corona. *AGU Fall Meeting Abstracts*, 1990 (2011)
- R.E. Erlandson, L.J. Zanetti, M.H. Acuña, A.I. Eriksson, L. Eliasson, M.H. Boehm, L.G. Blomberg, Freja observations of electromagnetic ion cyclotron ELF waves and transverse oxygen ion acceleration on auroral field lines. *Geophys. Res. Lett.* **21**, 1855–1858 (1994). doi:10.1029/94GL01363
- D.T. Farley Jr., A plasma instability resulting in field-aligned irregularities in the ionosphere. *J. Geophys. Res.* **68**, 6083 (1963)
- J.M. Fontenla, Chromospheric plasma and the Farley-Buneman instability in solar magnetic regions. *Astron. Astrophys.* **442**, 1099–1103 (2005). doi:10.1051/0004-6361:20053669
- J.M. Fontenla, E.H. Avrett, R. Loeser, Energy balance in the solar transition region. III - Helium emission in hydrostatic, constant-abundance models with diffusion. *Astrophys. J.* **406**, 319–345 (1993). doi:10.1086/172443
- J.M. Fontenla, W.K. Peterson, J. Harder, Chromospheric heating by the Farley-Buneman instability. *Astron. Astrophys.* **480**, 839–846 (2008). doi:10.1051/0004-6361:20078517
- J.M. Fontenla, E. Avrett, G. Thuillier, J. Harder, Semiempirical models of the solar atmosphere. I. The quiet- and active Sun photosphere at moderate resolution. *Astrophys. J.* **639**, 441–458 (2006). doi:10.1086/499345
- A. Fossum, M. Carlsson, Are high frequency acoustic waves sufficient to heat the solar chromosphere?, in *The Dynamic Sun: Challenges for Theory and Observations*. *ESA Special Publication*, vol. 600, 2005a
- A. Fossum, M. Carlsson, High-frequency acoustic waves are not sufficient to heat the solar chromosphere. *Nat.* **435**, 919–921 (2005b). doi:10.1038/nature03695
- A. Fossum, M. Carlsson, Determination of the acoustic wave flux in the lower solar chromosphere. *Astrophys. J.* **646**, 579–592 (2006). doi:10.1086/504887
- R. Fujii, S. Nozawa, S.C. Buchert, A. Brekke, Statistical characteristics of electromagnetic energy transfer between the magnetosphere, the ionosphere, and the thermosphere. *J. Geophys. Res.* **104**, 2357–2366 (1999). doi:10.1029/98JA02750
- T. Fuller-Rowell, C.J. Schrijver, On the ionosphere and chromosphere, in *Heliophysics I: Plasma Physics of the Local Cosmos*, ed. by Schrijver, C. J. and Siscoe, G. L. (Cambridge University Press, New York, 2009), pp. 324–359
- T.J. Fuller-Rowell, D. Rees, S. Quegan, G.J. Bailey, R.J. Moffett, The effect of realistic conductivities on the high-latitude neutral thermospheric circulation. *Planet. Space Sci.* **32**, 469–480 (1984). doi:10.1016/0032-0633(84)90126-0
- T.J. Fuller-Rowell, D. Rees, S. Quegan, R.J. Moffett, M.V. Codrescu, A Coupled Thermosphere-Ionosphere Model (CTIM), *STEP Handbook of Ionospheric Models 1996*, pp. 217–238
- H. Gilbert, G. Kilper, D. Alexander, Observational evidence supporting cross-field diffusion of neutral material in solar filaments. *ApJ* **671**, 978–989 (2007). doi:10.1086/522884
- H.R. Gilbert, V.H. Hansteen, T.E. Holzer, Neutral atom diffusion in a partially ionized prominence plasma. *ApJ* **577**, 464–474 (2002). doi:10.1086/342165
- G. Gogoberidze, Y. Voitenko, S. Poedts, M. Goossens, Farley-Buneman instability in the solar chromosphere.

- Astrophys. J. Lett. **706**, 12–16 (2009). doi:10.1088/0004-637X/706/1/L12
- M.L. Goodman, On the Mechanism of Chromospheric Network Heating and the Condition for Its Onset in the Sun and Other Solar-Type Stars. *Astrophys. J.* **533**, 501–522 (2000). doi:10.1086/308635
- M.L. Goodman, The Necessity of Using Realistic Descriptions of Transport Processes in Modeling the Solar Atmosphere, and the Importance of Understanding Chromospheric Heating*. *Space Science Review* **95**, 70 (2001).
- M.L. Goodman, On the efficiency of plasma heating by Pedersen current dissipation from the photosphere to the lower corona. *Astron. Astrophys.* **416**, 1159–1178 (2004). doi:10.1051/0004-6361:20031719
- M.L. Goodman, Conditions for photospherically driven Alfvénic oscillations to heat the solar chromosphere by Pedersen current dissipation. *Astrophys. J.* **735**, 45 (2011). doi:10.1088/0004-637X/735/1/45
- M.L. Goodman, P.G. Judge, Radiating current sheets in the solar chromosphere. *Astrophys. J.* **751**, 75 (2012). doi:10.1088/0004-637X/751/1/75
- G. Haerendel, Commonalities between ionosphere and chromosphere. *Space Sci. Rev.* **124**, 317–331 (2006). doi:10.1007/s11214-006-9092-z
- G. Haerendel, J.V. Eccles, S. akir, Theory for modeling the equatorial evening ionosphere and the origin of the shear in the horizontal plasma flow. *Journal of Geophysical Research: Space Physics* **97**(A2), 1209–1223 (1992). doi:10.1029/91JA02226. <http://dx.doi.org/10.1029/91JA02226>
- M.E. Hagan, M.D. Burrage, J.M. Forbes, J. Hackney, W.J. Randel, X. Zhang, GSWM-98: Results for migrating solar tides. *J. Geophys. Res.* **104**, 6813–6828 (1999). doi:10.1029/1998JA900125
- A.M. Hamza, J.-P. St.-Maurice, A fully self-consistent fluid theory of anomalous transport in Farley-Buneman turbulence. *J. Geophys. Res.* **100**, 9653–9668 (1995). doi:10.1029/94JA03031
- S.S. Hasan, A.A. van Ballegoijen, Dynamics of the solar magnetic network. II. Heating the magnetized chromosphere. *Astrophys. J.* **680**, 1542–1552 (2008). doi:10.1086/587773
- J.C. Henoux, B.V. Somov, The photospheric dynamo. I. Magnetic flux-tube generation. *Astron. Astrophys.* **241**, 613–617 (1991)
- J.C. Henoux, B.V. Somov, The photospheric dynamo. I. Physics of thin magnetic flux tubes. *Astron. Astrophys.* **318**, 947–956 (1997)
- A. Hillier, H. Isobe, K. Shibata, T. Berger, Numerical simulations of the magnetic Rayleigh-Taylor instability in the Kippenhahn-Schlüter prominence model. *Astrophys. J. Lett.* **736**, 1 (2011). doi:10.1088/2041-8205/736/1/L1
- A. Hillier, T. Berger, H. Isobe, K. Shibata, Numerical simulations of the magnetic Rayleigh-Taylor instability in the Kippenhahn-Schlüter prominence model. I. Formation of upflows. *Astrophys. J.* **746**, 120 (2012a). doi:10.1088/0004-637X/746/2/120
- A. Hillier, H. Isobe, K. Shibata, T. Berger, Numerical simulations of the magnetic Rayleigh-Taylor instability in the Kippenhahn-Schlüter prominence model. II. Reconnection-triggered downflows. *Astrophys. J.* **756**, 110 (2012b). doi:10.1088/0004-637X/756/2/110
- J.D. Huba, J. Krall, G. Joyce, Atomic and molecular ion dynamics during equatorial spread f. *Geophysical Research Letters* **36**(10), (2009a). doi:10.1029/2009GL037675. <http://dx.doi.org/10.1029/2009GL037675>
- J.D. Huba, G. Joyce, J. Krall, J. Fedder, Ion and electron temperature evolution during equatorial spread f. *Geophysical Research Letters* **36**(15), (2009b). doi:10.1029/2009GL038872. <http://dx.doi.org/10.1029/2009GL038872>
- J.D. Huba, G. Joyce, Global modeling of equatorial plasma bubbles. *Geophys. Res. Lett.* **37** 17104 (2013). doi:10.1029/2010GL044281. <http://adsabs.harvard.edu/abs/2010GeoRL...3717104H>
- H. Isobe, T. Miyagoshi, K. Shibata, T. Yokoyama, Filamentary structure on the Sun from the magnetic Rayleigh-Taylor instability. *Nat.* **434**, 478–481 (2005). doi:10.1038/nature03399
- H. Isobe, T. Miyagoshi, K. Shibata, T. Yokoyama, Three-dimensional simulation of solar emerging flux using the Earth Simulator I. Magnetic Rayleigh-Taylor instability at the top of the emerging flux as the origin of filamentary structure. *Pub. Astron. Soc. Jpn.* **58**, 423–438 (2006)
- W. Kalkofen, Is the solar chromosphere heated by acoustic waves? *Astrophys. J.* **671**, 2154–2158 (2007). doi:10.1086/523259
- F. Kamalabadi, J.M. Comberiate, M.J. Taylor, P.-D. Pautet, Estimation of electron densities in the lower thermosphere from guvi 135.6 nm tomographic inversions in support of spreadfex. *Annales Geophysicae* **27**(6), 2439–2448 (2009). doi:10.5194/angeo-27-2439-2009. <http://www.ann-geophys.net/27/2439/2009/>
- Y. Kamide, The relationship between field-aligned currents and the auroral electrojets - A review. *Space Sci. Rev.* **31**, 127–243 (1982). doi:10.1007/BF00215281
- A. Keiling, J.R. Wygant, C.A. Cattell, F.S. Mozer, C.T. Russell, The Global Morphology of Wave Poynting Flux: Powering the Aurora. *Science* **299**, 383–386 (2003). doi:10.1126/science.1080073
- M.C. Kelley, R.A. Hellis, *The Earth's Ionosphere: Plasma Physics and Electrodynamics* (Academic Press, New York, 1989)

- M.C. Kelley, D.J. Knudsen, J.F. Vickrey, Poynting flux measurements on a satellite. A diagnostic tool for space research. *J. Geophys. Res.* **96**, 201–207 (1991).
- E. Khomenko, M. Collados, Heating of the magnetized solar chromosphere by partial ionization effects. *Astrophys. J.* **747**, 87 (2012). doi:10.1088/0004-637X/747/2/87
- H. Kigure, K. Takahashi, K. Shibata, T. Yokoyama, S. Nozawa, Generation of Alfvén Waves by Magnetic Reconnection. *Pub. Astron. Soc. Jpn.* **62**, 993 (2010)
- J.A. Klimchuk, On solving the coronal heating problem. *Sol. Phys.* **234**, 41–77 (2006). doi:10.1007/s11207-006-0055-z
- J. Krall, J.D. Huba, G. Joyce, T. Yokoyama, Density enhancements associated with equatorial spread f. *Annales Geophysicae* **28**(2), 327–337 (2010). doi:10.5194/angeo-28-327-2010. <http://www.ann-geophys.net/28/327/2010/>
- V. Krasnoselskikh, G. Vekstein, H.S. Hudson, S.D. Bale, W.P. Abbett, Generation of electric currents in the chromosphere via neutral-ion drag. *Astrophys. J.* **724**, 1542–1550 (2010). doi:10.1088/0004-637X/724/2/1542
- A.P. Kropotkin, The generation of magnetic field via convective motions in the photosphere, Alfvén waves, and the origin of chromospheric spicules. *Astron. Rep.* **55**, 1132–1143 (2011). doi:10.1134/S10663772911120079
- J.E. Leake, T.D. Arber, The emergence of magnetic flux through a partially ionised solar atmosphere. *Astron. Astrophys.* **450**, 805–818 (2006). doi:10.1051/0004-6361:20054099
- J.E. Leake, M.G. Linton, Effect of ion-neutral collisions in simulations of emerging active regions. *Astrophys. J.* **764**, 54 (2013). doi:10.1088/0004-637X/764/1/54
- J.E. Leake, T.D. Arber, M.L. Khodachenko, Collisional dissipation of Alfvén waves in a partially ionised solar chromosphere. *Astron. Astrophys.* **442**, 1091–1098 (2005). doi:10.1051/0004-6361:20053427
- J.E. Leake, V.S. Lukin, M.G. Linton, Magnetic reconnection in a weakly ionized plasma. *Phys. Plasmas* **20**(6), 061202 (2013)
- J.E. Leake, V.S. Lukin, M.G. Linton, E.T. Meier, Multi-fluid simulations of chromospheric magnetic reconnection in a weakly ionized reacting plasma. *Astrophys. J.* **760**, 109 (2012). doi:10.1088/0004-637X/760/2/109
- J. Lei, R.G. Noble, B.A. Wang, S.R. Zhang, Electron temperature climatology at Millstone Hill and Arecibo. *J. Geophys. Res.* **112**, A02302 (2007). doi:10.1029/2006JA012041
- Y. Lin, O. Engvold, L.H.M. Rouppe van der Voort, M. van Noort, Evidence of traveling waves in filament threads. *Sol. Phys.* **246**, 65–72 (2007). doi:10.1007/s11207-007-0402-8
- G. Lu, A.D. Richmond, B.A. Emery, R.G. Roble, Magnetosphere-ionosphere-thermosphere coupling: Effect of neutral winds on energy transfer and field-aligned current. *J. Geophys. Res.* **100**, 19643–19660 (1995). doi:10.1029/95JA00766
- V.S. Lukin, Computational study of the internal kink mode evolution and associated magnetic reconnection phenomena, PhD thesis, Princeton University, 2008
- S. Lundquist, Studies in magneto-hydrodynamics. *Ark. Fys.* **5**, 297–347 (1952)
- C.A. Madsen, Y.S. Dimant, M.M. Oppenheim, J.M. Fontenla, The Multi-Species Farley-Buneman Instability in the Solar Chromosphere. *ArXiv e-prints* (2013)
- J.J. Makela, B.M. Ledvina, M.C. Kelley, P.M. Kintner, Analysis of the seasonal variations of equatorial plasma bubble occurrence observed from Haleakala, Hawaii. *Ann. Geophys.* **22**, 3109–3121 (2004). doi:10.5194/angeo-22-3109-2004
- J. Martínez-Sykora, B. De Pontieu, V. Hansteen, Two-dimensional radiative magnetohydrodynamic simulations of the importance of partial ionization in the chromosphere. *Astrophys. J.* **753**, 161 (2012). doi:10.1088/0004-637X/753/2/161
- E.T. Meier, U. Shumlak, A general nonlinear fluid model for reacting plasma-neutral mixtures. *Phys. Plasmas* **19**, 072508 (2012)
- G.H. Millward, R.J. Moffett, S. Quegan, T.J. Fuller-Rowell, A Coupled Thermosphere-Ionosphere Model (CTIM), STEP Handbook of Ionospheric Models 1996, pp. 239–280
- M. Mitchner, C.H. Kruger, *Partially Ionized Gases* (Wiley, New York, 1973)
- V.M. Nakariakov, L. Ofman, E.E. Deluca, B. Roberts, J.M. Davila, TRACE observation of damped coronal loop oscillations: Implications for coronal heating. *Science* **285**, 862–864 (1999). doi:10.1126/science.285.5429.862
- U. Narain, P. Ulmschneider, Chromospheric and coronal heating mechanisms. *Space Sci. Rev.* **54**, 377–445 (1990). doi:10.1007/BF00177801
- L. Ofman, Chromospheric Leakage of Alfvén Waves in Coronal Loops. *Astrophys. J. Lett.* **568**, 135–138 (2002). doi:10.1086/340329
- M.M. Oppenheim, Y.S. Dimant, Kinetic simulations of 3-D Farley-Buneman turbulence and anomalous electron heating. *Journal of Geophysical Research (Space Physics)* **118**, 1306–1318 (2013).

- doi:10.1002/jgra.50196
- S.L. Ossakow, Spread F theories: A review. *J. Atmos. Terr. Phys.* **43**, 437–452 (1981)
- N.F. Otani, M. Oppenheim, Saturation of the Farley-Buneman instability via three-mode coupling. *Journal of Geophysical Research (Space Physics)* **111**, 3302 (2006). doi:10.1029/2005JA011215
- E.N. Parker, Magnetic neutral sheets in evolving fields. I. General theory. *Astrophys. J.* **264**, 635–647 (1983). doi:10.1086/160636
- E.N. Parker, Dynamical oscillation and propulsion of magnetic fields in the convective zone of a star. VI. Small flux bundles, network fields, and ephemeral active regions. *Astrophys. J.* **326**, 407–411 (1988). doi:10.1086/166103
- E.N. Parker, The alternative paradigm for magnetospheric physics. *J. Geophys. Res.* **101**, 10587–10626 (1996). doi:10.1029/95JA02866
- E.N. Parker, *Conversations on Electric and Magnetic Fields in the Cosmos* (Princeton University Press, Princeton NJ, 2007)
- S.V. Poliakov, V.O. Rapoport, The ionospheric Alfvén resonator. *Geomagnetism and Aeronomy* **21**, 816–822 (1981)
- J.W.S. Rayleigh, Investigation of the character of the equilibrium of an incompressible heavy fluid of variable density. *Proc. Lond. Math. Soc.* **14**, 170–177 (1882)
- A.D. Richmond, J.P. Thayer, Ionospheric electrodynamics: A tutorial, in *Magnetospheric Current Systems*, ed. by Ohtani, S. and Fujii, R. and Hesse, M. and Lysak, R. L. Geophysical Monograph, vol. 118 (American Geophysical Union, Washington DC, 2000), pp. 131–146
- A.D. Richmond, E.C. Ridley, R.G. Roble, A thermosphere/ionosphere general circulation model with coupled electrodynamics. *Geophys. Res. Lett.* **19**, 601–604 (1992). doi:10.1029/92GL00401
- H. Rishbeth, Thermospheric Targets. *EOS Transactions* **88**, 189–193 (2007). doi:10.1029/2007EO170002
- R.G. Roble, E.C. Ridley, A thermosphere-ionosphere-mesosphere-electrodynamics general circulation model (TIMEGCM): Equinox solar cycle minimum simulations (30–500 km). *Geophys. Res. Lett.* **21**, 417–420 (1994). doi:10.1029/93GL03391
- R.G. Roble, E.C. Ridley, A.D. Richmond, R.E. Dickinson, A coupled thermosphere/ionosphere general circulation model. *Geophys. Res. Lett.* **15**, 1325–1328 (1988). doi:10.1029/GL015i012p01325
- A.J.B. Russell, L. Fletcher, Propagation of Alfvénic Waves from Corona to Chromosphere and Consequences for Solar Flares. *Astrophys. J.* **765**, 81 (2013). doi:10.1088/0004-637X/765/2/81
- R.W. Schunk, A.F. Nagy, *Ionospheres: Physics, Plasma Physics, and Chemistry* (Cambridge University Press, New York, 2000)
- M. Schwarzschild, On noise arising from the solar granulation. *Astrophys. J.* **107**, 1 (1948). doi:10.1086/144983
- P. Song, V.M. Vasyliūnas, Heating of the solar atmosphere by strong damping of Alfvén waves. *J. Geophys. Res.* **116**, 9104 (2011). doi:10.1029/2011JA016679
- P. Song, T.I. Gombosi, A.J. Ridley, Three-fluid Ohm’s law. *J. Geophys. Res.* **106**, 8149–8156 (2001). doi:10.1029/2000JA000423
- P. Song, V.M. Vasyliūnas, L. Ma, Solar wind-magnetosphere-ionosphere coupling: Neutral atmosphere effects on signal propagation. *Journal of Geophysical Research* **110**, 9309 (2005). doi:10.1029/2005JA011139
- J.P. St. Maurice, R.W. Schunk, Ion-neutral momentum coupling near discrete high latitude ionospheric features. *Journal of Geophysical Research* **86**, 11299 (1981).
- R.F. Stein, Solar surface magneto-convection. *Living Rev. Sol. Phys.* **9**, 4 (2012). doi:10.12942/lrsp-2012-4
- J.M. Stone, T. Gardiner, Nonlinear evolution of the magnetohydrodynamic Rayleigh-Taylor instability. *Phys. Fluids* **19**(9), 094104 (2007a). doi:10.1063/1.2767666
- J.M. Stone, T. Gardiner, The magnetic Rayleigh-Taylor instability in three dimensions. *Astrophys. J.* **671**, 1726–1735 (2007b). doi:10.1086/523099
- P.J. Sultan, Linear theory and modeling of the Rayleigh-Taylor instability leading to the occurrence of equatorial spread F. *J. Geophys. Res.* **101**, 26875–26892 (1996)
- E. Tandberg-Hanssen, *The Nature of Solar Prominences* (Kluwer, Dordrecht, 1995)
- G. Taylor, The instability of liquid surfaces when accelerated in a direction perpendicular to their planes. I. *Proc. R. Soc. (Lond.) A* **201**, 192–196 (1950). doi:10.1098/rspa.1950.0052
- J.P. Thayer, High-latitude currents and their energy exchange with the ionosphere-thermosphere system. *J. Geophys. Res.* **105**, 23015–23024 (2000). doi:10.1029/1999JA000409
- J.P. Thayer, J. Semeter, The convergence of magnetospheric energy flux in the polar atmosphere. *J. Atmos. Solar-Terr. Phys.* **66**, 807–824 (2004). doi:10.1016/j.jastp.2004.01.035
- J.P. Thayer, J.F. Vickrey, R.A. Heelis, J.B. Gary, Interpretation and modeling of the high-latitude electromagnetic energy flux. *J. Geophys. Res.* **100**, 19715–19728 (1995). doi:10.1029/95JA01159
- W.K. Tobiska, T. Woods, F. Eparvier, R. Viereck, L. Floyd, D. Bouwer, G. Rottman, O.R. White, The SOLAR2000 empirical solar irradiance model and forecast tool. *J. Atmos. Solar-Terr. Phys.* **62**, 1233–1250

- (2000). doi:10.1016/S1364-6826(00)00070-5
- S. Tomczyk, S.W. McIntosh, S.L. Keil, P.G. Judge, T. Schad, D.H. Seeley, J. Edmondson, Alfvén waves in the solar corona. AGU Fall Meeting Abstracts, 289 (2007)
- M.R. Torr, D.G. Torr, The seasonal behaviour of the F2 layer of the ionosphere. *J. Atmos. Terr. Phys.* **35**, 2237–2251 (1973)
- J. Tu, P. Song, On the concept of penetration electric field. *Radio Sounding and Plasma Physics* **974**, 81–85 (2008).
- J. Tu, P. Song, V.M. Vasyliūnas, Ionosphere/thermosphere heating determined from dynamic magnetosphere-ionosphere/thermosphere coupling. *Journal of Geophysical Research (Space Physics)* **116**, 9311 (2011). doi:10.1029/2011JA016620
- J. Tu, P. Song, A Study of Alfvén Wave Propagation and Heating the Chromosphere. *Astrophysical Journal* **777**, 53 (2013). doi:10.1088/0004-637X/777/1/53
- Y.-K. Tung, C.W. Carlson, J.P. McFadden, D.M. Klumpar, G.K. Parks, W.J. Peria, K. Liou, Auroral polar cap boundary ion conic outflow observed on FAST. *J. Geophys. Res.* **106**, 3603–3614 (2001). doi:10.1029/2000JA900115
- P. Ulmschneider, Acoustic heating of stellar chromospheres and coronae, in *Cool Stars, Stellar Systems, and the Sun*, ed. by G. Wallerstein Astron. Soc. Pac. Conf. Ser., vol. 9 (ASP, San Francisco, 1990), pp. 3–14
- V. Väisälä, Über die Wirkung der Windschwankungen auf die Pilotbeobachtungen. *Soc. Sci. Fenn. Comment. Math. Phys.* **2**, 19–37 (1925)
- V.M. Vasyliūnas, Electric field and plasma flow: What drives what?. *Geophys. Res. Lett.* **28**, 2177–2180 (2001). doi:10.1029/2001GL013014
- V.M. Vasyliūnas, Time evolution of electric fields and currents and the generalized Ohm’s law. *Ann. Geophys.* **23**, 1347–1354 (2005). doi:10.5194/angeo-23-1347-2005
- V.M. Vasyliūnas, Relation between magnetic fields and electric currents in plasmas. *Ann. Geophys.* **23**, 2589–2597 (2005). doi:10.5194/angeo-23-2589-2005
- V.M. Vasyliūnas, P. Song, Meaning of ionospheric Joule heating. *J. Geophys. Res.* **110**, 2301 (2005). doi:10.1029/2004JA010615
- V.M. Vasyliūnas, Physics of Magnetospheric Variability. *J. Geophys. Res.* **158**, 91–118 (2011). doi:10.1007/s11214-010-9696-1
- V.M. Vasyliūnas, The physical basis of ionospheric electrodynamics. *Ann. Geophys.* **30**, 3157–369 (2012). doi:10.5194/angeo-30-357-2012
- J.E. Vernazza, E.H. Avrett, R. Loeser, Structure of the solar chromosphere. III. Models of the EUV brightness components of the quiet Sun. *Astrophys. J. Suppl. Ser.* **45**, 635–725 (1981). doi:10.1086/190731
- Y. Voitenko, M. Goossens, Excitation of high-frequency Alfvén waves by plasma outflows from coronal reconnection events. *Sol. Phys.* **206**, 285–313 (2002). doi:10.1023/A:1015090003136
- J. Vranjes, P.S. Krstić, Collisions, magnetization, and transport coefficients in the lower solar atmosphere. *Astron. Astrophys.* **554**, 22 (2013). doi:10.1051/0004-6361/201220738
- W. Wang, A.G. Burns, M. Wiltberger, S.C. Solomon, T.L. Killeen, Altitude variations of the horizontal thermospheric winds during geomagnetic storms. *J. Geophys. Res.* **113**, 2301 (2008). doi:10.1029/2007JA012374
- R.F. Woodman, Spread F – An old equatorial aeronomy problem finally resolved? *Ann. Geophys.* **27**, 1915–1934 (2009). doi:10.5194/angeo-27-1915-2009
- T.V. Zaqarashvili, M.L. Khodachenko, H.O. Rucker, Magnetohydrodynamic waves in solar partially ionized plasmas: two-fluid approach. *Astronomy and I/Tysics* **529**, 82 (2011). doi:10.1051/0004-6361/201016326